Assessing the Performance of Horizontal Axis Marine Current Turbines: The Impact of Evaluation Methods and Inflow Parameters

by

Masoud Rahimian, B.E., M.E

National Centre for Maritime Engineering and Hydrodynamics

Australian Maritime College

Submitted in fulfilment of the requirements for the degree of Doctor of Philosophy

University of Tasmania
August 2018

Declarations

I declare that ‘This thesis contains no material which has been accepted for a degree or diploma by the University or any other institution, except by way of background information and duly acknowledged in the thesis, and to the best of my knowledge and belief no material previously published or written by another person except where due acknowledgement is made in the text of the thesis, nor does the thesis contain any material that infringes copyright.’

This thesis may be made available for loan and limited copying in accordance with the Copyright Act 1968

Signed:

_____

Masoud Rahimian

Date: 01 May 2018

Statement of Published Work Contained in Thesis

The publishers of the papers comprising Chapters 2 to 4 hold the copyright for that content, and access to the material should be sought from the respective journals. The remaining non-published content of the thesis, Chapter 5, are submitted and under review, and may be made available for loan and limited copying and communication in accordance with the Copyright Act 1968.

Statement of Co-Authorship

The following people and institutions contributed to the publication of work undertaken as part of this thesis:

- Masoud Rahimian, University of Tasmania (Candidate)
- Doctor Jessica Walker, Primary Supervisor, University of Tasmania (Author 1)
- Associate Professor Irene Penesis, Co-Supervisor, University of Tasmania (Author 2)
- Michael Sos, University of Tasmania (Author 3)
- Luke Johnston, University of Tasmania (Author 4)

Author details and their roles:

Paper 1: **Rahimian M, Walker J, Penesis I. Numerical assessment of a horizontal axis marine current turbine performance.** ***International Journal of Marine Energy*****. 2017;20: 151-64.**

Chapter 2 was based on this paper. The Candidate was the primary author. Author 1 and Author 2 assisted with research direction, advice, and presentation. [Candidate: 80%, Author 1: 10%, Author 2: 10%].

Paper 2: **Rahimian M, Walker J, Penesis I. Performance of a horizontal axis marine current turbine– A comprehensive evaluation using experimental, numerical, and theoretical approaches. *Energy*. 2018; 148:965-76.**

Chapter 3 and parts of Chapter 4 were based on this paper. The Candidate was the primary author. Author 1 and Author 2 assisted with research direction, advice, and presentation. [Candidate: 80%, Author 1: 10%, Author 2: 10%].

Paper 3: **Rahimian M, Walker J, Penesis I. The influence of shear flow and waves on the performance characteristics of a horizontal axis marine current turbine. *Journal of Applied Energy*. 2018. (submitted for review)**

Chapter 5 is based on this paper. The Candidate was the primary author. Author 1 and Author 2 assisted with research direction, advice, and presentation. [Candidate: 80%, Author 1: 10%, Author 2: 10%].

Paper 4: **Sos M, Johnston L, Walker J, Rahimian M. The impact of waves and immersion depth on horizontal axis tidal turbine performance. *12th European Wave and Tidal Energy Conference (EWTEC2017)*. Cork, Ireland. p. 1-8.**

This conference paper is included in the appendix. Author 3 and Author 4 completed the experimental work presented in the paper and contributed to the drafting of the paper. Author 1 contributed to the conception and design of the project, the analysis and interpretation of the research data, and prepared the paper. The Candidate contributed to the conception and design of the project and the analysis and interpretation of the research data. [Author 3: 35%, Author 4: 35%, Author 1: 20%, Candidate: 10%].

We the undersigned agree with the above stated proportion of work undertaken for each of the published (or submitted) peer-reviewed manuscripts contributing to this thesis.

Signed:

_____

Dr Jessica Walker
Primary Supervisor
National Centre for Maritime Engineering and Hydrodynamics
Australian Maritime College
University of Tasmania

Date: 02 May 2018

_____

Assoc/Prof Irene Penesis
Co-Supervisor
National Centre for Maritime Engineering and Hydrodynamics
Australian Maritime College
University of Tasmania

Date: 02 May 2018

_____

Assoc/Prof Michael Woodward
Director
National Centre for Maritime Engineering and Hydrodynamics
Australian Maritime College
University of Tasmania

Date: 02 May 2018

Acknowledgements

Finally, this wonderful chapter of my life has come to an end. It has been filled with joy and tribulations, and I certainly was not able to make it through on my own.

Firstly, I would like to express my sincere gratitude to my supervisory team, Dr Jessica Walker and Assoc/Prof Irene Penesis for their continuous support, patience, encouragement, and immense knowledge. They have been great supervisors as well as tremendous mentors for me. It has been a pleasure to work with them and I hope I can pass on what I have learnt from them.

My genuine thanks also goes to Dr. Zhi Leong, and Dr. Philip Marsh for sharing their CFD knowledge, which helped me make through CFD difficulties. Special thanks must also go to Rowan Frost, Jock Ferguson, and Tim Lilienthal for their technical support in the setup and execution of experimental works.

I would like to express my appreciation to the turbine research team led by Prof Karen Flack at the United States Naval Academy for sharing their rotor design, which was used as the basis for the AMC turbine.

Last but not the least, thanks to Zhinous, my love, who brought colours into my life. This work is dedicated to you.

Abstract

The oceans offer a considerable sustainable energy resource in the form of wave, marine currents and thermal energy and provide a potential alternative to fossil fuels. Marine current, or tidal, energy can be harnessed using horizontal axis marine current turbines (HAMCTs). In this work, the performance of a 2-bladed HAMCT was extensively investigated using experimental, theoretical and numerical models under different flow conditions. The motivation behind the study was to assess the influence of various parameters, associated with an evaluation method and those involved in the environment of a deployment site, on turbine performance. The employed evaluation methods were compared to find the best practice for performance assessment in various operational conditions.

For this purpose, two physical scale models with diameters of 500 mm and 800 mm were tested in the Australian Maritime College Towing Tank and Circulating Water Channel (CWC). Towing tank results from the United States Naval Academy were also employed for facility comparison as well as CFD model verification. The experimental results provide the hydrodynamic characteristics of the turbine under the different inflow conditions in each facility. The difference between the performances of the two scale models was found to be mainly due to the effect of Reynolds number and possibly attributed to the blockage effect. To predict the performance of a full-scale turbine, experiments on a scale model in conditions with Reynolds number independency, in this study $Re > 2 \times 10^5$, in a facility with little blockage is suggested. Unlike the towing tanks, the CWC did not have a uniform inflow. Using the equivalent flow velocity, obtained from kinetic energy flux over the rotor swept area, in dimensional analysis of the CWC data resulted in a better correlation with the towing tank results. It shows that although the shear flow profile practically has little effect on the mean power output per se, selecting the flow velocity by which the performance is analysed is essential in scale model tests. The impact of facility bias on the performance assessment appeared to be induced mainly from blockage and partially from the flow velocity profile.

An experimentally validated Blade Element Momentum (BEM) model was modified to consider shear flow profile and Reynolds number in the performance calculations. In addition, QBlade software was employed as a tool to investigate the effect of using local Reynolds number over the blade span. No significant changes were seen in the BEM model results by incorporating the shear flow in the code. Comparing the QBlade and BEM model results

showed that using local sectional Reynolds numbers in the prediction may be not worth the effort to achieve results that were slightly more accurate than the model with a single reference Reynolds number. BEM theory provides reasonable performance predictions for turbines in steady flow conditions.

To establish detailed hydrodynamic characteristics of the turbine in ideal flow conditions, an experimentally validated numerical model using Computational Fluid Dynamics (CFD) was developed. Different CFD approaches were applied to the model to find the best numerical practice for the performance evaluation of HAMCTs. The CFD model was modified to account for sheared inflow and surface waves using volume of fluid (VOF) and single-phase methods. A steady moving reference frame (MRF) simulation of the whole turbine model using the k-ω SST turbulence model with the wall-function model was found to be the best approach for the performance prediction of HAMCTs under steady inflow conditions in a balance between simulation time and result accuracy. Conversely, a transient solution with the sliding mesh method provided a better fit to the experimental results for turbine under waves and sheared inflow velocity profiles. The CFD simulations showed that a sheared inflow velocity profile had a cyclic effect on the blade loadings and almost no significant effect on the mean power production of the turbine. The effect of turbine depth and waves on the mean power yield was also negligible when the tip immersion depth of the turbine was more than half the turbine radius. Since both wave and sheared flow velocity affect the quality of power output even in deeper positions, they should be considered during the turbine design stage. Regardless the angular position of the blades, the maximum values of C_P and C_T occurred at the passing wave peaks and the minimum values at the troughs.

This study comprehensively evaluated the methods available to predict the performance of HAMCTs and provided a detailed discussion of the different parameters that affect both turbine and model performance. Overall, the BEM model provided accurate performance results in the steady flow condition, though it was unable to capture the effect of shear velocity on the turbine hydrodynamics. The QBlade model yielded similar results to the BEM model with the possibility of investigating Reynolds number effect; a user-friendly tool for quick performance prediction of a full-scale turbine. The CFD approach provided detailed information about the turbine hydrodynamics in both steady and unsteady conditions; however, an extensive verification and validation of the model is essential to achieve trustworthy results. The scale model tests were found to be a reliable way for performance assessment of HAMCTs.

However, it is important to know how to account for blockage, inflow velocity profile and model scale effects when extrapolating the results to the full-scale turbine.

Table of Contents

List of Figures

List of Tables

Nomenclature

Greek Symbols

α	Local angle of attack	rad
β	Seabed friction	-
γ	Power law of velocity profile	-
δ	Local blade twist	rad
ε	Change in key variable	-
η_P	Precision error	-
η_B	Bias error	-
η_{cal}	Calibration error	-
θ	differential angle of the element	rad
λ_r	Local tip speed ratio	rad
μ	Viscosity	kg / m.s
υ	Kinematic viscosity	m^2 / s
ρ	Density	kg / m^3
σ_i	Root mean square of velocity fluctuations	m / s
σ_s	Standard deviation	-
τ	Shear stress	N / m^2
ϕ	Key variable of simulation (Torque/Thrust)	-
φ	Relative flow angle	rad
ψ	Local solidity ratio	rad
ω_w	Wave angular frequency	rad / s
ω	Rotational velocity	rad / s
$\forall$	Volume	m^3

Roman Symbols

a	Axial induction factor	-
a'	Angular induction factor	-
A	Rotor swept area	m^2

A_w	Wave amplitude	m
B	Number of blades	-
C	Cross-sectional area of facility	m^2
C_B	Blockage correction factor	-
C_L	Lift coefficient	-
C_D	Drag coefficient	-
C_T	Thrust coefficient	-
C_P	Power coefficient	-
dr	Differential radius	m
dt	Time step	s
dT	Differential thrust	N
dQ	Differential torque	N m
c	Local blade chord	m
e	Relative error of key variable	-
F	Tip loss factor	-
g	Gravity	m / s^2
h	number of mesh	-
H	Total water depth	m
I	3D turbulence intensity	-
I_x	streamwise turbulence intensity	-
k	Wave number	1 / m
N	Number of grids	-
N_S	Number of measured samples	-
p_e	Apparent order of mesh	-
P	Pressure	Pa
Q	Torque	N m
r	Local blade radius	m
rf	Mesh refinement factor	-
R	Rotor radius	m
Re_c	Chord based Reynolds number	-
S	Surface	m^2
S_M	Source term	N – N m

SEE	Standard error of estimate	-
SS_R	Summed square of residuals	-
S_E	Standard error	-
t	Time	s
th	Local blade thickness	m
t_{n-2}	t-random variable with n − 2 degrees of freedom	-
T	Thrust	N
u	Velocity vector	m / s
U	Freestream velocity	m / s
u_τ	Friction velocity	m/s
u'	Velocity fluctuations	m / s
$\bar{u}$	Mean velocity	m / s
$u_{w\,x}$	Wave velocity in x-direction	m / s
$u_{w\,z}$	Wave velocity in z-direction	m / s
$U1$	Velocity at turbine location	m / s
$U2$	Velocity in wake	m / s
$U3$	Bypass velocity	m / s
$\bar{U}$	Depth averaged velocity	m / s
U_z	Velocity at depth z	m / s
U_{eq}	Equivalent velocity	m / s
U_{rel}	Relative velocity	m / s
v	Analogue voltage recorded by sensor	Volt
Y^+	Dimensionless distance from wall	-
y_w	Distance from wall	m
z	Distance from free surface	m

Abbreviations

AMC	Australian Maritime College
ADV	Acoustic Doppler Velocimeter
ADCP	Acoustic Doppler Current Profiler
AoA	Angle of Attack
BEM	Blade Element Momentum
BSL EARSM	Baseline Explicit Algebraic Reynolds Stress Model
CAD	Computer-Aided Design
CFD	Computational Fluid Dynamics
CWC	Circulating Water Channel
FSI	Fluid-Structure Interaction
GCI	Grid Convergence Index
HAMCT	Horizontal Axis Marine Current Turbine
ITTC	International Towing Tank Committee
KE	Kinetic Energy
MRF	Moving Reference Frame
MSWT	MARIN Stock Wind Turbine
NACA	National Advisory Committee for Aeronautics
NREL	National Renewable Energy Laboratory
RANS	Reynolds Averaged Navier Stokes
SPh	Single-Phase
SST	Shear Stress Transport
TKE	Turbulence Kinetic Energy
TSR	Tip Speed Ratio
TT	Towing Tank
USNA	United States Naval Academy
VOF	Volume of Fluid

Chapter 1

Thesis Introduction

1.1. Introduction

Fossils fuels are currently the main resource providing global energy requirements. Huge dependence on this conventional source of energy is raising significant concerns. In addition to their negative environmental impacts, given the current rate of exploitation these resources are expected to be depleted within the next few decades. Thus, many studies are being performed to develop various renewable energy resources as sustainable alternatives. Oceans cover more than 70% of the earth, which store a vast renewable energy resource. The forms of ocean energy can be categorised into tidal, wave, current, thermal gradient and salinity gradient [1]. Tides and waves can provide predictable and consistent power generation, compared to solar and wind energy, which are highly dependent on weather condition [2]. Global tidal and marine current energy capacity is estimated to be in the order of 570 TWh/yr [3] well over twice electricity consumption of Australia in 2014 [4].

Horizontal-axis marine current turbines (HAMCTs) are devices that can convert the kinetic energy of the oceans to electricity [5]. Full scale HAMCTs are in the range of 1 MW and have 2 or 3-bladed rotors. The turbine blades rotate about a horizontal axis, parallel to the direction of the water flow. Ocean current velocities in a range of 2 to 3 m/s are optimal for the operation of these turbines. In those currents, a tidal turbine generates the same amount of energy as a wind turbine four times the size. Despite the performance of a horizontal-axis turbine depending on the current direction, they have slightly higher efficiency than vertical turbines [6]. Some examples of HAMCTs are the AR-1000, shown in Fig. 1.1, presented by Atlantis Resource Corporation [7], the HS1000 designed by Andritz Hydro Hammerfest [8] and the 1.2 MW SeaGen in Northern Ireland [9].

1.2. Problem Definition

In spite of recent advancements in tidal energy technology, it has not yet become technologically competitive with other renewable energy sources [10, 11]. One of the main concerns is the reliability and performance of these devices in the harsh marine environment [12]. Although many researchers have been striving to enhance the technology of these devices for many years, there are not yet many commercialised HAMCTs around the world [13, 14]. To date, operational records of only a few tidal energy devices have been demonstrated [15]. Turbine performance is influenced by various parameters, such as the flow condition of deployment site, which may be different from that the turbine was designed. Thus, it is crucial

to ensure that the performance of a turbine is optimum for a particular site in the primary design stages [16]. Various flow conditions that a turbine may experience, for example, are shear velocity profile due to seabed friction, change in flow direction, turbulence and fluctuations in the flow, depth variation and surface waves. Despite recent studies trying to assess the effect of these conditions on the turbine performance, more investigation is required to address the influence of each flow condition on the hydrodynamic characteristics of HAMCTs.

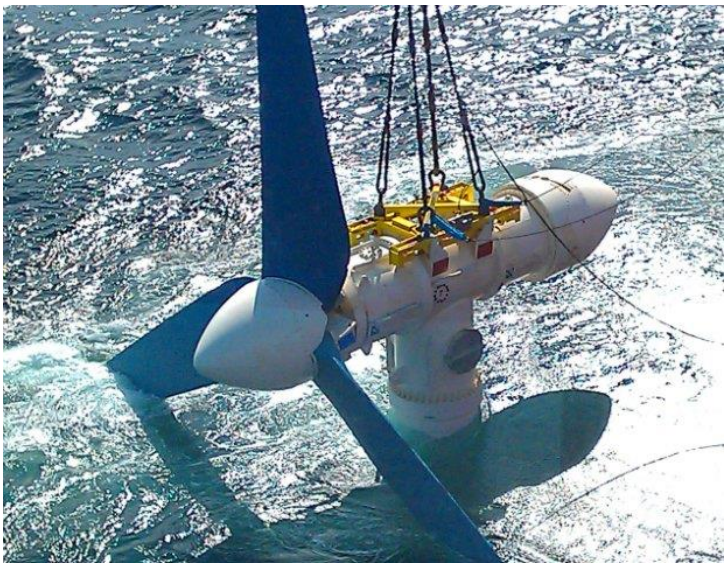

Fig. 1.1. Deployment of AR-1000 at a tidal site [7]

There are several approaches available to study the performance of a full-scale turbine, among which selecting an appropriate and accurate method that characterises the turbine hydrodynamics in various operational conditions is crucial. Among all of the theoretical approaches for analysing turbine performance, Blade Element Momentum (BEM) Theory represents the state-of-the-art. This theory is based on the assumption that each stream flow passing through the screw disc can be analysed independently from the rest of the flow. Therefore, the variations in the fluid dynamic quantities occur in the plane along the axial and radial directions from strip to strip, without considering expressly the radial equilibrium among the strips [17]. The Blade Element Momentum (BEM) theory is a useful tool to attain a quick power prediction of a marine current turbine [18]. A comprehensive description of BEM theory is given by Manwell, et al. [19]. Studies that have applied BEM theory to HAMCTs include [18, 20-24].

Experimental approaches are common practice to predict the hydrodynamic characteristics of marine systems. However, experimental tests are expensive to perform on full-scale turbines. It is common practice to test scale models before fabrication of the full scale device. The main

drawback of model tests is the unwanted effects of scaling that influence the viscous flow over the turbine blades. Nevertheless, they offer a realistic condition for performance evaluation and parametric study. Developing successful testing procedures and scaling methods has always been a key issue to predict valid full-scale performance. Having the ability to extrapolate results from model test data reduces some of the costs and challenges in turbine development. Besides the scale effects, there are parameters, such as facility bias, blockage and flow conditions, that should be taken into account when analysing the results. In this regard, different methods and facilities are proposed to see the effects of various factors, such as facility bias, on the performance of HAMCTs. Most facilities employed to test marine current turbines, such as towing tanks, have no turbulence and present a uniform flow. Thus, the performance curves developed from testing in such facilities represents the ideal case. Turbine performance in a real environment will be different due to the flow unsteadiness, which is demanding to be accounted for in a model test procedure. Key experimental studies on HAMCT include [25-32].

In addition to results from the above-mentioned approaches, an accurate and detailed performance prediction can be achieved if the assessment method considers the viscous effect over the turbine blades. Computational fluid dynamics (CFD) is an approach that inherently captures viscous flow. Although CFD may come with a great computation cost, the advantages of providing a better understanding of the flow field around the blade should not be neglected [33]. CFD is mainly being utilised as a tool for complex flow studies [34]. In addition, CFD can be employed to improve the design of a turbine in order to optimise the performance [35]. However, due to the vast variety of methods that can be employed for performance assessment, selecting a proper CFD approach is challenging. Some key CFD studies on HAMCT are [18, 36-42].

1.3. Research Objectives

The core aim of this work was to evaluate the performance of a horizontal axis marine current turbine in both steady and unsteady flow conditions. To find the best practice for performance evaluation, an in-depth investigation on the various methods and their limitations and benefits was completed. This allows quantification of the parameters of importance relative to the environmental conditions at a deployment site. The two overarching research questions for this project were:

"How do flow conditions, such as shear inflow velocity, waves and submergence depth, and evaluation parameters, such as blockage and model scale, influence the performance of HAMCTs?"

"What are the best approaches to characterise the hydrodynamic performance of HAMCTs in steady and unsteady flow conditions?"

To address these questions, three methodologies including theory, scale model tests and CFD modelling were employed to assess the performance of the turbine. Based on the outcomes of this study, guiding principles are presented on how best to assess turbine performance. Conclusions about the hydrodynamic behaviour of the turbine in different flow conditions are also presented.

1.4. Description of Model Geometry

The experiments for this study consisted of tests on scale models in both the Towing Tank (TT) and Circulating Water Channel (CWC) of the Australian Maritime College (AMC), University of Tasmania. The physical turbine models were two-bladed rotors, which are $1/20^{th}$ and $1/32^{th}$ scale of the commercial-scale design of a HAMCT developed at the U.S. National Renewable Energy Laboratory (NREL). The rotors and hubs , made from 6061 T6 Aluminium alloy, were based on those designed at the United States Naval Academy [21], which have a NACA 63-618 model blade profile. Lift and drag coefficient data for this blade is available from Miley et al. [43] and X-Foil predictions [44]. The diameters of the two models were 500 mm and 800 mm. The lift and drag coefficients of the blades in the operating range should be Reynolds number independent to allow scaling of the model-scale results to full-scale. The Reynolds number independency of the lift and drag coefficient data at the operating Reynolds number was investigated by Walker et al [21]. The blade details are provided in Table 1.1; where *r* is local radius, *c* and *th* are local chord and local thickness of the blade, respectively and *R* is the overall blade radius. The rotors are shown in Fig. 1.2.

Fig. 1.2. Turbine models used in the experiments (top – 800 mm rotor, bottom – 500 mm rotor)

Table 1.1. Blade Geometry

Section	r/R	c/R	th/c (%)	Twist (deg)	Shape
1	0	0	100	12.9	circle
2	0.115	0.08	100	12.9	circle
3	0.175	0.117	62.9	12.9	ellipse
4	0.205	0.136	46	12.9	ellipse
5	0.243	0.161	29.8	12.9	ellipse
6	0.261	0.17	25.4	12.9	thick foil
7	0.299	0.165	21	11.5	thick foil
8	0.336	0.16	18.5	10.2	thick foil
9	0.355	0.158	18	9.5	foil
10	0.385	0.153	18	8.7	foil
11	0.445	0.145	18	7.4	foil
12	0.475	0.141	18	6.9	foil
13	0.505	0.137	18	6.5	foil
14	0.565	0.128	18	5.7	foil
15	0.595	0.124	18	5.4	foil
16	0.625	0.119	18	5.1	foil
17	0.685	0.11	18	4.5	foil
18	0.715	0.106	18	4.3	foil
19	0.745	0.101	18	4.0	foil
20	0.805	0.092	18	3.6	foil
21	0.835	0.087	18	3.4	foil
22	0.895	0.078	18	2.9	foil
23	0.925	0.073	18	2.7	foil
24	0.985	0.063	18	2.2	foil
25	1	0.06	18	2.1	foil

The experimental results provide a solid dataset, describing the hydrodynamic behaviour of the HAMCT. In addition, a key objective of this work was to validate the theoretical and numerical models. The experimental dataset together with data available in the literature were utilised for validation in this thesis. The CAD design of the turbine generated in Rhino modeller is shown in Fig. 1.3. The CAD model was identical to the physical scale turbine, which allows for validation of the CFD models.

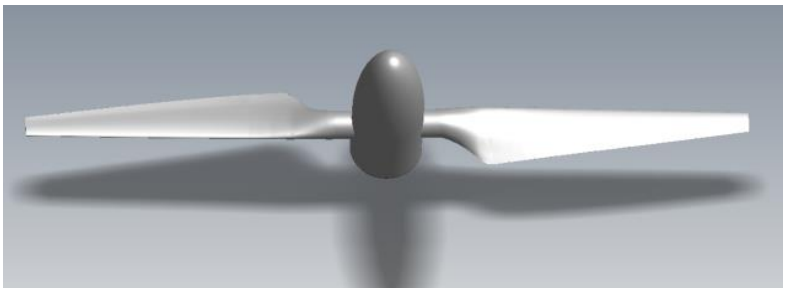

Fig. 1.3. Turbine CAD model

1.5. Novel Aspects

The contributions of this study are through the application of different methodologies in assessing the turbine hydrodynamic characteristics in conditions rarely studied. The novel aspects of this study are as follows:

Experimental investigation of scale effect by conducting tests on two physical model sizes of the turbine. Some previous works have studied the effect of scaling on wind turbines using numerical methods. Make and Vaz [45], Giahi and Dehkordi [46], in similar efforts, conducted some CFD simulations on the performance of wind turbines at model and full-scale Reynolds numbers conditions. There is a lack for experimental study of scale effect in the literature. This thesis is pioneering in evaluating the scale effect on marine turbines performance using experimental methods.

Evaluation of the facility bias effects on the turbine performance assessment by comparing towing tank and circulating water channel results. Despite recent research by Gaurier, et al. [30] which performed experiments on a tidal turbine model in two towing tanks and two circulating water tanks, a detailed study was needed on the parameters associated with facility bias, such as flow condition and blockage ratio.

Quantifying the effect of shear flow velocity on the turbine performance using experiments in the CWC and CFD simulations. Although there are some previous studies on the effect of shear velocity on wind turbines, such as Bardal, et al. [47] and Wagner, et al. [48], few studies have been performed on marine turbines, such as a numerical study by Tatum, et al. [41]. In a recent experimental effort, Forbush, et al. [49] developed a method to account for spatial and temporal velocity variations in performance assessment of a full-scale cross-flow hydrokinetic turbine in an intended river. However, providing a general approach to consider shear in the performance assessment of marine turbines was required.

A theoretical approach was employed to check the effect of Reynolds number and shear on the turbine by developing a BEM code and modelling the turbine in QBlade. Previous BEM studies on marine turbines were performed in steady condition of flow, such as [20]. In an effort by Koh and Ng [20], the effect of Reynolds number in BEM theory accuracy was investigated using lift and drag coefficients obtained from XFoil. This was performed using various blade pitch angles in one uniform flow velocity. In a work performed by Masters, et al. [50] modifications were made for non-uniform, three-dimensional analysis of horizontal axis

turbine using BEM. However, this thesis has employed various inflow velocities to see the effect of Reynolds number on BEM results in addition to the influence of sheared flow in BEM calculations.

The interaction of shear and waves on the hydrodynamic characteristics of the turbine was simulated using numerical modelling. There are some studies on wave effects on marine current turbines ([42, 51-53]) and recently an investigation was conducted by Tatum, et al. [41] on the turbine performance under the interaction of shear and waves using CFD modelling. A point of difference in this thesis is that two CFD models were evaluated to find the best approach to account for shear, surface proximity and wave. The model was validated against experimental results and then the impact of various waveforms and shear flow profiles were studied using the validated model. Finally, the interactive effect of submergence depth, shear and wave was investigated on the HAMCT performance.

A comparison presented, in this work, among the theoretical, numerical and experimental methods employed for the performance assessment of the HAMCT. The impacts of different parameters associated with an assessment approach or those involved in environmental condition were examined and recommendations were provided on how to deal with them. Although these methods are common practice among researchers, comparing all the methods for a turbine is rare.

1.6. Thesis Outline

This work, completed in a chapter structure, consists of introduction, scientific chapters and conclusion. The chapters follow the development of the methods employed for the performance evaluation of the turbine, including numerical, experimental and theoretical approaches, to study the effects of various operational parameters. The structure of the thesis is as follows:

Chapter 1: The introductory chapter defines the research problem, the research objectives and explains the geometric models employed in this research. The novel aspects of the work were presented with respect to other studies in this field.

Chapter 2: In this chapter, CFD approaches were compared and discussed to find an optimum numerical method for marine current turbine modelling. The influences of using these approaches on the numerical results were assessed against experimental results from the literature. The governing equations utilised for numerically modelling the turbine were defined

using incompressible Navier Stokes equations, continuity and momentum conservation. Then the CFD model setup, including geometry modelling, grid generation and solver setting in the ANSYS CFX were presented. Two turbulence models of k-ω SST and BSL EARSM were applied on the model. Steady state and transient solutions using moving reference frame (MRF) and sliding mesh method were compared. The effect of modelling a single blade instead of the whole turbine was evaluated. Three approaches of boundary layer modelling over the blade, including wall function, near wall method, and transitional gamma-theta model were studied. A grid sensitivity and a Y^+ study were implemented on the numerical models. Finally, the proposed CFD approach should be able to predict the hydrodynamic characteristics of different scales of the turbine.

Chapter 3: The third chapter presented the experimental approaches for the performance assessment of the turbine. The performance was characterised by testing two physical scale models. The experiments were implemented in the towing tank and the CWC of the AMC, enabling an investigation on the effect of facility bias. Blockage and flow velocity profile are the main differences between the two facilities. Moreover, the scale effect was studied by comparing the results from the two scale models. The independency of the results from Reynolds number was checked in order to predict the full-scale turbine performance.

Chapter 4: This chapter provides a comparison among the performance evaluation methods. To see the effect of Reynolds number in BEM prediction, the larger turbine was modelled in the QBlade, a BEM based software. To find the best BEM approach, the turbine performance results from the QBlade using lift and drag coefficients from local sectional Reynolds numbers were compared with the BEM model with a single reference Reynolds number. The BEM model was developed to model the turbine in the shear velocity profile of the CWC. The results from the theoretical models introduced in this chapter were compared with the experimental and the numerical models in the previous chapters, which would signify the advantages and limitations of each analysis method for HAMCT characterisations.

Chapter 5: In this chapter, the experiments on the 800 mm diameter scale model of the turbine in the CWC were presented for different depths and shear flow profiles. The CWC flow characteristics were measured using an acoustic Doppler velocimeter. Then an experimentally validated CFD model was developed to account for shear and surface waves. Results from the towing tank [54] and the CWC were utilised to validate CFD model for wave and shear respectively. Two numerical methods were compared in the CFD modelling to find the best

practice for performance evaluation of the turbine in presence of wave and shear flow profile. Finally, the hydrodynamic characteristics of the turbine under the influence of wave and shear were assessed using the validated CFD model.

Chapter 6: The concluding chapter of this work provides a summary of the project by presenting the key findings together with recommendations for future researchers in this field. It also discusses the implication of findings and limitations of the approaches employed to tackle the research objectives.

Chapter 2

Numerical Assessment of a Horizontal Axis Marine Current Turbine under Steady Flow Conditions

A refereed journal paper was published based on this Chapter in the International Journal of Marine Energy. The citation for this journal paper is:

Rahimian M, Walker J, Penesis I. Numerical assessment of a horizontal axis marine current turbine performance. *International Journal of Marine Energy*. 2017;20:151-64.

2.1. Introduction

Marine current turbines work on a similar basis to wind turbines. Therefore, a lot can be learnt from wind turbine studies to develop performance prediction methods for HAMCTs. Blade element momentum theory and the vortex element approach are two conventional methods for the performance evaluation of wind turbines, shown to be applicable to marine current turbines by many studies, such as Wu, et al. [55], and Baltazar and De Campos [56]. Despite helpful results from these two methods, an accurate performance prediction needs to consider the viscous effect on the turbine blades. Computational fluid dynamics (CFD) is an approach that can capture viscous flow. Although CFD may come with a great computation cost, the advantages of providing a better understanding of the flow field around the blade should not be neglected [33]. Thus, CFD is being utilised as a tool for complex flow studies [34]. In addition, CFD can also be employed to improve the design of a turbine in order to optimise the performance [35]. A detailed study was performed by Make and Vaz [45] to analyse the scaling effect on the performance of two well-known National Renewable Energy Laboratory (NREL) 5MW and MARIN Stock Wind Turbine (MSWT) wind turbines using Reynolds Averaged Navier-Stokes (RANS) simulation. Giahi and Dehkordi [46] also did a similar study on developing a RANS model to assess the effect of scaling on aerodynamic behaviour of an NREL 2MW wind turbine.

In recent decades, by increasing the power of computers, CFD has been used extensively as a viable tool to predict the hydrodynamics of marine current turbines. However, due to the vast variety of methods that can be employed for performance assessment, selecting an appropriate CFD approach is challenging. Xu [57] applied three methods of vortex lattice, boundary element method and a RANS solver to predict the performance of a HAMCT. Based on the developed RANS method, he proposed a design procedure and assessed the effect of non-uniform flow on the performance. Bai, et al. [36] employed an immersed boundary method to couple the simulation of a turbulent flow and the solid body of a three-bladed turbine using a 3D finite volume solver. Shi, et al. [58] used the viscous flow solver ANSYS CFX to predict the hydrodynamic characteristics of a HAMCT focusing on the impact of flow separation on turbine performance. A RANS model of a three-bladed HAMCT in unsteady flow was developed in STAR-CCM by Gunawan, et al. [59] using the rotating reference method with a k-ε turbulence model.

In this chapter, CFD approaches for marine turbine modelling from the literature were compared and discussed to find an optimum numerical model, compromising between accuracy and computational time. The impact of using these various approaches was assessed by comparing the numerical output with experimental results from the United States Naval Academy (USNA) [21]. Pointwise mesh software was employed for grid generation. The well-known solver ANSYS CFX was used to set up the simulations. Two turbulence models, k-ω SST and BSL EARSM, were applied to the model. Steady state and transient solutions using a moving reference frame (MRF) and a sliding mesh method were compared. The effect of modelling a single blade instead of the whole turbine was evaluated. Three approaches of boundary layer modelling over the blade, including wall function, near wall method, and transitional gamma-theta model were studied.

2.2. Problem Description

The main objective of this study was to propose a CFD model that can predict the performance of a two-bladed HAMCT in the fully submerged condition. It assumes that the effects of the free surface and the seabed are negligible. Some common approaches in CFD were utilised to generate the numerical models. The models were compared in terms of their assessment of the hydrodynamic performance of the turbine and their pros and cons were discussed. The proposed CFD approach should be able to predict the hydrodynamic characteristics of different scales of the turbine.

The turbine model was a $1/20^{th}$ scale of a two-bladed HAMCT based on a design developed at the US NREL. The blade profile was a NACA 63-618, with the lift and drag coefficients data available from 2D wind tunnel tests [21] and X-Foil predictions [44]. The lift and drag coefficients were Reynolds number independent for $Re_c > 5 \times 10^5$. Re_c is based on the chord length at 70% of the span. The diameter of the model was 800 mm. The blade geometry was detailed in Table 1.1 of Chapter 1. The hub had a diameter of 41 mm and a total length of 123 mm. The CAD design of the turbine was generated in Rhino modeller and is shown in Fig. 1.3 of Chapter 1. The CAD model was identical to the physical scale turbine from the literature, which allows for validation of the CFD results.

The hydrodynamic performance of a turbine with the radius of R (m) rotating at a rotational speed of ω (rad/s) in an inflow speed of U (m/s) is assessed based on power coefficient (C_P) and thrust coefficient (C_T) with respect to tip speed ratio (TSR), defined as follows:

$$TSR = \frac{\omega R}{U} \quad \textbf{(2-1)}$$

$$C_T = \frac{T}{0.5\rho\pi R^2 U^2} \quad \textbf{(2-2)}$$

$$C_P = \frac{Q\omega}{0.5\rho\pi R^2 U^3} \quad \textbf{(2-3)}$$

where Q and T are torque (N.m) and thrust (N), respectively and ρ is the water density (kg/m^3).

2.3. Governing Equations

To model the hydrodynamics of the turbine, the Reynolds-averaged Navier-Stokes (RANS) method was applied to solve the incompressible Navier-Stokes equations, continuity and momentum conservation, written in finite volume format as follows:

$$\frac{d}{dt}\int_V \rho dV + \int_S \rho u_i dn_i = 0 \quad \textbf{(2-4)}$$

$$\frac{d}{dt}\int_V \rho u_i d\forall + \int_S \rho u_i u_j dn_j = -\int_S P dn_j + \int_S (\tau_{ij} - \rho u_i' u_j')dn_j + \int_{\forall} S_M d\forall \quad \textbf{(2-5)}$$

where $\forall$ and S indicate integration regions of volume and surface respectively; and dn is the outward normal surface vector. u is velocity vector and indices i or j = 1, 2, 3 define the direction. p is pressure and S_M is a source term. If μ is dynamic viscosity, shear stress (τ_{ij}), is defined by:

$$\tau_{ij} = \mu\left(\frac{\partial u_i}{\partial x_j} + \frac{\partial u_j}{\partial x_i}\right) \quad \textbf{(2-6)}$$

The Reynolds stress term is $\rho u_i' u_j'$, determined by turbulence models. k-ω SST (shear stress transport) and BSL EARSM were the two models utilised in this study to predict the turbulent flow around the turbine blades.

The k-ω SST model is based on the k-ω model in the near wall region but utilised k-ε formulation in the far field. It considers the transport of the turbulence shear stress in calculations which helps to predict the flow separation over a surface as a result of an adverse

pressure gradient [60]. Because of these improvements it is commonly used in modelling of wind and marine turbines [33].

Baseline k-ω or BSL is another two equation model proposed by Menter [61] to resolve the k-ω model sensitivity to free stream condition. Explicit Algebraic Reynolds Stress Model (EARSM) is an extension to the BSL, which enables the turbulence model to capture the secondary flows as well as flows with streamline curvature and system rotation [62] [63]. Therefore, BSL EARSM is expected to predict the turbulent flow around a rotating turbine properly.

2.4. CFD Model

2.4.1. Geometry and Flow Domain

The first step in the CFD modelling was to produce an accurate geometry of the turbine and fluid domains. The 3D CAD model, by which the physical scale turbine was fabricated, was used for CFD simulation. Two cylindrical fluid domains were generated around the turbine to have one stationary and one rotating domain. In addition, given the periodic condition of the turbine geometry, the turbine together with the two domains was halved, which reduces the number of grids and consequently the computational time of the simulations. This model is referred to as the half turbine in this Chapter. The influence of using one blade instead of the whole turbine in simulations was evaluated in this study. For transient solutions with the sliding mesh method the whole turbine must be modelled. Thus, the steady state solution was used for comparison between the half and the whole turbine.

2.4.2. Grid Generation

A hybrid mesh was generated by Pointwise software, discretising the fluid domains and the turbine surfaces. The grids over the blade surface were structured. Higher grid resolution close to the leading and trailing edges, the kink and the tip of the blade was considered to properly discretise the curves of the blade. For the other regions including the fluid domains, the blade tip and hub surfaces, an unstructured mesh was produced, see Fig. 2.1. The total number of grids, including hexahedral, tetrahedral and prismatic elements, was approximately 8 million for the whole turbine model. The number of prismatic inflation layers and the growth rate over the blade covering the boundary layers varied depending on the required Y^+. The average Y^+ over the blade surface monitored during the simulation at TSR ~ 6 was chosen as the reference

for presenting Y^+ in this Chapter. Y^+ is the non-dimensional wall distance which determines the level of grid refinement. It is defined by the wall friction velocity, $u_\tau = \sqrt{\tau/\rho}$, and fluid kinematic viscosity, ν, as follows:

$$Y^+ = \frac{u_\tau y_w}{\nu} \qquad \textbf{(2-7)}$$

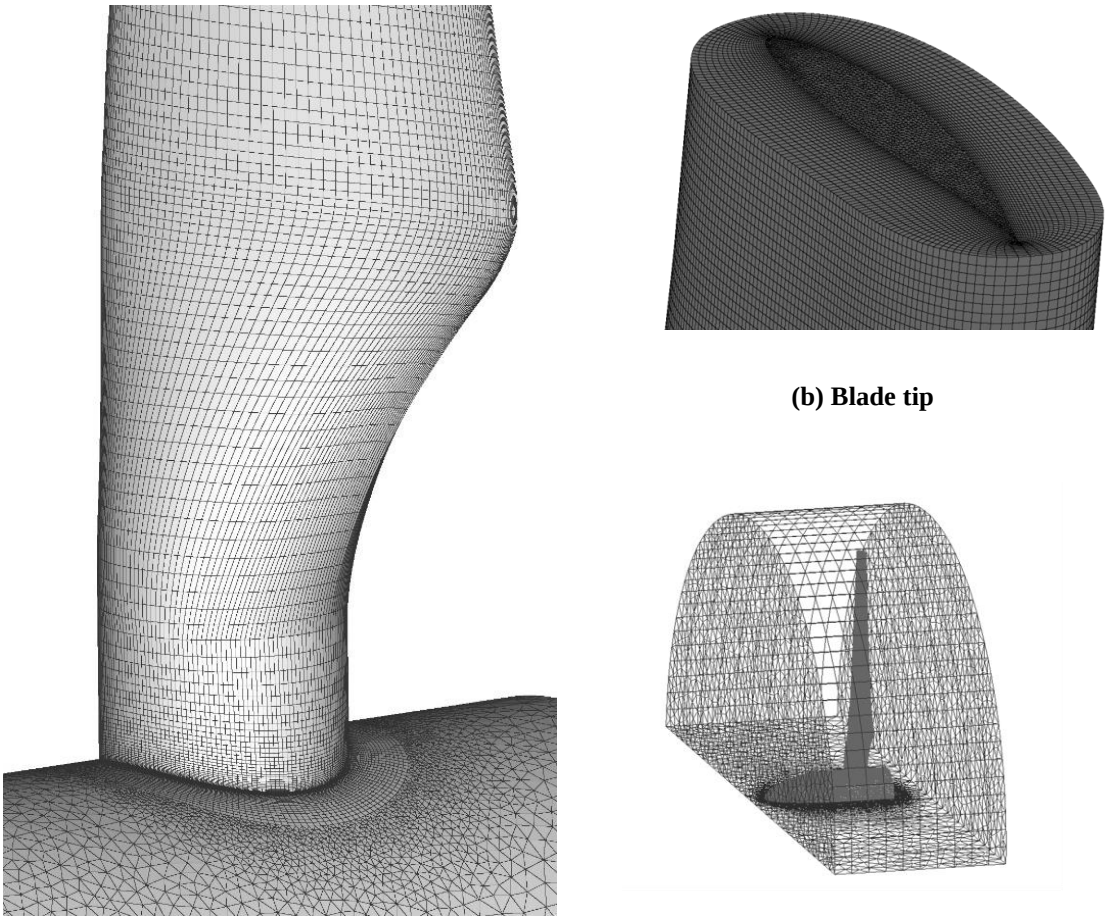

(a) Blade root and hub

(b) Blade tip

(c) Inner domain

Fig. 2.1. Hybrid grid generated over the turbine and flow domains for the numerical model

A Y^+ in the order of 1 should be considered for the model to accurately capture the turbulent flow over the blade surfaces for the numerical models using a "viscous sub-layer modelling" approach [33]. This method is also known as "near-wall modelling". On the other hand, a Y^+ less than 300 is recommended when a wall function applies in the turbulence model [64]. Calculating the Reynolds number for the operating point of the scale model reveals that the

blades are mostly operating in the transitional flow condition. Hence, the effect of the transition model was also checked by adding the Gamma-Theta formulation to the *k-ω* SST turbulence model. Overall, the influence of turbulence model and boundary layer model were evaluated by using four different models as follows:

- Fully turbulent *k-ω* SST with near wall method, provided by $Y^+ \sim 1$
- Fully turbulent *k-ω* SST with wall function, provided by $Y^+ \sim 30$
- Transitional *k-ω* SST with near wall method, using $Y^+ \sim 1$ and the Gamma-Theta transition model
- BSL EARSM turbulence model with wall function, provided by $Y^+ \sim 30$

All of the above simulations were performed on a same mesh, where only the grid resolution close to the wall has changed according to the required Y^+, which had insignificant effect on the total number of grids.

2.4.3. Solver Setup

Ansys CFX R15.0 was utilised to set up the solver. It uses a conservative element-based finite volume method to solve the RANS model [65]. Fig. 2.2 shows the domains together with the boundaries of the half turbine model. The condition of the boundaries, domains and interfaces were detailed in Table 2.1. A normal velocity of 2 m/s with a turbulence intensity of 1% was set at the inlet. A zero relative pressure was considered for both the outlet and the opening. The surfaces of the blade and the hub were specified as no slip walls. The inner domain has a general grid interface with the outer domain. A rotational periodicity condition was applied on the bottom faces of the two domains for half turbine model.

A moving reference frame (MRF) was described using a “frozen rotor” in ANSYS CFX to simulate the rotation of the turbine in the steady state solution. In the MRF method, the fluid around the blade in the inner domain was set as a MRF, while the blade and hub were stationary relative to the inner fluid. Thus, a solution was achieved without moving the grids during the numerical solution. The induced acceleration of the fluid was added to the momentum equation as an extra source term. The MRF approach was performed for the transient solution as well to see the difference between the results of CFD for the two solution methods.

Table 2.1: CFD setup

Boundary	Condition
Inlet	Uniform flow of 2 m/s normal to inlet
Outlet	Relative Pressure = 0 Pa
Opening	Relative Pressure = 0 Pa
Blade	No Slip Wall
Hub	No Slip Wall
Domain	**Condition**
Inner Domain	Fluid (Rotating)
Outer Domain	Fluid (Stationary)
Interface	**Condition**
Bottom Interfaces	Rotational Periodicity
Domains Interfaces	General Grid Interface (GGI)

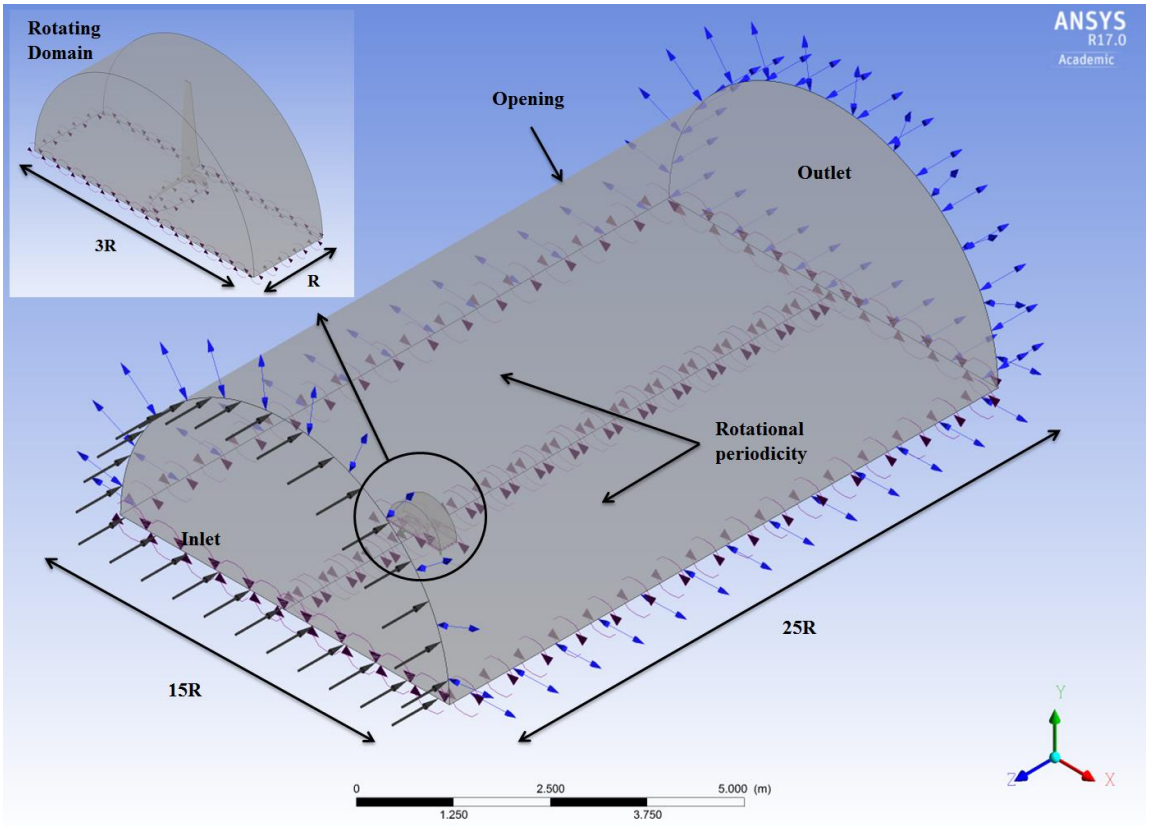

Fig. 2.2. Boundary conditions of the domains around the half turbine model

A sliding mesh method was performed to model the rotation of the rotor for the transient solution of the whole turbine model. The transient rotor stator condition was set for the interface between the two domains in the ANSYS CFX. The inner domain rotated at each time step for a certain amount based on the rotational speed set for the rotor. Thus, the boundary cells of the two domains slid relative to each other. The sliding mesh was the most similar technique to the

real situation when modelling the flow in rotating cases; but unlike MRF, it is computationally demanding [66]. The result from the steady solution was set as an initial condition for the transient rotor stator solution to help with convergence achievement in less computational time.

ANSYS CFX uses a pressure-velocity coupled method proposed by Rhie [67] to discretise the governing equations. The high resolution scheme was chosen for discretising the advection term as well as for the turbulent viscosity. In the transient rotor stator solutions, the second order backward Euler scheme was used for the transient scheme.

In addition to the model scale, the CFD model of the full-scale turbine was generated to provide a better understanding of the scale effect as well as an estimate of the full-scale performance.

2.4.4. Solution

Torque and thrust together with power and thrust coefficients were monitored during the solution iterations and used as criteria for solution convergence. The judgement of solution convergence was achievement of less than 2% deviation of torque and thrust values over at least 200 iterations. Given the higher unsteadiness for higher TSRs, for convergence achievement in the steady condition, a number of iterations from 1500 for TSR ~ 4 to 5000 for TSR ~ 9 were required.

The efficiency of the CFD models used for performance evaluation of the HAMCTs was presented in Table 2.2 and Table 2.3, for the steady and transient solutions, respectively. The tables outline the wall clock time required to achieve simulation convergence at TSR ~ 6. All of the simulations were done on 32 cores of a high performance computing cluster with 16 GB RAM. Total time of 3 rotations was enough to achieve convergence for the transient rotor-stator solution using a time step corresponding to 1^{o} of rotation. The transient time step was defined as:

$$dt = \frac{2\pi}{\omega \times 360} \qquad \textbf{(2-8)}$$

The solution time for the transient sliding mesh, in Table 2.3, was high because of the need to have a steady MRF result as the initial condition, which leads to a longer computational time. The transient MRF simulation was run by setting the total time to 20 s and time step to 0.01s.

All the simulations were performed in double precision in order to have infinitesimal round-off error due to the computers precision. The number of cells for the whole turbine model was 6.1 million, which was approximately halved for the half turbine model. The effect of changing Y^+ on the number mesh was insignificant. The residual of the momentum equation in the streamwise direction for the steady and transient solutions was presented in Table 2.2 and Table 2.3, respectively. The lower residual represents a lower truncation error, which means higher accuracy of the converged results.

Table 2.2: Simulation time and momentum residual in steady state solutions at TSR ~ 6

CFD model	Whole turbine				Half turbine	
	SST-wall function (Y^+ ~ 30)	SST-near wall (Y^+ ~ 1)	SST-transition (Y^+ ~ 1)	BSL EARSM (Y^+ ~ 30)	SST (Y^+ ~ 30)	BSL EARSM (Y^+ ~ 30)
Time (minutes)	724	1052	883	620	380	350
Residual	8.0e-05	2.2e-04	3.0e-04	8.8e-05	8.9e-05	1.0e-04

Table 2.3: Simulation time and momentum residual in transient solutions at TSR ~ 6

CFD model	Sliding Mesh - Whole turbine		MRF - SST	
	SST	BSL-EARSM	Half turbine	Whole turbine
Time (minutes)	2500	2420	1477	1500
Residual	2.0e-07	1.7e-05	8.9e-08	7.0e-07

2.4.5. Grid Sensitivity

Grid sensitivity was estimated by the grid convergence index (GCI), which is actually a measure of the discretisation error. For this purpose, three different meshes were generated over the half turbine model by changing the grid resolution over the blade surfaces and in the regions closer to the turbine. A factor of grid refinement greater than 1.3 was considered for generating the meshes. The cell numbers for these three meshes were 2.15 million (coarse), 3.01 million (medium) and 4.36 million (fine). The GCI calculation in this Chapter was performed based on the method proposed by Slater [68]. The first step to find the GCI was to define a representative cell size:

$$h = \left(\frac{1}{N} \sum_{i=1}^{N} (\Delta \forall_i) \right)^{1/3} \quad \textbf{(2-9)}$$

where N is the total number of cells and $\Delta\forall_i$ is the volume of the ith cell. Then the grid refinement factor $rf = h_{coarse}/h_{fine}$ was calculated; e.g. $rf_{21} = h_2/h_1$. A key variable ϕ important to the study objectives, torque in this study, was selected for error calculation. In turn, the apparent order p_e was computed using:

$$p_e = \frac{1}{\ln(r_{21})}\left|\ln\left|\varepsilon_{32}/\varepsilon_{21}\right| + q(p_e)\right| \quad \textbf{(2-10)}$$

$$q(p_e) = \ln\left(\frac{rf_{21}^{p_e} - s}{rf_{32}^{p_e} - s}\right) \quad \textbf{(2-11)}$$

where $\varepsilon_{21} = \phi_2 - \phi_1$, $\varepsilon_{32} = \phi_3 - \phi_2$ and s is the sign of $\varepsilon_{32}/\varepsilon_{21}$. If the relative error of the torque is

$$e_{21} = \left|\frac{\phi_1 - \phi_2}{\phi_1}\right|, \quad \textbf{(2-12)}$$

Finally, GCI is obtained for the fine mesh by

$$GCI_{21} = \frac{1.25e_{21}}{rf_{21}^{p_e} - 1} \quad \textbf{(2-13)}$$

Table 2.4 summarises a sample of the GCI calculation performed for the three selected meshes. It can be seen that the fine-grid convergence index is about 2%. In addition to the GCI calculation, the grid independency of the CFD solutions was conducted on the MRF steady technique over the different mesh resolutions. Fig. 2.3 illustrates the grid independency of the steady solution for torque at TSR ~ 6 by showing the torque difference relative to the torque value of the USNA results, which means $|Q-Q_{USNA}|/Q_{USNA}$. It signifies that the results are grid independent for a cell number higher than 4 million.

2.4.6. Y^+ Study

Fig. 2.4 shows the effect of Y^+ on the torque values relative to the experimental value. Changing the Y^+ was important in terms of accounting for the viscous effect near the walls. Both the turbulence models used in this study were embedded with an automatic wall function in ANSYS CFX R15.0. In the case of using $Y^+ \sim 1$, the near wall method was applied to the turbulence model. Having a $Y^+ \geq 20$ activated the wall function method in the turbulence model. Although the higher Y^+ results in less mesh density and consequently less computational time, the relative difference of the torque increases for $Y^+ \geq 30$. Provided the

mesh independency condition was met, comparing the simulations with different Y^+ resulted in an optimal $Y^+ \sim 30$. Later in this Chapter, this conclusion based on the correlation with the experiments will be discussed further.

Table 2.4: Sample Calculation of Grid Convergence Index for Numerical Models

Parameter	Value
N_1, N_2, N_3	4.36, 3.05, 2.15 million
h_1, h_2, h_3	3.2, 4.6, 6.5 x 10^{-5}
ϕ_1, ϕ_2, ϕ_3	29.1, 28.7, 28.5 Nm
rf_{21}, rf_{32}	1.43, 1.41
p_e	1.74
e_{21}, e_{32}	1.37%, 0.69%
GCI_{21}, GCI_{32}	1.98%, 1.04%

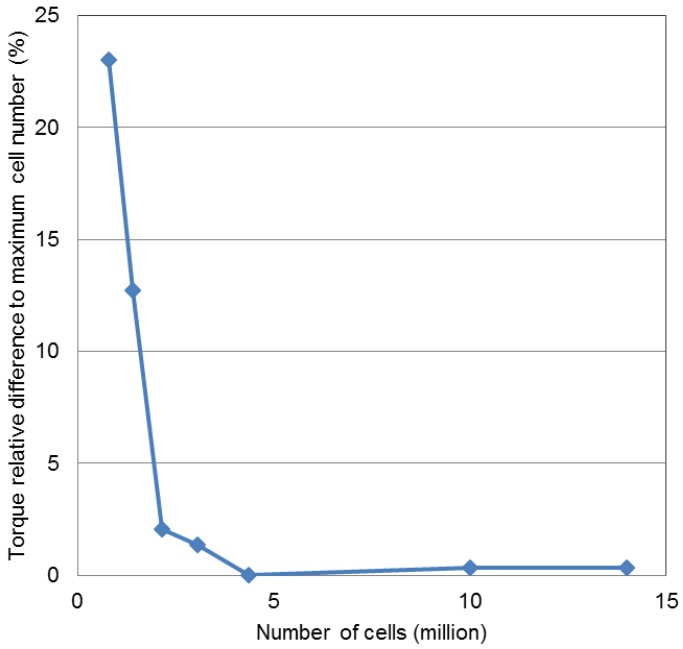

Fig. 2.3. Grid independency for the half turbine in the steady state solution

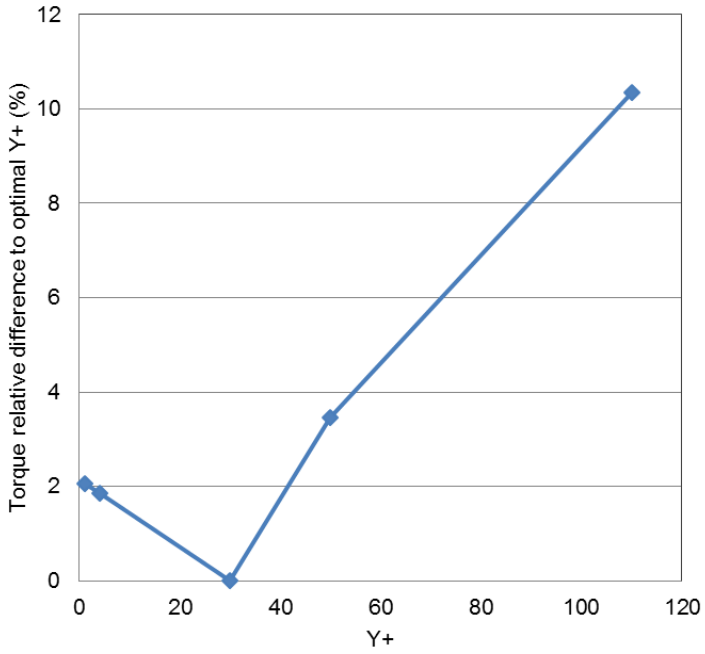

Fig. 2.4. Effect of different Y$^+$s on the torque outputs of the CFD models

2.5. Results and Discussion

Different output parameters, including velocity, turbulence kinetic energy, eddy viscosity and pressure obtained from transient MRF solution of the whole turbine model at TSR 6 using SST turbulence model with wall function are depicted over the planes passing through the turbine centre in Fig. 2.5 to Fig. 2.8.

2.5.1. Validation of Numerical Models with Experimental Results

The CFD computations was validated using experimental results from the USNA towing tank [21]. The USNA towing tank is 116 m long, 7.9 m wide and 4.9 m deep. The ratio of the rotor area to the tank cross-sectional area is small enough to have negligible blockage effect. The power and thrust coefficients with respect to tip speed ratio are plotted in Fig. 2.9 and Fig. 2.10 respectively, for the steady state CFD models using the MRF technique together with the towing tank results. Generally, it can be seen that both the C_T and C_P curves show reasonable agreement with the USNA curves, which validates the CFD models. Although all the C_T curves collapse on the experimental curve, there are some discrepancies in the C_P curves. Among all the power coefficient curves, the whole turbine model using the k-ω SST turbulence model has the best correlation with the experiments.

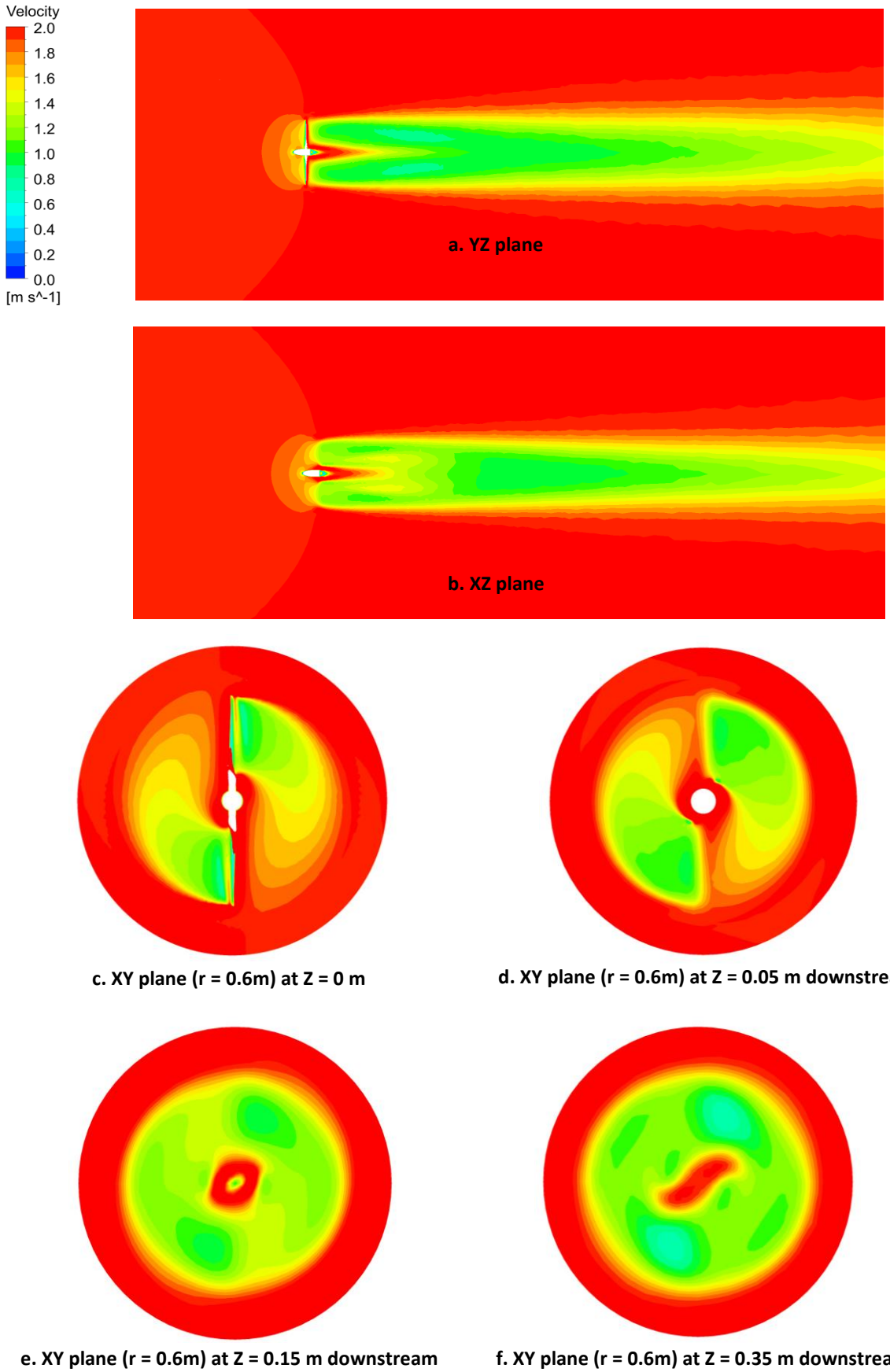

Fig. 2.5. Velocity distribution over the turbine planes for transient MRF simulation at TSR = 6 and inflow velocity of 2 m/s using SST turbulence model and wall function

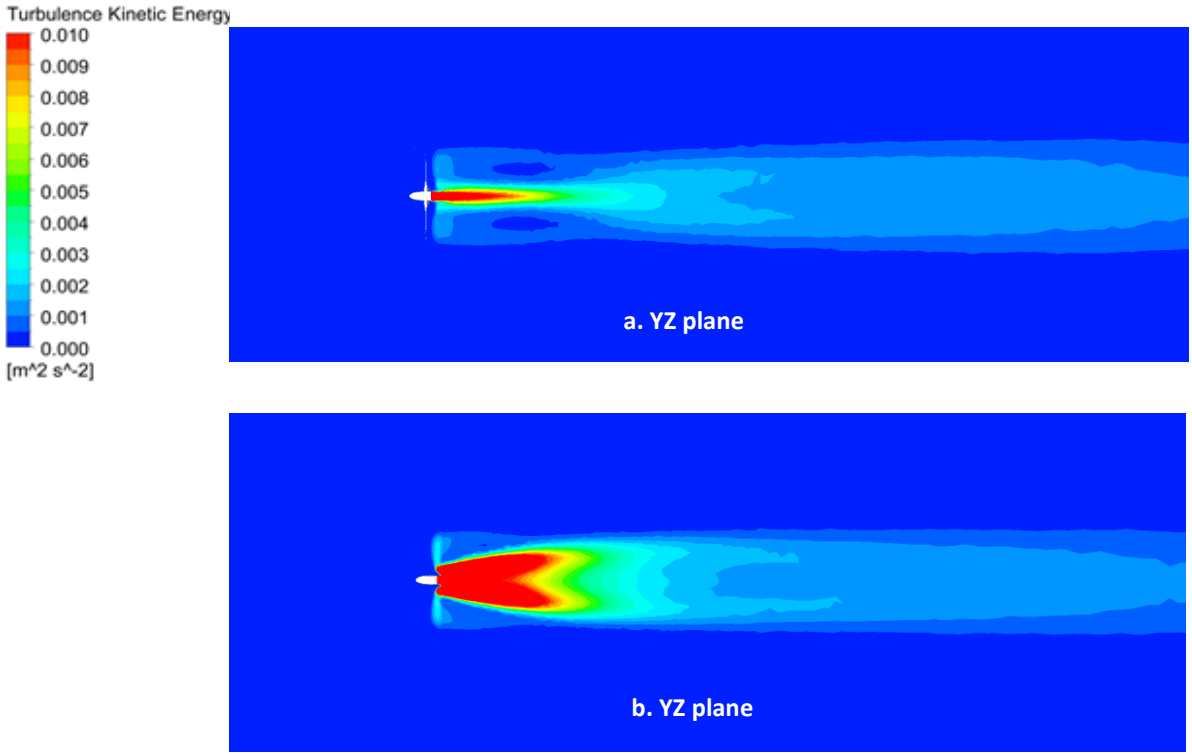

c. XY plane (r = 0.6m) at Z = 0 m downstream

d. XY plane (r = 0.6m) at Z = 0.05 m downstream

e. XY plane (r = 0.6m) at Z = 0.15 m downstream

f. XY plane (r = 0.6m) at Z = 0.35 m downstream

Fig. 2.6. Distribution of turbulence kinetic energy over the turbine planes for transient MRF simulation at TSR = 6 and inflow velocity of 2 m/s using SST turbulence model and wall function

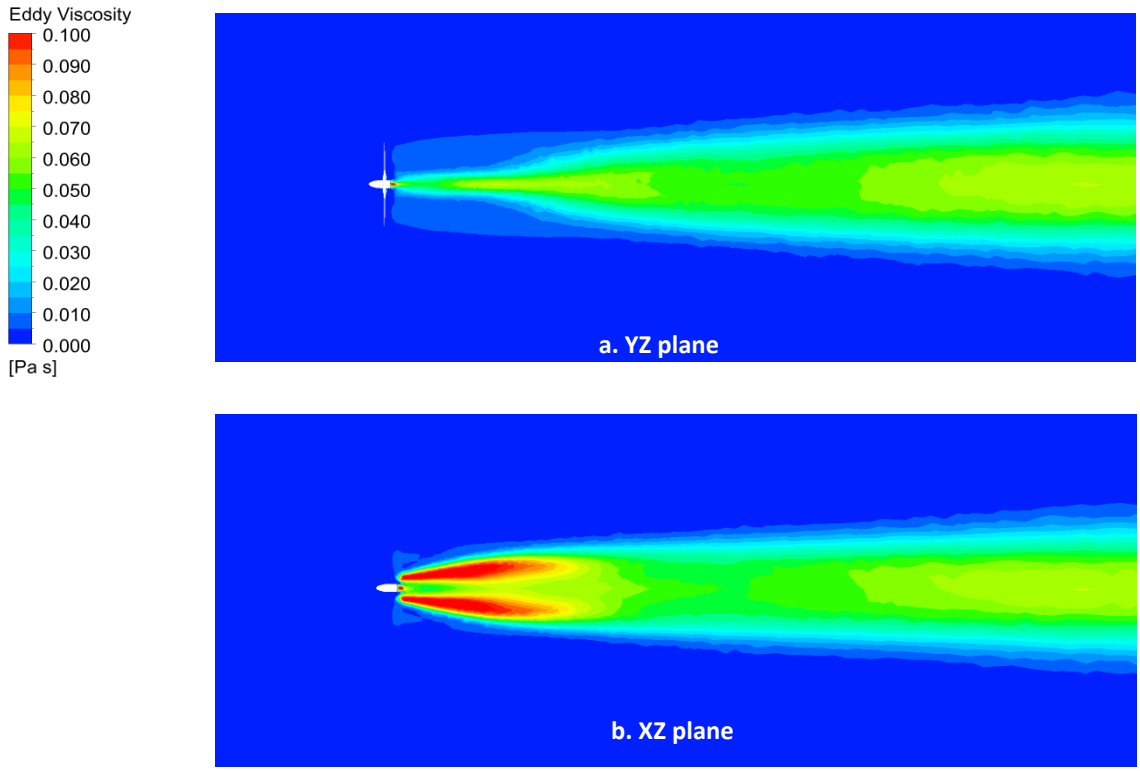

c. XY plane (r = 0.6m) at Z = 0 m

d. XY plane (r = 0.6m) at Z = 0.05 m downstream

e. XY plane (r = 0.6m) at Z = 0.15 m downstream

f. XY plane (r = 0.6m) at Z = 0.35 m downstream

Fig. 2.7. Eddy viscosity distribution over the turbine planes for transient MRF simulation at TSR = 6 and inflow velocity of 2 m/s using SST turbulence model and wall function

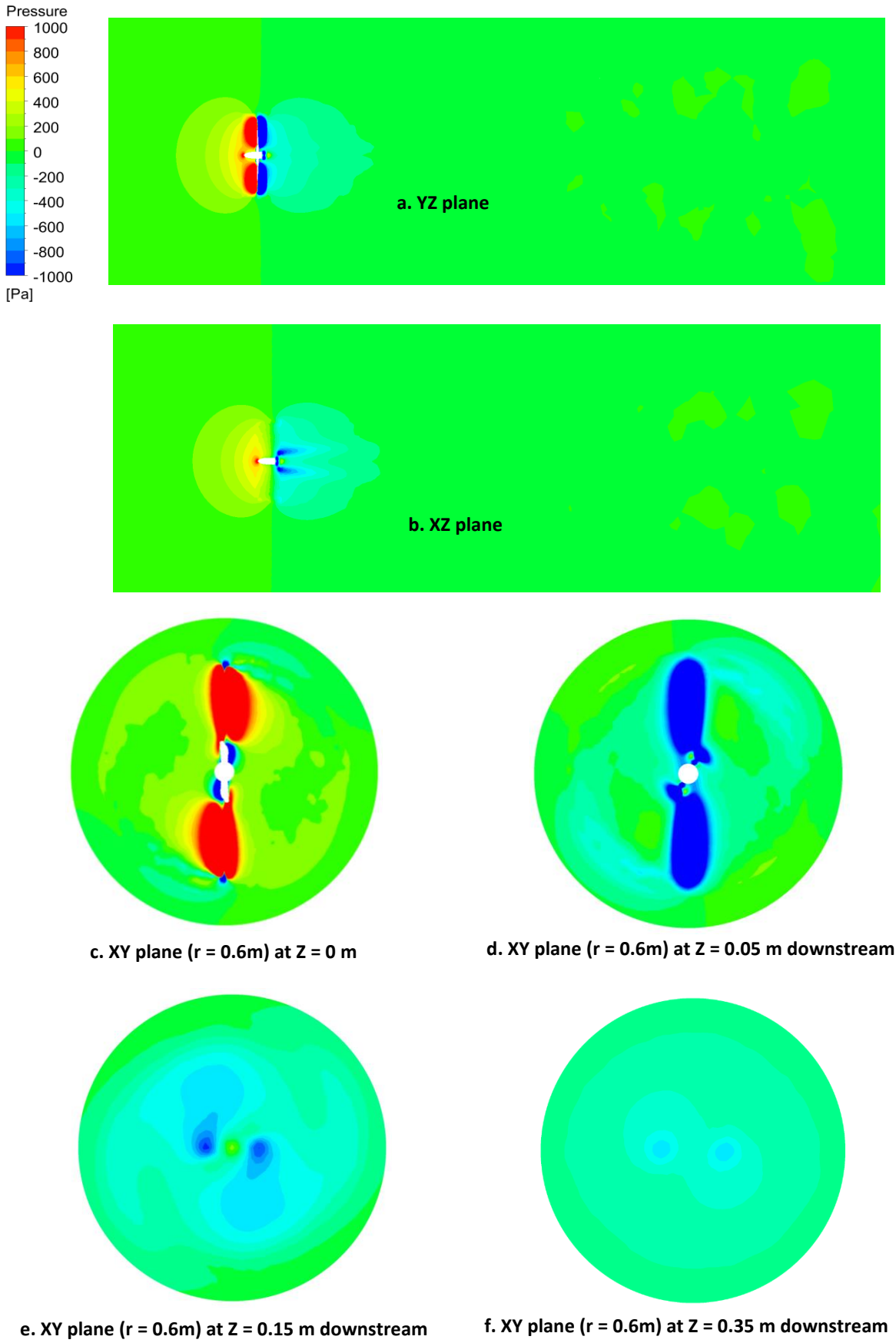

Fig. 2.8. Pressure distribution over the turbine planes for transient MRF simulation at TSR = 6 and inflow velocity of 2 m/s using SST turbulence model and wall function

The agreement between the experimental results and the numerical models validates the employed numerical methodology, including the grid generation approach and the selected turbulence model and solver setup, for the performance evaluation of HAMCTs.

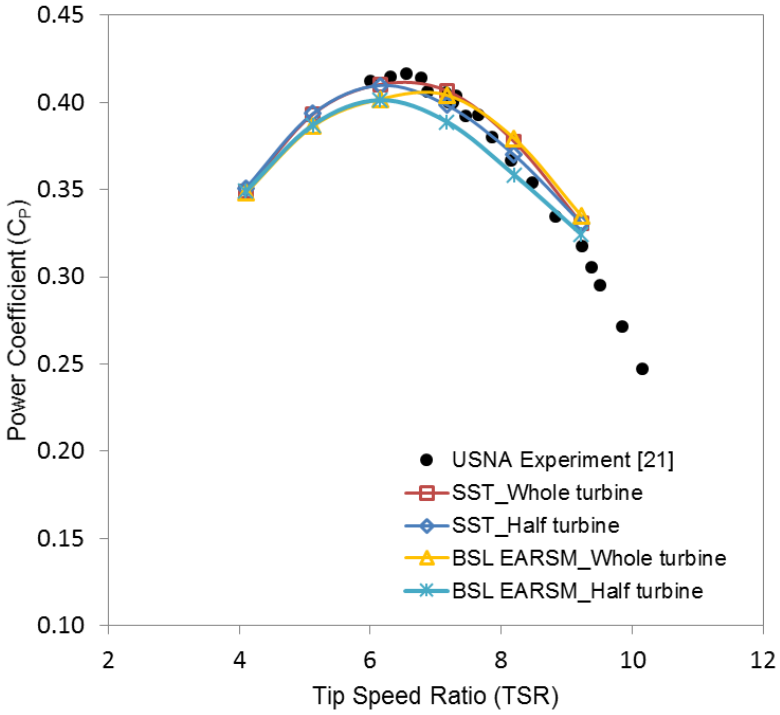

Fig. 2.9. Comparison of power coefficient curves between CFD models and USNA experimental results

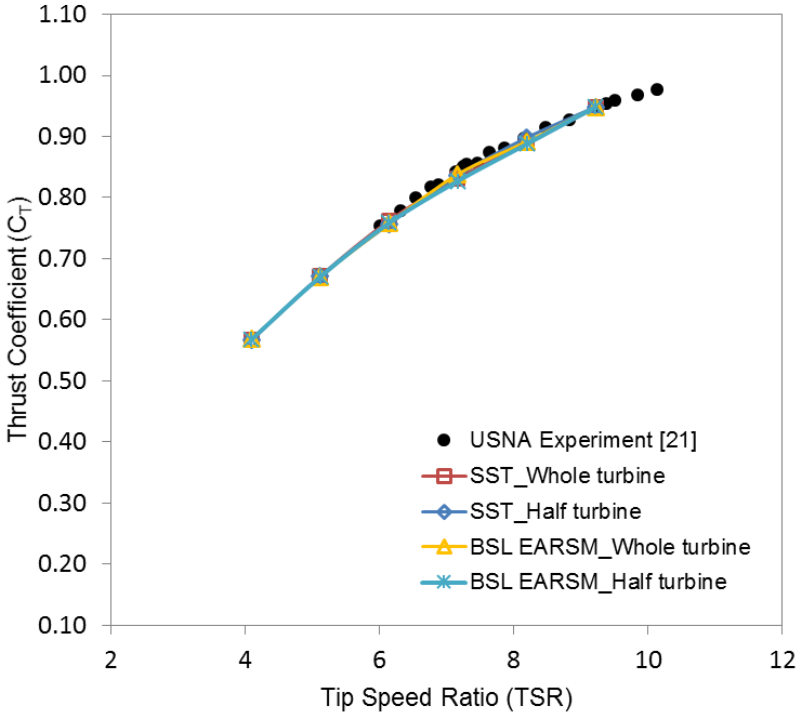

Fig. 2.10. Comparison of thrust coefficient curves between CFD models and USNA experimental results

2.5.2. Reynolds Number and Scale Effects

The pressure distributions together with the limiting streamlines on the suction side of the blade in the transient rotor stator solutions using the *k-ω* SST are depicted in Fig. 2.11. It can be seen that low pressure occurs mainly in the tip area near the leading edge, which is extended by increasing the TSR; see Fig. 2.11 (a) to (c). Comparing the contours for the scale model and the full-scale turbine at TSR ~ 6, Fig. 2.11 (b) and (d) respectively, shows a similar pressure distribution for the blades; i.e. they should have similar C_P and C_T, considering the scale/Reynolds effects between the two models.

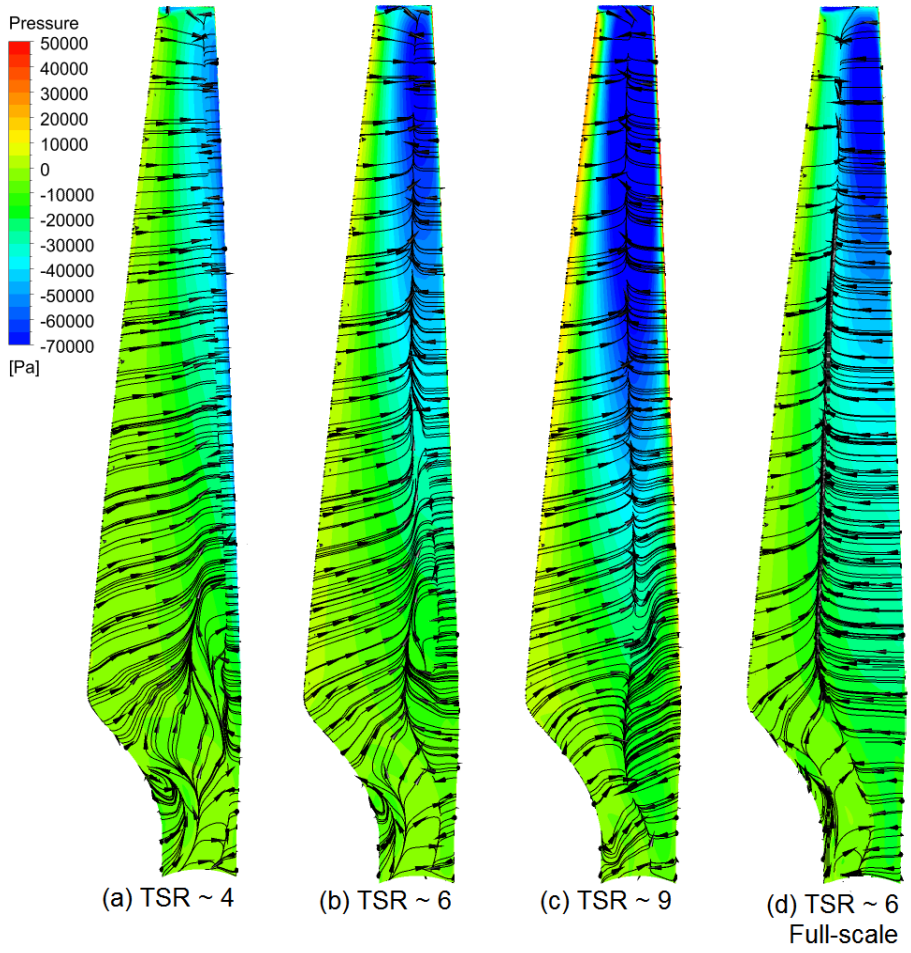

Fig. 2.11. Pressure distribution and limiting streamlines over the suction side of the blade

The limiting streamlines over the blade (Fig. 2.11) illustrate that the stagnation point, where separation occurs due to adverse pressure gradients, is closer to the leading edge for TSR ~ 4, especially in the tip area. However, by increasing the TSR which leads to a higher relative flow velocity over the blade and consequently higher Re and lower angles of attack, the separation line moves further from the leading edge in the chord wise direction. The limiting streamlines

of the full-scale blade (see Fig. 2.11 (d)), show that the flow is attached for approximately 2/3 of the blade area, due to being fully turbulent $Re_c \sim 7.4 \times 10^6$, and the separation line is closer to the trailing edge. The separation line over the entire blade span shows that the blade is working in the stall condition [69]. The separation line closer to the leading edge indicates a larger angle of attack as well as a higher pressure difference between the two sides of the blade; hence increased drag and reduced lift [70]. The pressure distribution over the blade was also depicted in the Fig. 2.11. As can be seen low pressure area is located closer to the tip over the suction side of the blade which grows larger by increasing TSR.

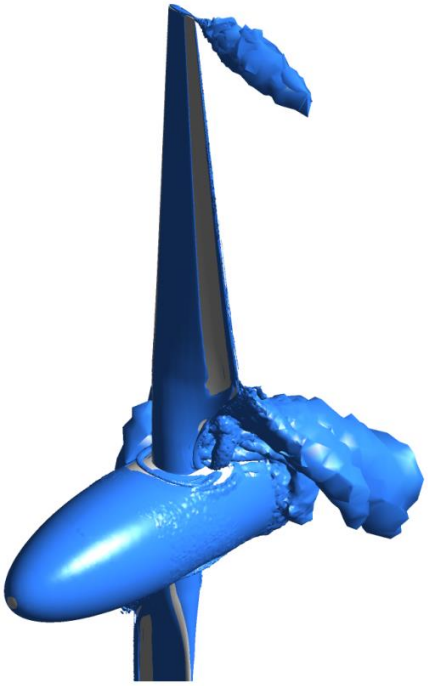

Fig. 2.12. Unsteady flow around the blade using Q-criterion of 0.004 for transient MRF simulation at TSR = 6 and inflow velocity of 2 m/s using SST turbulence model and wall function

A source of unsteadiness around the blade was the root sections with an annular shape near the hub similar to one reported by Otto, et al. [71]. Unsteady flow was shown by an iso-surface using the Q-criterion of 0.004 in Fig. 2.12 for transient MRF simulation at TSR = 6 and inflow velocity of 2 m/s using SST turbulence model and wall function. Tip vortex shedding was also seen near the tip region, which leads to tip power loss of the turbine [72].

The pressure difference between the two sides of the blade accounts for lift, and hence torque, generation [35]. The pressure coefficient, which is the ratio of the static pressure over the dynamic pressure, is plotted in Fig. 2.13 for r/R = 0.9, close to the tip, and r/R = 0.4, near

the root. It can be inferred that the pressure difference was reduced between the two sides of the blade by increasing the TSR. Thus, lift and torque are smaller for higher TSRs.

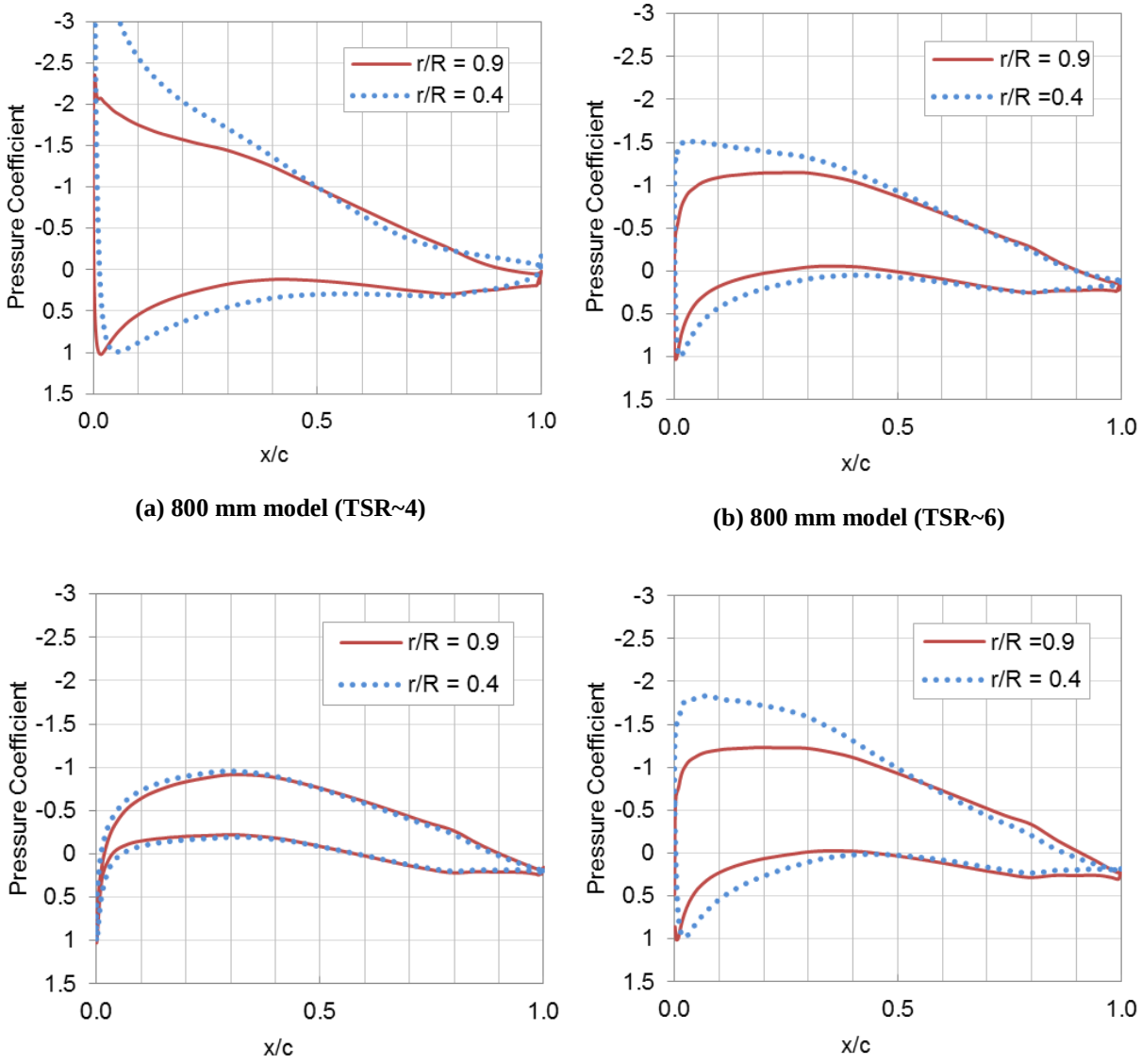

(a) 800 mm model (TSR~4)

(b) 800 mm model (TSR~6)

(c) 800 mm model (TSR ~ 9)

(d) Full scale (TSR ~ 6)

Fig. 2.13. Pressure coefficient over the blade surface at two radial cross sections for an inflow speed of 2 m/s at different TSRs

Comparing the pressure coefficients drawn for the two blade sections in Fig. 2.13 shows that the pressure difference is lower for larger radius of the blade at all TSRs. It means that a higher amount of lift is generated by blade sections with lower radii. However, torque and power induced from lift also depends on incorporated distance from the centre of rotation. Calculating torque and power on regions along the blade span showed that areas closer to the tip generate more torque and power than the areas near the root. The pressure coefficients at r/R = 0.7 for different TSRs of the 800 mm model as well as full-scale turbine at TSR ~ 6 are

shown in Fig. 2.14. This section showed to have the highest contribution in generating torque and power among all blade radii. This graph confirms the reduction of pressure difference by increasing the TSR. Moreover, as it can be seen there is little difference between the pressure coefficient of the full-scale turbine and the scale model. Thus, the scale effect is negligible when the operating condition of the scale model is Reynolds number independent. It can be concluded that the results from the scale model can be used for predicting the full-scale turbine performance.

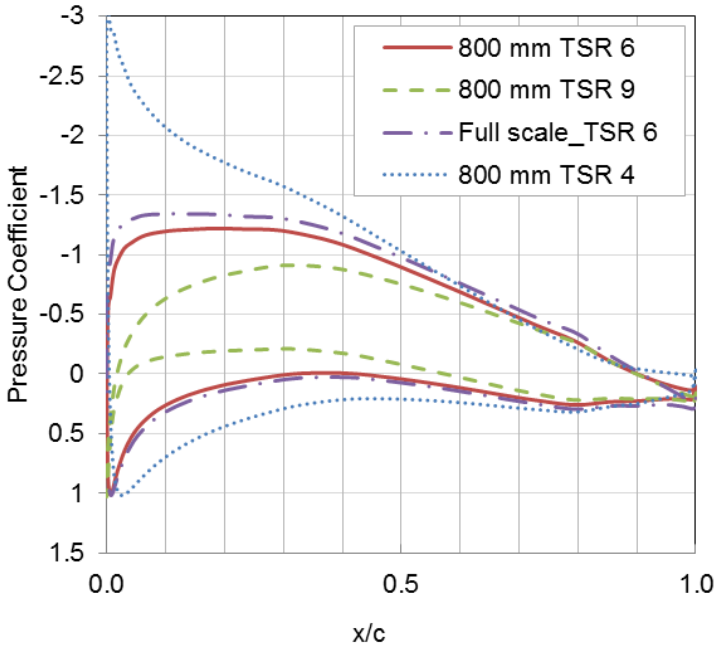

Fig. 2.14. Pressure coefficient at r/R = 0.7 for different TSRs of the scale model and full-scale turbine

2.5.3. Effect of Chosen Turbulence Model

A comparison was made between the steady state results from the *k-ω* SST and the BSL EARSM models to investigate the influence of chosen turbulence model on the performance of the turbine, shown in Fig. 2.9. Since the results for the two turbulence models were available for both the whole turbine and the half turbine models, it was also possible to study the effect of selecting the half or whole turbine.

Generally, all of the CFD curves showed good agreement with the experimental data. The discrepancy among the CFD curves increased for TSR > 5 and then decreased at TSR ~ 9. The CFD results for the whole turbine model with BSL EARSM had a maximum C_P at a TSR ~ 7; while the other CFD models had maximum C_P at TSR ~ 6.5, showing better agreement with the experimental data. Comparing the C_P curves of the two turbulence models for the half

turbine revealed that the BSL EARSM had lower values, while the *k-ω* SST had better agreement with the experimental results. Thus, *k-ω* SST is recommended to be used as the turbulence model for turbine performance evaluation. According to the Table 2.2 and Table 2.3, the residual of the *k-ω* SST in the transient solution is less than the residual for the BSL EARSM; however, the opposite is true for the steady MRF simulations, whilst the simulation time is similar for the two turbulence models. Overall, *k-ω* SST is recommended to be used as the turbulence model for the turbine performance evaluation.

2.5.4. Effect of Chosen Boundary Layer Model

The influence of the chosen boundary layer model was studied using three boundary layer techniques of near wall, wall function and transition Gamma-Theta models using the *k-ω* SST turbulence model for the steady state solution of the whole turbine. Fig. 2.15 compares the C_P curves obtained from simulations conducted using these three approaches with the experimental results. It can be seen that the near wall technique underestimated the power coefficients for the entire range of TSRs. On the other hand, the results from the wall function approach showed good agreement with the experimental data. Given the chord based Reynolds number ranges in which the turbine blade is operating, it could be expected that the transitional turbulence model should have results that are more accurate. However, compared to the fully turbulent near wall model, the transitional model using the Gamma-Theta formulation overestimated the C_P values.

It should be noted that simulations with the transitional boundary layer model as well as the near wall method did not converge based on less than 2% deviation criterion even after 5000 iterations. However, the results are presented in this study, considering higher errors, because the fluctuations were within 5% deviation. It can be seen in Table 2.3 that the residual for these two models are larger than the wall function, showing higher truncation error in the results. In addition, compared to the other two boundary layer models, the wall function is computationally less expensive. Overall, the wall function model is recommended for HAMCT studies.

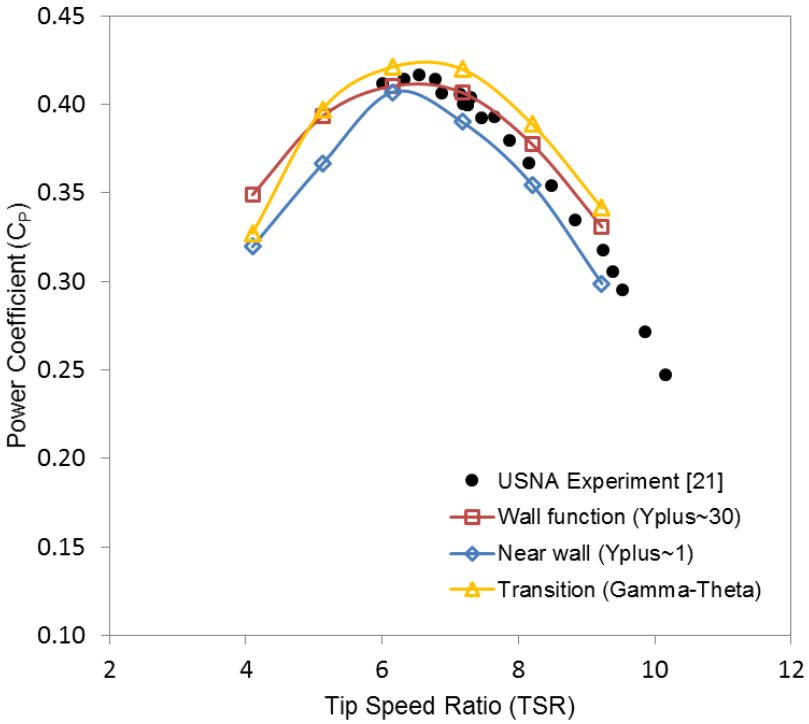

Fig. 2.15. Comparison of C_P curves from CFD simulations with different boundary layer models

2.5.1. Evaluation of Transient vs Steady State Solutions

Fig. 2.16 shows the effect of using a moving reference frame (MRF) or sliding mesh for simulating the rotation as well as the influence of using a steady state or transient solution. Simulations were performed on the whole turbine using the k-ω SST turbulence model. Generally, all three CFD models predicted the power coefficient of the turbine for the entire range of the TSRs. The curves of the transient MRF and the steady state MRF coincide. Thus for a moving reference frame model, the selection of a steady state or transient model provides the same results. Based on Table 2.2 and Table 2.3, the transient solutions have much lower residuals than the steady state solutions, indicating the higher accuracy of the transient solution than the steady state solution. However, the steady state solution is computationally less expensive. Therefore, the steady state solution is recommended for assessing the hydrodynamics of HAMCTs in steady flow conditions.

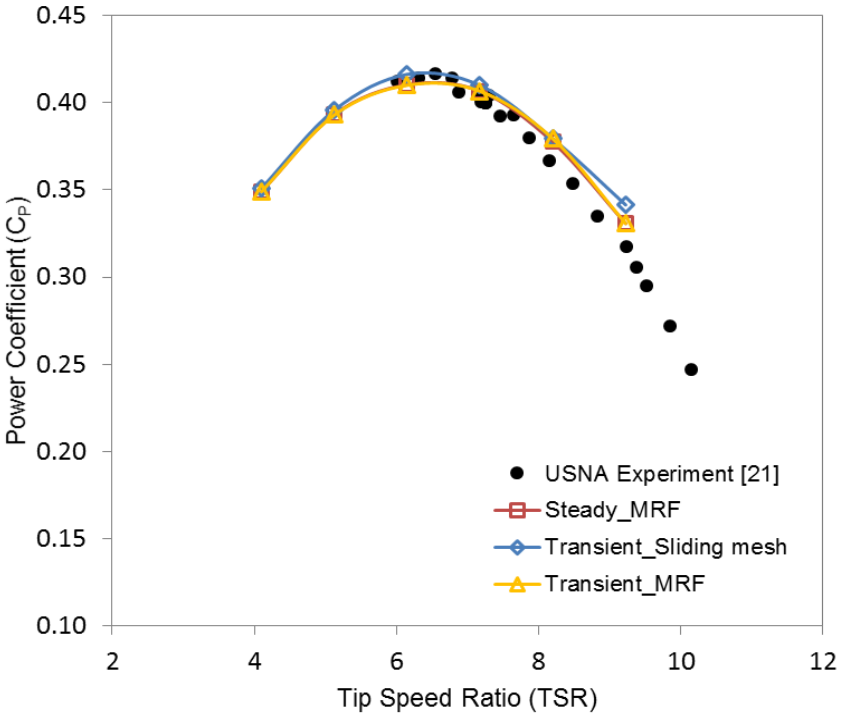

Fig. 2.16. Comparison between the C_P curves of the steady and transient simulations with MRF and sliding mesh method

The velocity profile around the turbine is compared between the sliding mesh and the MRF in Fig. 2.17. Although the velocity distributions in the two graphs look similar, the tip vortices were only captured by the sliding mesh. It is because of setting the rotating zone in the MRF method as a moving reference frame; which causes the blades remains stationary during the CFD solution. The wake distribution behind the turbine, marked in Fig. 2.17, for the two methods was also different. It is obvious that the wake behind the turbine was not periodic for the sliding mesh method. It shows that using a half turbine model with a periodic boundary condition instead of the whole turbine is not suitable for turbine wake studies. The half turbine simulations can only be performed using the MRF method. Even though the turbine is geometrically periodic, the wake propagation and the blade vortices are not always periodic [73], which leads to different simulation results for the half and the whole turbine models. From Fig. 2.9, it can also be inferred that the whole turbine model was a better fit to the experimental data than the single blade model. Thus, using the whole turbine is recommended for both the performance and wake study of HAMCTs.

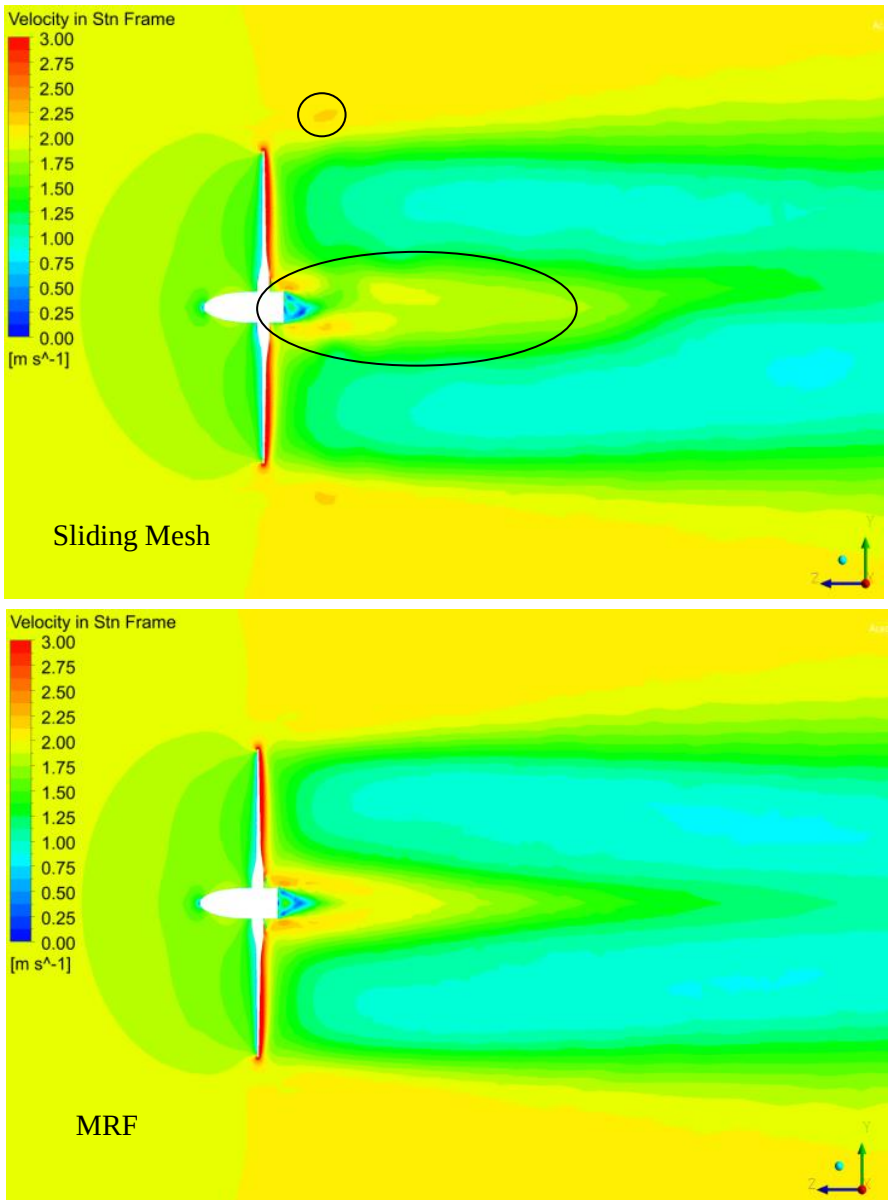

Fig. 2.17. Comparing the flow velocity profile around the turbine between the sliding mesh and MRF methods.

2.6. Conclusion

The hydrodynamic characteristics of a two-bladed turbine scale model were investigated using different CFD approaches. The CFD approaches were compared with experimental results from the USNA towing tank to evaluate the best numerical modelling approach for studying turbine performance.

Comparison between the turbulence models showed that even though the results from BSL EARSM can reasonably predict the hydrodynamic behaviour of the turbine for a range of TSRs, k-ω SST results have closer agreement with the experiments.

The influence of using two rotating approaches on the numerical results was assessed. It is found that moving reference frame (MRF) technique, which had a close agreement with the experimental data, achieved the convergence criteria faster. However, the sliding mesh technique provided more realistic conditions to the actual turbine operation; e.g. helical vortices and wake of the turbine in downstream region. Even though the C_P and C_T curves from the sliding mesh method were in good correlation with the experimental results, the computational time was much higher than the MRF. Thus, it is recommended that the MRF method be used in the case of needing quick and reasonable performance assessment of a turbine with limited computing resources. Conversely, in the case of investigating the wake or interaction between the turbines, the sliding mesh technique should be used.

Different boundary layer models were applied on the k-ω SST turbulence model in the steady state solution. Among all of the applied boundary layers, the wall-function model had the best agreement with the experimental data with the least computational time. Conversely, given the high resolution mesh required for near wall region compared to the other two methods, the transitional gamma-theta model and the near wall model were computationally demanding as well as having higher truncation error. Therefore, the wall-function model is recommended for HAMCT studies.

Running the numerical simulations on a single blade instead of the whole turbine reduces the simulation time significantly. However, the single blade models had lower C_P estimates than the whole turbine models. It shows that despite the turbine geometry being periodic; the operation in terms of wake propagation and the blade vortices is not always periodic.

Overall, the steady MRF simulation on the whole turbine using the wall-function with k-ω SST model provided the best balance between accurately predicting the turbine performance and modelling the flow physics with computational time.

The next step in the development of the numerical model was to modify it to be able to evaluate the performance of the HAMCT under the influence of shear, proximity to the free surface, and surface waves. The following chapter presents the experimental data used to validate the modified numerical model (presented in Chapter 5).

Chapter 3

Experimental Evaluation of a Horizontal Axis Marine Current Turbine

A refereed journal paper was published based on this Chapter and a part of Chapter 4 in Journal of Energy. The citation for this journal paper is:

Rahimian M, Walker J, Penesis I. Performance of a horizontal axis marine current turbine–A comprehensive evaluation using experimental, numerical, and theoretical approaches. *Energy*. 2018;148:965-76.

3.1. Introduction

Ensuring the optimum performance of a marine current turbine is essential in the design stage, including determining if the turbine is cost-effective and viable for a particular deployment site [16]. Experimental approaches are common practice to predict the hydrodynamic characteristics of marine systems. In this regard, different methods and facilities are used to study the effects of various factors on the performance of HAMCTs.

Bahaj et al. [25] conducted experiments in a cavitation tunnel and a towing tank to investigate the effects of various hydrodynamic flow conditions on the performance of a 3-bladed HAMCT model. They studied the effect of blockage, depth, direction of the flow and cavitation on the performance of the turbine. In 2013, Walker et al. [21] performed wind tunnel and towing tank experiments together with a numerical study to investigate the influence of Reynolds number, blade roughness and biofouling on HAMCT performance. Myers [26] studied the wake and hydrodynamic characteristics of a 0.4 m diameter HAMCT by testing in a circulating water channel. Gaurier, et al. [27] as well as Tutar and Veci [28] in separate works conducted flume tank experiments on 3 bladed HAMCTs to study the effect of different current and wave characteristics on the hydrodynamic performance and blade loading. In an effort by Ross and Polagye [29], the effect of blockage on the hydrodynamics of current turbines was investigated. They experimentally characterised the performance and the wake of a cross-flow turbine and an axial-flow turbine using flume tank tests on physical scale models and porous plates. Gaurier, et al. [30] performed experiments on a tidal turbine model in two towing tanks and two circulating water tanks to study the impact of facility bias on the test results. The performance results were found to be very similar in all facilities; however, fluctuations were seen in torque and thrust measured data. Among all the characteristics of a facility, blockage had the most impact on the results.

In this study, the performance of a 2 bladed HAMCT was characterised by testing two scale models of 500 mm and 800 mm diameter, representing $1/32^{th}$ and $1/20^{th}$ scale of operational turbines with 16 m of diameter such as SeaGen [9]. The experiments were implemented in two test facilities with different blockage and flow characteristics enabling an investigation on the effect of facility bias on the test results. Moreover, the scale effect was studied by comparing the results from the two scale models. The independency of the results from Reynolds number was checked in order to predict the performance of the full-scale turbine. The experimental

data presented in this Chapter was used to validate the numerical model presented in Chapter 5.

3.2. Experimental Approach

The experiments were performed on two scale models in the circulating water channel (CWC) and the towing tank (TT) of the Australian Maritime College (AMC) at the University of Tasmania. There are some intrinsic differences in the characteristics of the two facilities, which provide different flow conditions for the tests. Comparing the results between these two facilities and the two scale models allows assessment of the impact of testing marine current devices in different hydrodynamic facilities as well as the implications of using scale models to predict full-scale turbine performance.

3.2.1. Test Facilities

Circulating Water Channel

Fig. 3.1 shows the configuration of the test setup in the CWC. The water in the channel was circulated in the tank using four axial pumps located at the end of the tank, as shown in schematic view in Fig. 3.2. A conveyor belt was utilised along the bottom of the tank, which operated at the same speed as the flow, in order to reduce the boundary layer formation. There were two series of flow straighteners before the inlet to damp the vortices in the free stream produced by the pumps and reduce the fluctuations in the flow. Details of this testing facility are presented in Table 3.1. The turbine rotor was located at a distance of 2.87 m downstream from the inlet as flow profiling showed this location to have the least spatial and temporal fluctuations in the flow due to the acceleration of the flow from the pumps and the mixing of the inlet flow. The flow profiling was performed using an Acoustic Doppler Velocimeter (ADV), explained later in this Chapter.

Towing Tank

Fig. 3.3 shows the test setup configuration in the towing tank and Fig. 3.4 depicts the schematic view of the test setup. Details of the facility are given in Table 3.1. Although the overall length of the towing tank is 100 m, the useful length for testing was approximately 60 m, due to the need to gradually accelerate and decelerate the carriage at the beginning and end of each test. Data recording time depended on the carriage speed. For example, at carriage

speed of 2 m/s the data acquisition cannot be performed for more than 30s. Thus, the acquisition time for all experiments was considered 30 s.

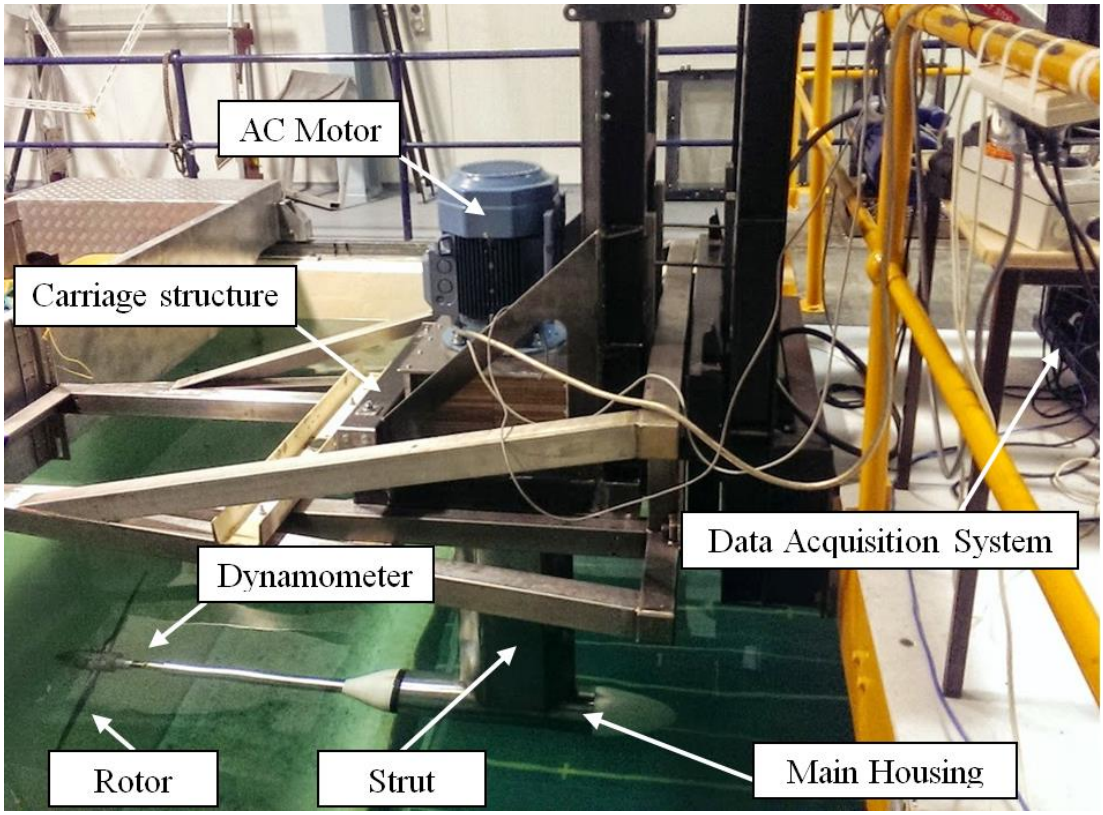

Fig. 3.1. Test setup configuration in CWC

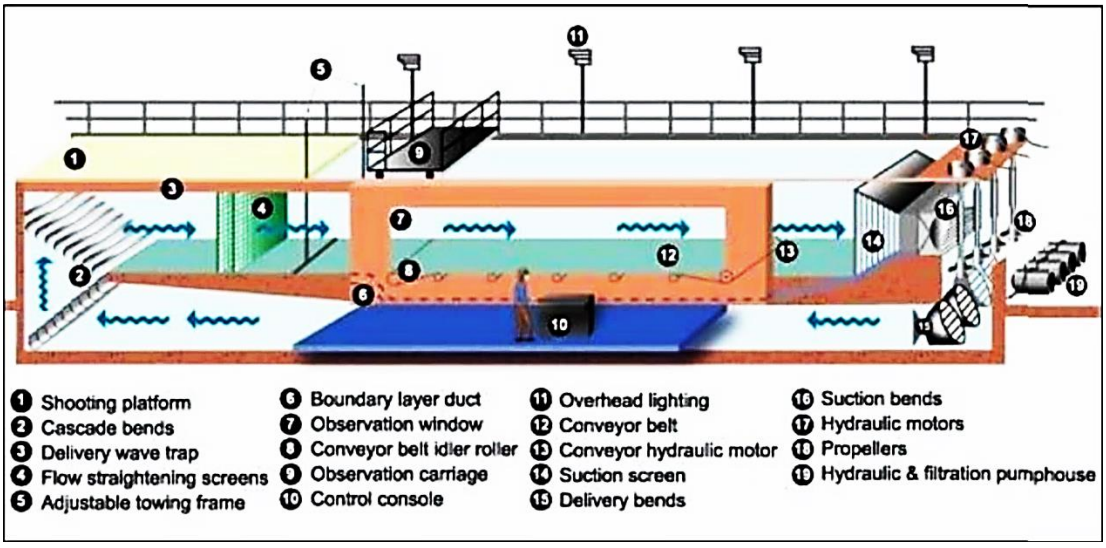

Fig. 3.2. Schematic configuration of CWC

Fig. 3.3. Test setup configuration in Towing Tank

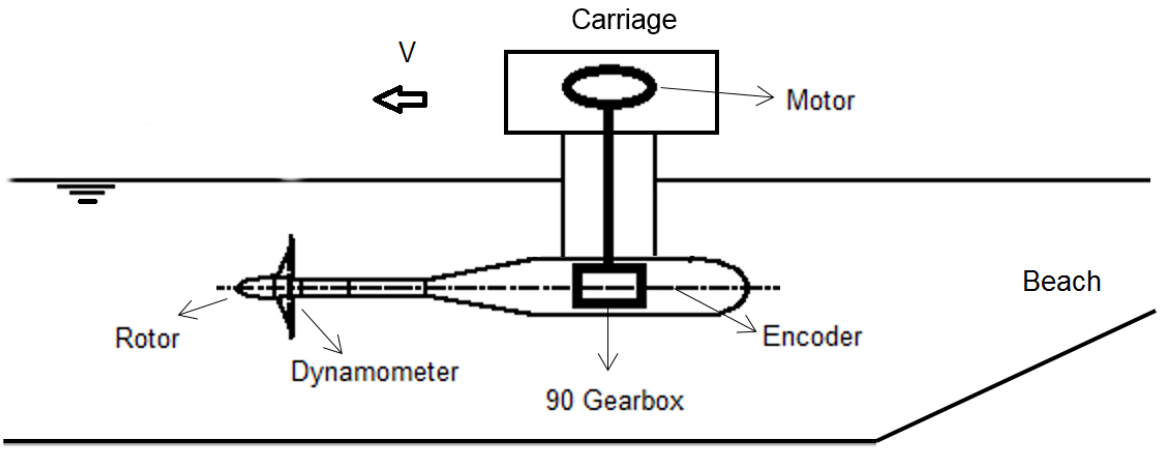

Fig. 3.4. Schematic configuration of the test setup in Towing Tank

Table 3.1. Details of the experimental testing facilities

Facility	**Circulating Water Channel**	**Towing Tank**
Length (m)	11	100
Width (m)	5	3.55
Depth (m)	2.5	1.5
Cross-sectional area (m^2)	12.5	5.325
Current velocity tested (m/s)	1.3	1 to 2

3.2.2. Test Rig

A test rig was fabricated to perform experiments in the two facilities. Fig. 3.1 shows the setup of the test rig in the CWC. The rig includes a streamlined vertical strut that holds the housing of the internal equipment. The strut was clamped to the support frame but can slide vertically in order to adjust the depth of the turbine before a test. Fig. 3.5 shows the internal instruments of the test rig. A QT255 Marin Tech dynamometer was employed to measure the torque and thrust. It was mounted in the wet area immediately adjacent to the turbine rotor before any bearing or sealing. Hence, the logged data is not affected by the losses in connections. The dynamometer data wires were connected to a slip ring which transfers data to a signal conditioner and transmitter. The signal conditioner reduces noise in the signal captured by the sensor. A 90^{o} gearbox was utilised to convert the axis of rotation from vertical shaft, driven by an AC motor from the top, to the horizontal shaft connected to the turbine. An AMCI Dura Coder analogue encoder was attached to the other side of the gearbox to log the rotational speed of the shaft. It was used as a feedback for the shaft rotational speed in addition to the built-in encoder of the motor.

Marin dynamometer

AMCI encoder

90^{O} Gearbox (ratio 1:1)

Fig. 3.5. Internal equipment of the test rig

3.2.3. Physical Models

The Froude-scaled turbine models were of a 2-bladed HAMCT based on a design developed at the U.S. National Renewable Energy Laboratory (NREL). The blade profile was a NACA 63-618, with the lift and drag coefficient data available from 2D wind tunnel tests [21] and X-Foil predictions [44]. The diameters of the two models are 500 mm and 800 mm. These are $1/32^{th}$ and $1/20^{th}$ scale of the 16 m diameter full-scale turbines. The blade geometry was detailed

in Table 1.1 of Chapter 1. The two turbine scale models are shown in Fig. 1.2 of Chapter 1. In this Chapter, the main discussions are performed on the larger turbine results. The results from 500 mm diameter scale model were used to investigate the effect of scaling/Reynolds number on the performance of the turbine.

3.2.4. Flow Characterisation

An understanding of the flow characteristics in each test facility was necessary before any turbine performance evaluation. Water was stationary in the towing tank, which is considered as a steady state condition. However, the water is circulated in the CWC, leading to both spatial and temporal fluctuations in velocity together with significant turbulence intensity. Thus, a Sontek 16-MHz Micro Acoustic Doppler Velocimeter (ADV) was utilised to characterise the flow condition in the CWC.

Fig. 3.6 shows the ADV attached to a traversing system which provides an accurate positioning for data acquisition in the sampling section. Sampling was performed for a section with 0.9 m of width and 2.1 m of depth, at the same location as the rotor installation in the CWC. The ADV recorded the 3D flow velocity components at each spatial point for 3 minutes with sampling rate of 50 Hz, providing around 15000 samples per point.

The ADV measured the time-varying velocity, u_x, which was subject to some noise. Two other parameters were logged by the ADV, signal to noise ratio (SNR) and correlation, which can be used for filtering the noise from the velocity signal. These two factors are mainly related to the quality of the acoustic signal that an ADV receives. In addition to the signal filtering using SNR (Signal to Noise Ratio) and the correlation criteria, recommended by the sensor manufacturer [74], a maximum/minimum threshold method described in [75] was used to discard or replace bad data points and large spikes from all the raw velocity data. The velocity profile for an inflow velocity of 1.3 m/s is plotted in Fig. 3.7.a, which demonstrates the spatial velocity fluctuation of the CWC flow at the testing section. The maximum velocity variation within the swept area of the rotor was approximately 0.2 m/s.

Fig. 3.6. ADV velocity measurement

In addition to the time-averaged velocity, temporal fluctuation was determined by turbulence intensity. The streamwise turbulence intensity, I_x, defined as the ratio of the root mean square, $\sigma_x = \sqrt{\overline{u_x'^2}}$, of the velocity fluctuations, $u_x' = u_x - \overline{u}_x$, to the mean velocity, $\overline{u}_x$, was calculated in the flow direction by

$$I_x = \frac{\sigma_x}{\overline{u}_x} \qquad \textbf{(3-1)}$$

Fig. 3.7 (b) shows the turbulence intensity profile in the testing section for an inflow velocity of 1 m/s. The 3D turbulence intensity, *I*, which contain transverse and vertical fluctuating velocities in addition to the streamwise, was computed using

$$I = \frac{\sqrt{2TKE}}{U} \qquad \textbf{(3-2)}$$

where $TKE = \frac{1}{2}(\sigma_x^{\,2} + \sigma_y^{\,2} + \sigma_z^{\,2})$ is turbulence kinetic energy and *U* is the 3D mean flow velocity. The average streamwise and 3D turbulence intensities for the swept area were approximately 7.5% and 10.2% respectively.

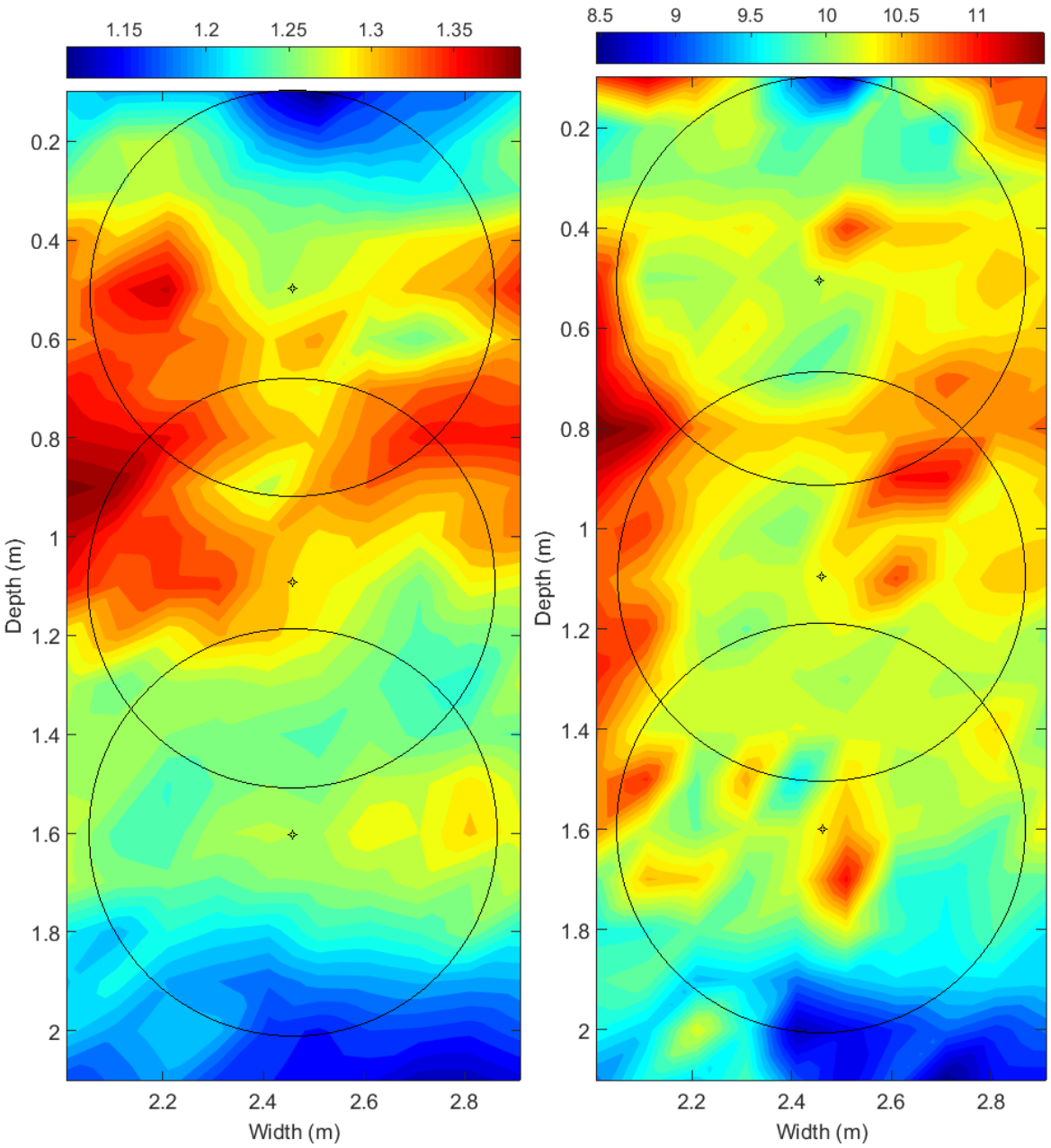

(a) Velocity (m/s) **(b) 3D turbulence intensity (%)**

Fig. 3.7. Results from ADV measurement for a streamwise flow velocity of 1.3 m/s

Although the flow characteristics of the CWC were influenced by the pumps used to drive the flow, the general flow condition was more comparable to the real environment, where the full-scale turbine operates in a flow with shear velocity profile and fluctuations, than the towing tank. Turbulence intensity is important in terms of the loadings on the blades which cause fluctuating forces, leading to fatigue. It does not affect the mean power of a single turbine [76]. However, it plays a major role in the power output of a turbine which operates in the wake of other turbines in a tidal farm [77]. Shear flow velocity has a similar fluctuating effect on torque and thrust, since in a single rotation the turbine blades are under varying velocity and pressure,

and consequently varying lift and drag. In addition, the flow velocity value by which the power is calculated should be selected wisely; particularly if the rotor is operating in an environment with an uneven or sheared velocity distribution, otherwise the predicted power output would be different from the real performance. The velocity derived from the kinetic energy of the flow passing through the swept area of the rotor was the method employed in this study.

3.2.5. Test Procedure

The main objective of the experimental tests was measuring torque and thrust over a range of inflow speeds and turbine rotational speeds. In order to have a united criterion to characterise the turbine performance, a non-dimensional analysis was performed on the measured data. The power and thrust coefficients of the turbine with respect to tip speed ratio were determined using the equations (2-1) to (2-3) of Chapter 2.

Following ITTC[1] procedures [78], prior to each series of experiments the dynamometer was calibrated for thrust and torque up to 1240 N and 50 Nm, respectively; following the instruction recommended by the manufacturer [79]. A calibration formula was generated at the end of the calibration for each of thrust and torque, which was used to convert the output voltage from the dynamometer to torque and thrust values. The encoder in the test rig was analogue, hence there was no need for calibration. However, the encoder results were double-checked by the results from the AC motor built-in encoder, to make sure that the turbine was rotating with the same speed as the one set on the motor controller. The water temperature was measured at the beginning and end of the two series of experiments in order to estimate the water density.

To conduct a test in the towing tank, first, zero values were acquired at the beginning of each test, while the carriage, rotor and water were stationary. Then, the rotor rpm was set and in turn, the carriage towed the test rig at the pre-determined speed. It was important to conduct tests in steady state flow. Thus, a minimum of 10 minutes was allowed between each two consecutive tests to allow the water to settle. At each carriage speed, 10 values of rotor rotational speeds were applied to cover a range of TSRs from 4 to 9, with smaller increments around TSR ~ 6. Experiments were performed at six carriage speeds from 1 m/s to 2.25 m/s/ The turbine hub was positioned at a depth of 720 mm from the surface. Although it was possible

[1] International Towing Tank Committee

to increase the carriage speed up to 4 m/s, given the vibration of the system during the tests of the 800 mm rotor at 2.25 m/s, no higher speeds were undertaken.

For the CWC experiments, the zero values for the dynamometer were calculated based on static tests taken at the beginning and end of the test series. The static test was a normal test run but in stationary condition of the rotor and the water. The zero value was used to reduce the bias error of the sensor. The inflow speed of the tank was then set to the maximum velocity of the tank, 1.3 m/s. The flow velocity profile at the testing section is depicted in Fig. 3.6. The experiments were conducted at hub immersion depths of 0.5 m, 0.72 m, 1.1 m and 1.6 m. Eleven rotational speeds were applied to the rotor to cover a range of tip speed ratios (TSRs) from 3 to 9 with higher resolution around TSR ~ 6, which was potentially the TSR where the maximum C_P occurs according to the Walker, et al. [21]. The sampling frequency was 1 kHz and each test run was 30 seconds. At the end of experiments, a crucial check was done on the measured data to see if they were within the sensitivity of the dynamometer. Hence, measured data of lower than 0.275 Nm for torque and 11 N for thrust were discarded from the results.

3.2.6. Blockage Correction

The size of hydrodynamic facilities, such as towing tank and flume tank, is one of the parameters that introduce an inherent interference in model test results due to flow confinement. It is associated with the concept of blockage, an effect on an object obstructing passing flow in a finite cross sectional area. The blockage effect is generally assessed using the ratio of the turbine swept area to the tank cross sectional area. It is known that the results in blockage ratio higher than 10% are questionable [80]. The level of blockage affects the acceleration of the turbine bypass flow in a confined area, attributed to the turbine geometry and its wake. As a result, the dynamic pressure will increase on the turbine, hence higher loadings [38].

The blockage ratio for the larger rotor in the towing tank and the CWC were 10% and 4%, respectively. The towing tank results were corrected using the method suggested by Bahaj, et al. [25]. This method is based on the continuity and momentum balance between the upstream and downstream of the turbine. The index T and F represent tunnel and freestream condition respectively. A is the rotor swept area and C is tank cross-sectional area. If U1 is the flow velocity at the turbine location; U2 and U3 are wake and bypass velocity in the far downstream respectively, it can be written:

$$\frac{U1}{U2}=\frac{-1+\sqrt{1+(A/C)\left((U3/U2)^2-1\right)}}{(A/C)\left((U3/U2)-1\right)} \quad \textbf{(3-3)}$$

$$\frac{U_T}{U2}=\frac{U3}{U2}-\frac{A}{C}\frac{U1}{U2}\left[\frac{U3}{U2}-1\right] \quad \textbf{(3-4)}$$

The thrust coefficient can be obtained non-dimensionally by:

$$C_T=\left(\frac{U2}{U_T}\right)^2\left[\left(\frac{U3}{U2}\right)^2-1\right] \quad \textbf{(3-5)}$$

By rearranging equation (3-5) for $U_T/U2$ and equating equation (3-4), $U3/U2$ can be found by solving the equations iteratively. Then the ratio of tunnel velocity to freestream velocity is the blockage correction factor, defined as below:

$$C_B=\frac{U_T}{U_F}=\frac{U1/U_T}{(U1/U_T)^2+C_T/4} \quad \textbf{(3-6)}$$

The corrections to C_P, C_T and TSR can be conducted using C_B as below:

$$C_{Pc}=C_P.C_B^{\,3} \quad \textbf{(3-7)}$$

$$C_{Tc}=C_T.C_B^{\,2} \quad \textbf{(3-8)}$$

$$TSR_c=TSR.C_B \quad \textbf{(3-9)}$$

The corrections at TSR ~ 6 at a flow velocity of 1.7 m/s led to 11% and 7% reduction for the larger turbine and 3% and 2% decrease for the smaller turbine in C_P and C_T, respectively, in the towing tank. Due to the larger cross-sectional area of the facility, the blockage correction factors for the CWC results in the calculations were approaching 1. Thus, no blockage corrections were applied to the CWC results.

3.2.7. Uncertainty Analysis

It is important to know the uncertainty of any measured data, which shows the quality of an experimental result [81]. The first step in this regard was to estimate the calibration uncertainty, due to the deviation of the measured data from the fitted curve as well as the accuracy of the calibration instruments. The fitted curve provides a calibration formula written as $v=b\phi+a$, where v is voltage, ϕ is applied torque or thrust, and a and b are the calibration constants. The

uncertainty associated with calibration was estimated using the method suggested by the ITTC [78]. The precision error (η_P) of the calibration was computed according to [82], based on standard error of estimate (*SEE*) with 95% confidence interval.

$$\eta_{P,cal} = t_{n-2} SEE \tag{3-10}$$

$$SEE = \sqrt{SS_R / (n-2)} \tag{3-11}$$

$$SS_R = \sum_{i=1}^{N} (v_i - a - b\phi_i)^2 \tag{3-12}$$

where *n* is number of samples, *i* is the sample number, SS_R is summed square of residuals and t_{n-2} is a t-random variable with n − 2 degrees of freedom. The calibration bias error, for example, for torque ($Q = mgl$) was based on the measuring uncertainty of mass, length and gravitational constant, expressed as:

$$\eta_{B,cal,Q} = Q\sqrt{\frac{\eta_m^2}{m^2} + \frac{\eta_g^2}{g^2} + \frac{\eta_l^2}{l^2}} \tag{3-13}$$

where the measuring uncertainty for all the three quantities were in the order of 0.001. Finally, the total calibration uncertainty was obtained by:

$$\eta_{cal} = \sqrt{\eta_{p,cal}^2 + \eta_{B,cal}^2} \tag{3-14}$$

An uncertainty analysis was also done on the measured data based on the Taylor series method [83] and in accordance with ITTC [78]. First, the precision and bias errors were defined for all measured parameters, including thrust, torque, inflow speed and RPM. Then, the errors were propagated to determine the uncertainty in the calculated variables, such as power and thrust coefficients, and TSR. The standard error, S_E, in each measured variable was estimated from ten repeated runs at TSR ~ 6 using the method presented in Figliola and Beasley [81]. The precision errors, μ_P, were then calculated using equation (3-15) with confidence interval of 95% and $t_{v,95}$ = 2.262 for N = 10 repeats. S_E is the standard random error, computed by the standard deviation, σ_S; as shown in equation (3-16).

$$\eta_P = t_{v,95} \times S_E \tag{3-15}$$

$$S_E = \frac{\sigma_S}{\sqrt{N_S}} \tag{3-16}$$

The bias error (η_B) for the dynamometer was calculated based on the sensitivity of the sensor. The bias error for the CWC flow velocity was as a result of the ADV accuracy as well as spatial fluctuations of the flow in the tank. The uncertainty of the data acquisition system, National instrument board model PCI-6254, in logging voltage from the sensors was negligible. Using the error propagation method, the uncertainty of the thrust coefficient, power coefficient and TSR was also calculated. Table 3.2 shows the uncertainty analysis performed for the 800 mm turbine experiments in the CWC at inflow speed of 1.3 m/s and in the towing tank at carriage speed of 1.25 m/s for TSR ~ 6. The uncertainties are +/- amounts in respective units of the provided parameters. Comparing the uncertainties between the two facilities shows the significant effect of flow velocity uncertainty on the total uncertainties of C_P, C_T and TSR. Although the total error of torque and thrust measurements were marginally higher in the towing tank, since the error associated with the flow velocity was higher for the CWC, the total uncertainty of the dimensionless parameters are much larger for the CWC results.

Table 3.2. Uncertainty of experimental results in each facility at TSR ~ 6 (data given is +/- amount in the relevant units)

Parameter	CWC at 1.3 m/s				Towing Tank at 1.25 m/s			
	Calibration	Bias	Precision	Total	Calibration	Bias	Precision	Total
Torque (Nm)	0.113	0.066	0.014	0.132	0.116	0.066	0.113	0.175
Thrust (N)	0.985	1.810	0.170	2.067	0.992	1.672	1.816	2.660
Velocity (m/s)	-	0.025	0.017	0.030	-	0.010	2.2e-4	0.010
RPM	-	0	4.1e-03	4.1e-3	-	0	7.1e-3	7.1e-03
TSR	-	-	-	0.141	-	-	-	0.048
C_P	-	-	-	0.031	-	-	-	0.013
C_T	-	-	-	0.039	-	-	-	0.014

3.2.8. Equivalent Inflow Velocity

As discussed in Section 3.2.4, the inflow velocity in the CWC was not uniform. A method was proposed by Wagner, et al. [48] to account for wind velocity shear in the performance evaluation of wind turbines. Conventionally when the performance of a turbine is assessed, the velocity at the hub location is taken as being representative for the entire rotor swept area in calculating the performance parameters (C_P, C_T, and TSR). However, ignoring the velocity shear will cause inaccuracies when the flow is not steady, such as flow in the CWC and the real environment. The idea behind this approach is that the turbine is converting the kinetic energy in the flow passing through the entire swept area of the rotor. Hence, using the velocity at the hub is not an accurate way to find the kinetic energy of flows with shear. If the rotor

section area is divided into horizontal segments according to the wind shear and the inflow velocity, u_i, is measured separately at each segment area, A_i, then kinetic energy flux can be calculated by:

$$KE = \sum_i \tfrac{1}{2} \rho u_i^3 A_i \qquad \textbf{(3-17)}$$

The flow kinetic energy flux, *KE*, derived from the velocity profile over the whole rotor swept area is utilised in this method to compute an equivalent velocity, U_{eq}, as an alternative for the hub inflow speed, which is defined as follows:

$$U_{eq} = \left(\frac{KE}{0.5 \rho A} \right)^{\frac{1}{3}} \qquad \textbf{(3-18)}$$

Unlike wind shear, the flow in the CWC did not have a horizontal shear. Hence, it was impossible to divide the flow profile into a number of horizontal segments. In this Chapter, the flow profile, depicted in Fig. 3.7 (a) over the rotor swept area was divided to elements with an angle of 5° and radius of 5 mm, as shown in Fig. 3.8. To find the equivalent velocity (U_{eq}) in order to calculate the power and thrust coefficient, equations (3-17) and (3-18) were employed.

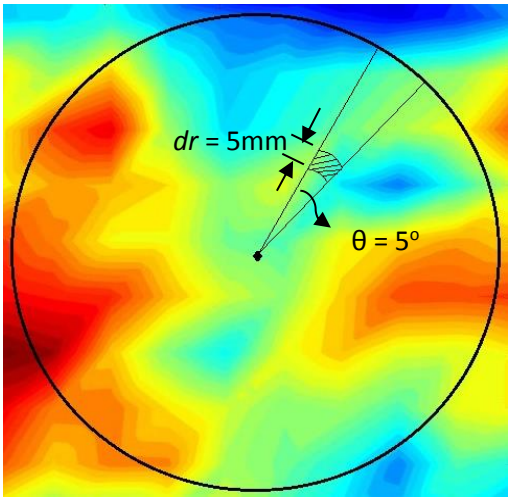

Fig. 3.8. Dividing the rotor swept area to small elements for calculating equivalent inflow velocity based on kinetic energy flux through the rotor swept area

3.3. Results and Discussion

3.3.1. Towing Tank Results

Fig. 3.9 and Fig. 3.10 show the hydrodynamic performance of the two scale turbine models in the towing tank tests using dimensionless coefficients, i.e. power and thrust coefficients with

respect to tip speed ratio, after blockage corrections. Each marker is an average value from 20 second of measured data of an individual test. The uncertainty of the results is shown by error bars only at test speed of 1.25 m/s at TSR ~ 6.

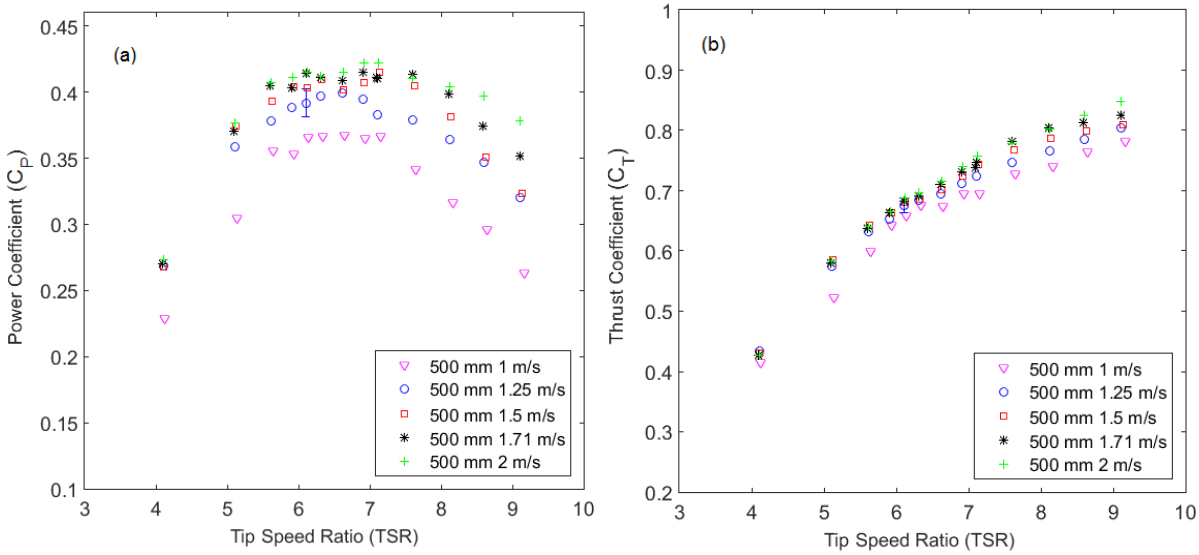

Fig. 3.9. Towing tank performance curves of the 500 mm diameter turbine after blockage correction (a) Power coefficient (b) Thrust coefficient

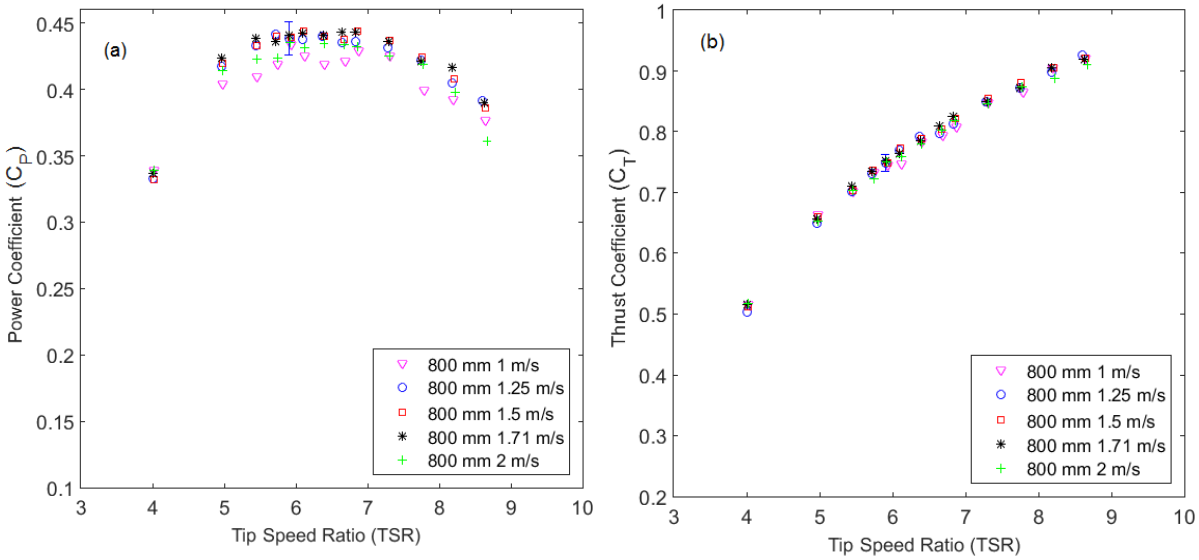

Fig. 3.10. Towing tank performance curves of the 800 mm diameter turbine after blockage correction (a) Power coefficient (b) Thrust coefficient

Although some discrepancies are seen in the C_P curves, almost all the C_T curves collapse on a same curve with an upward trend. The larger turbine had less scattered results than the smaller one. The C_P curves correlated well within the experimental uncertainty, with the exception of the test velocity of 1 m/s for the larger turbine and below test velocities of 1.5 m/s for the smaller turbine. In addition, C_P and C_T values for the 800 mm diameter model were larger than

the smaller turbine for the same range of TSRs, similar to what is seen in the CWC results shown in Fig. 3.11 to Fig. 3.14. The main reason is that the 500 mm turbine blades are working at smaller Reynolds numbers, and hence produce less lift.

Since a full-scale HAMCT works in conditions with high Reynolds numbers, the turbine performance is not affected by Re variation. Thus, only the scale model results that are not sensitive to Reynolds number can be utilised for performance prediction of the full-scale turbine. Comparing the C_P curves of the towing tank results helps to find Reynolds number independency condition. The USNA turbine tests results are reported Re independent, where Re_{c70} is in the range of 4×10^5 [21]. However, based on the correlation among C_P curves in Fig. 3.9 and Fig. 3.10, results are Re independent excluding the tests for the larger turbine at 1 m/s and for the smaller model at 1 m/s and 1.25 m/s. Hence it can be inferred that a Re_{c70} in the range of 2×10^5 at TSR ~ 6 is required to achieve the independency of the results, which was verified by the lift coefficients from XFoil predictions [44]. Note that Re_{c70} is based on the chord length at 70% of the span.

3.3.2. Circulating Water Channel Results

The results for the 500 mm and 800 mm diameter turbines in the CWC are presented in Fig. 3.11 to Fig. 3.14 at four hub submersion depths of 0.5 m, 0.72 m, 1.1 m and 1.6 m. The uncertainty of the results is shown by error bars only at hub depth of 0.5 m at TSR ~ 6. The C_P and C_T values for the 800 mm diameter turbine are larger than the 500 mm diameter turbine for the same range of TSRs; the same trend was observed for the TT results. The CWC results in Fig. 3.11 and Fig. 3.13 are presented based on the flow velocity at the turbine hub, whereas the results in Fig. 3.12 and Fig. 3.14 are based on the equivalent inflow velocity, calculated using the kinetic energy of the flow passing through the entire swept area of the rotor (equation (3-18)). Using the equivalent inflow velocity resulted in maximum reduction of approximately 5% on the C_P values and 2% on the C_T values for the larger turbine. The presence of a shear flow profile leads to a change in the water power input, kinetic energy flux, which is taken into consideration using the equivalent velocity in the analysis.

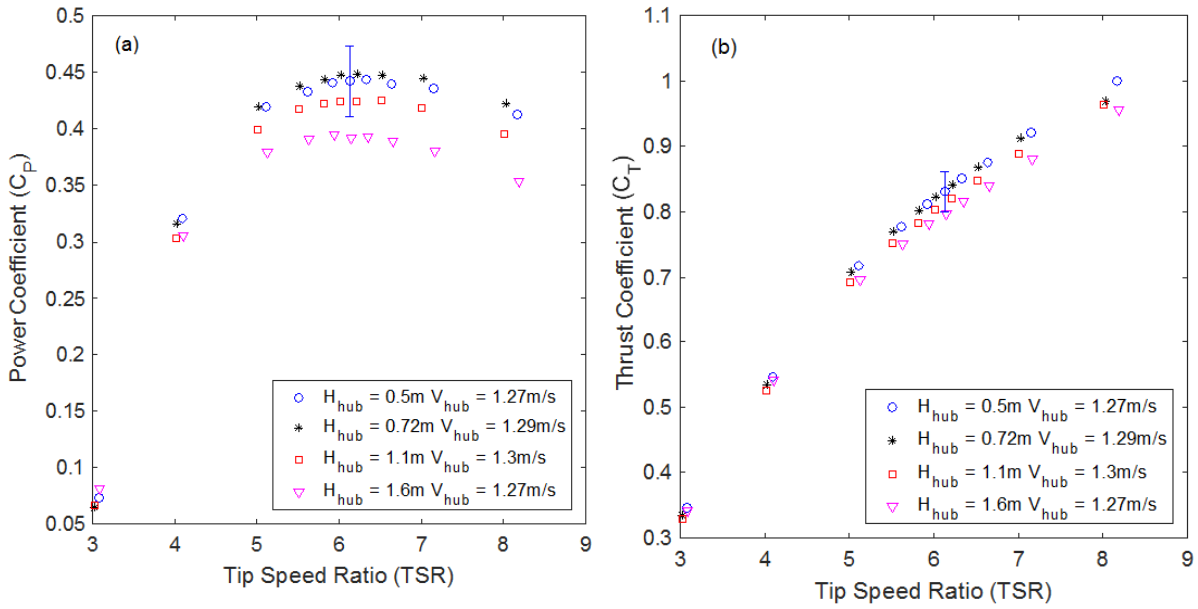

Fig. 3.11. Circulating water channel (CWC) performance curves of 800mm turbine using velocity at the hub (a) Power coefficient (b) Thrust coefficient

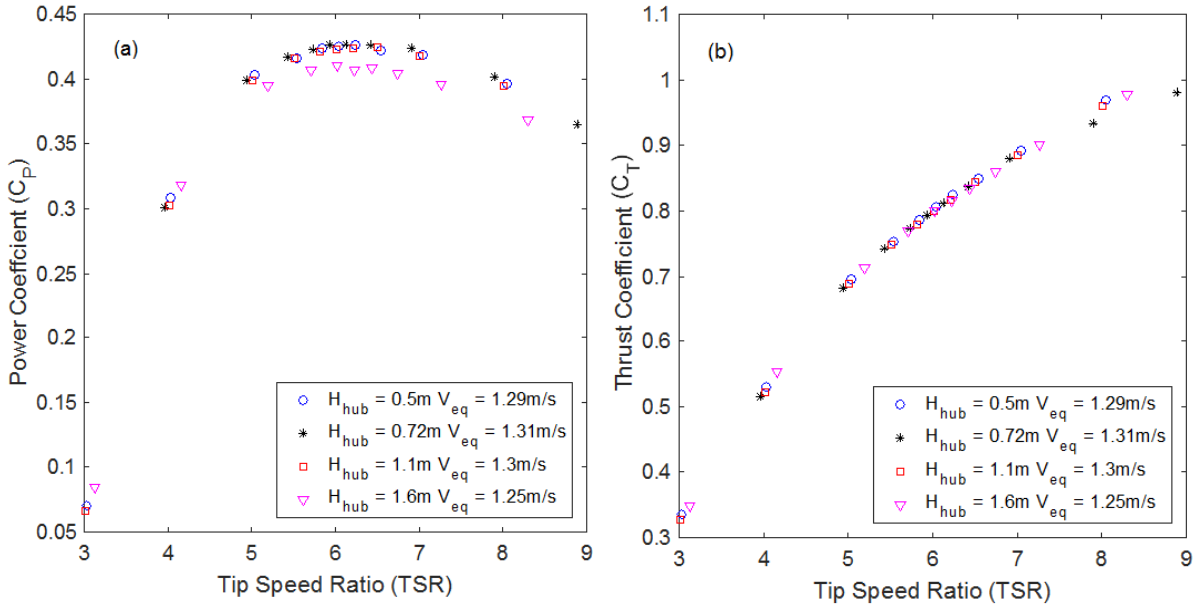

Fig. 3.12. Circulating water channel (CWC) performance curves of 800mm turbine using equivalent velocity (a) Power coefficient (b) Thrust coefficient

All the curves, except for 1.6 m of depth, in Fig. 3.12 and Fig. 3.14 are collapsing on a same curve, whilst there are discrepancies among the curves in Fig. 3.11 and Fig. 3.13 where the hub velocity was used. The C_P curve obtained using the equivalent velocity is a better fit for the USNA curve, as shown in Fig. 3.16. Thus, employing the equivalent flow velocity is recommended for turbine performance evaluation in a shear flow condition. However, since a turbine is usually designed for uniform flows, the cyclic effect of sheared inflow velocity on blades may change the ability of the rotor to extract the power depending on the shear flow and

also the blades design [84]. The lower values in the C_P curve with 1.6 m depth in Fig. 3.12.a and Fig. 3.14.a might be due to a slight incline of the strut from the vertical axis, observed during the test at this depth, which misaligned the rotor from the horizontal plane during test runs. It can be inferred from the CWC results that depth had little effect on the performance per se, even for tip immersion depths lower than half a rotor radius.

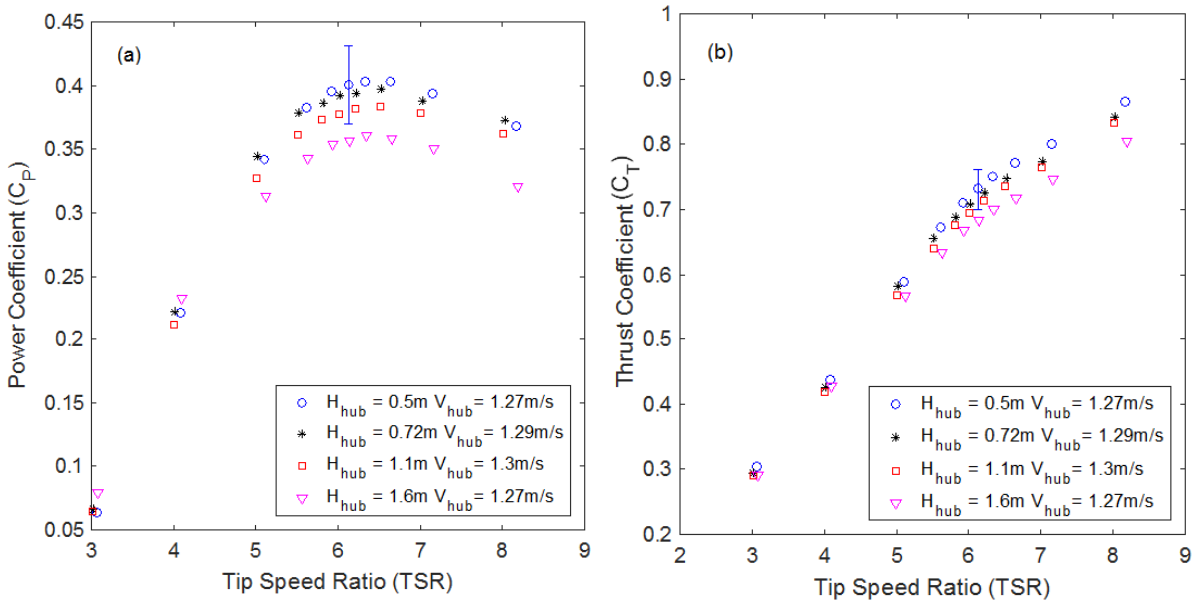

Fig. 3.13. Circulating water channel (CWC) performance curves of 500mm turbine using velocity at the hub (a) Power coefficient (b) Thrust coefficient

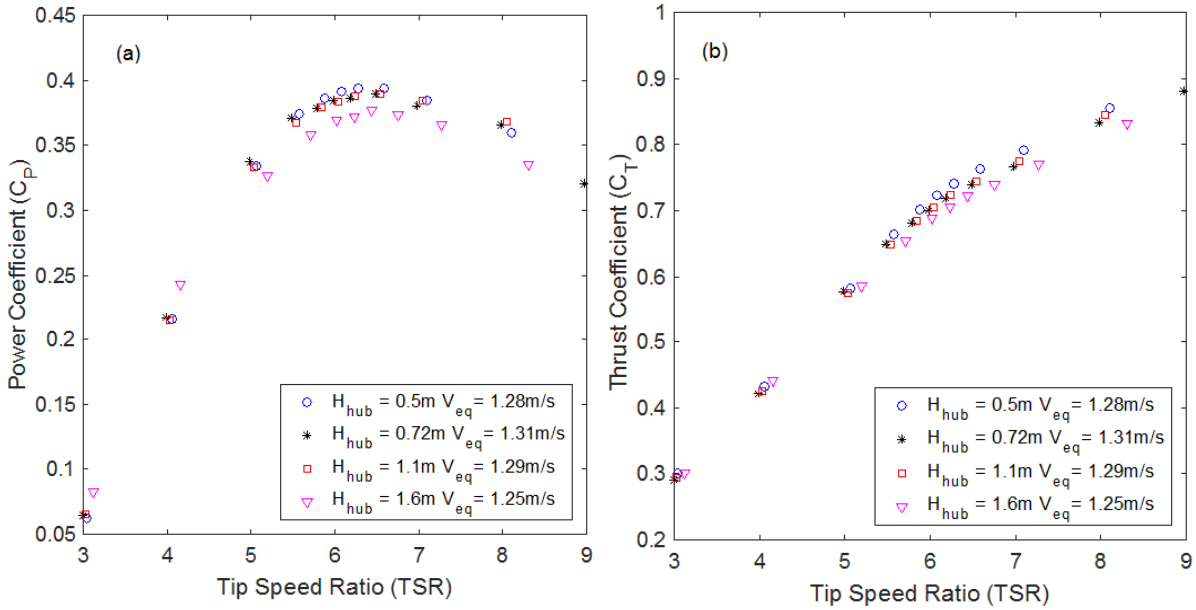

Fig. 3.14. Circulating water channel (CWC) performance curves of 500mm turbine using equivalent velocity (a) Power coefficient (b) Thrust coefficient

3.3.3. Blockage, Facility Type and Model Scale

Fig. 3.15 demonstrates the significant impact of blockage on the AMC towing tank results by comparing the C_P and C_T curves before and after blockage correction of the larger turbine at a carriage speed of 1.71 m/s. The blockage correction reduces the C_P and C_T by 12% and 7% at a TSR ~ 7, respectively. The results from towing tank tests on a turbine scale model [21], with a similar geometry to the 800 mm diameter turbine, at a speed of 1.68 m/s are also provided for comparison with our results in Fig. 3.15. The testing section of the USNA towing tank was 7.9 m × 4.9 m; large enough to have almost no blockage effect on the results. Although the size of the turbine model in the USNA test was the same as the larger turbine used in the present study, its C_P curve mostly collapses on the smaller 500 mm diameter turbine curve, which has approximately 7% difference with the large turbine curve at TSR ~ 6. It shows that the results from the two series of experiments with little blockage effect have a better correlation with each other. Thus, to have a reliable performance assessment, it is recommended to avoid testing in facilities with high blockage effect.

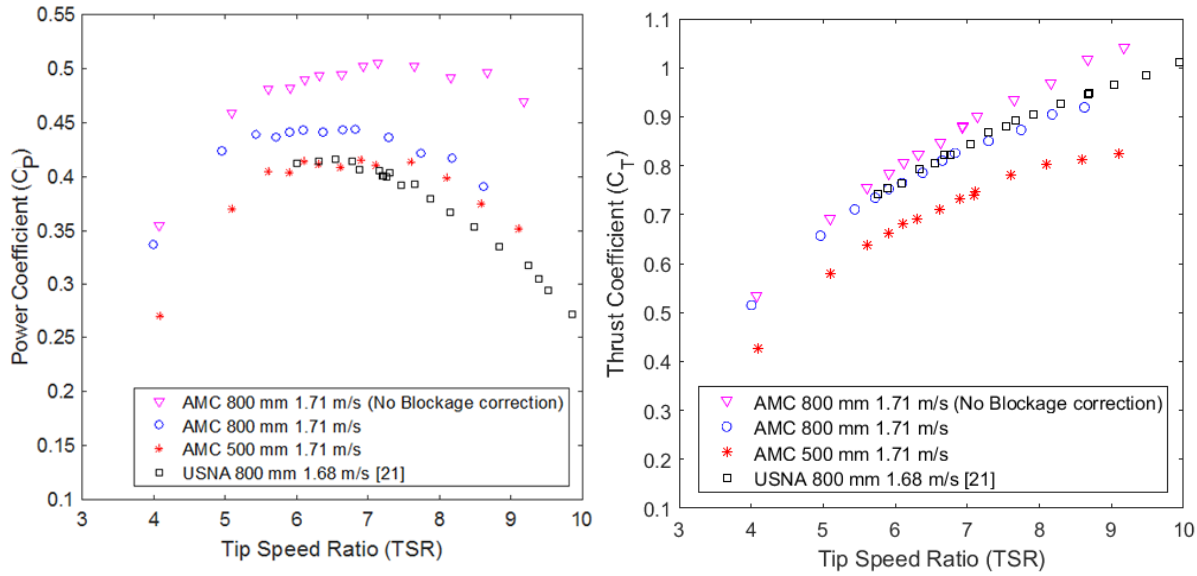

Fig. 3.15. Blockage effect on turbine performance evaluation (towing tank results)

There are other facility characteristics that may affect the results. For example, since the water in the towing tank was stationary, the flow condition was steady state and the flow profile passing through the blades was uniform with no turbulence intensity (TI). It is an ideal condition, which is far removed from conditions at a real deployment site. On the other hand, in the CWC the flow was unsteady and full of temporal and spatial fluctuations, resulting in an average of 10% TI, which was considered more representative of the conditions in which a

full-scale turbine would operate. The flow unsteadiness resulted in higher uncertainties for the measurements in the CWC (see Table 3.2). In addition, the speed limitation is another factor that influences the results. In the CWC, the maximum flow speed was 1.3 m/s, which for the smaller turbine was not high enough to achieve Reynolds number independency. Thus, these factors should be kept in mind before selecting the hydrodynamic facility for the performance assessment of a HAMCT.

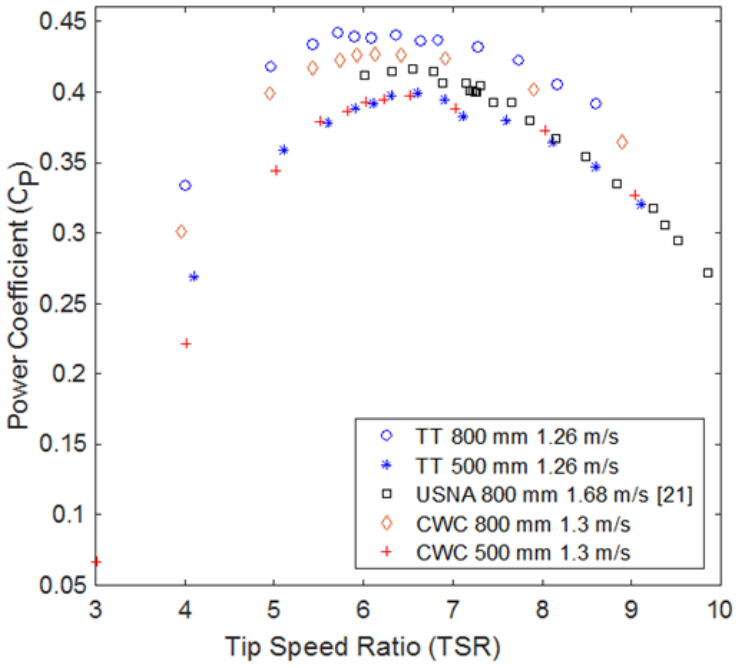

Fig. 3.16. The effect of scaling/Reynolds number and facility bias on the turbine performance

The effect of hydrodynamic facility and scaling on the experimental results can be seen in Fig. 3.16, which compares the C_P curves of the two scale models in the Towing Tank and the CWC at the AMC with the USNA towing tank results of the 800 mm turbine model. The same range of speed for the AMC facilities was selected for better comparison. Despite the higher C_P values of the larger turbine compared to the smaller turbine, each scale model shows a similar performance characteristic in the two facilities. Although there is small difference between the results of the larger turbine, the smaller turbine results match well with each other in the two facilities. This difference in the results can be partially attributed to blockage, even though the blockage corrections were applied. The blockage ratio was 10% for the 800 mm turbine and 4% for the 500 mm rotor in the towing tank; whilst, blockage was negligible for the two models in the CWC.

As can be seen in Fig. 3.15, although the results were Re independent at inflow velocity of 1.71 m/s, there is an obvious difference between the C_P curves of the two scale models. This difference is higher at an inflow speed of 1.25 m/s, shown in Fig. 3.16, where the smaller turbine was in a condition of Re dependency. The maximum power coefficient in the towing tank was approximately 0.44 and 0.4; and in the CWC, it was 0.43 and 0.4 for the larger and the smaller models, respectively. It shows about 8% difference of the maximum C_P between the two scale models. The TSR at which the maximum C_P occurred is approximately 6.5 for the two AMC facilities. However having the uncertainty of TSR, presented in Table 3.2, as well as blockage correction performed on the towing tank TSRs, the exact value is uncertain. The results of the USNA shows similar trend to the both AMC facilities, though it has lower C_P values, especially at higher TSRs.

3.4. Conclusion

A performance evaluation of a 2 bladed horizontal axis marine current turbine was presented using an experimental approach. Experiments were performed on two scale models with 500 mm and 800 mm diameters in two different hydrodynamic facilities. Experiments were undertaken in the AMC towing tank with a 3.5 m × 1.5 m test section for a range of carriage speeds from 1 m/s to 2 m/s. Experiments were also undertaken in the AMC circulating water channel with a cross-sectional area of 5 m × 2.5 m at an inflow velocity of 1.3 m/s. The results were compared to experimental data from the USNA towing tank (cross-sectional area of 7.9 m × 4.9 m).

During the experiments, torque and thrust were measured using a dynamometer together with rotational speed using an encoder. The flow profile in the CWC was measured using an ADV, which in addition to flow velocity provides temporal and spatial fluctuations of the flow over the testing section, showing an average of 10% turbulence intensity. A dimensional analysis was performed on the measured data to present the performance of the turbine. The maximum power coefficient of the larger turbine is 0.44 at TSR ~ 6.5 in the towing tank and is 0.42 at TSR ~ 7 in the CWC.

Experimental results revealed that the type of testing facility affects turbine performance. Facility bias was found to be a result of different flow conditions and blockage effects varying between the two scale models and the two facilities. The blockage correction on the towing tank results led to a 12% C_P reduction for the larger turbine. Using equivalent flow velocity

instead of the inflow speed at the hub in dimensional analysis of the CWC data resulted in maximum 5% of C_P reduction, which led to similar C_P and C_T curves for various shear flow velocity profiles and consequently a better correlation with the towing tank results, especially for the 500 mm turbine. In addition, equivalent inflow velocity is a better representative of the kinetic energy passing through the rotor swept area than the velocity at the hub. Therefore, it is recommended that the equivalent flow velocity be used for turbine performance evaluation in a shear flow conditions.

Comparing the two scale models results revealed similar performance curves, though the larger turbine had larger C_P values, approximately 8% higher at TSR ~ 6, than the smaller model. The difference between the two scale models performance was mainly due to the effect of Reynolds number and may be attributed to the blockage effect. In a similar test condition the smaller turbine was working in lower Reynolds numbers which lead to lower lift coefficients and higher drag coefficients that propagates to power coefficient. Since the C_P curves of the tests with Re_{c70} less than 2×10^5 were more scattered and do not collapse on other curves, 2×10^5 was considered as the criterion for Reynolds number independency. There was a difference between the C_P curves of the two scale models after blockage correction, even for Re independent condition, which could be due to high blockage effect on the 800 mm rotor in the towing tank. Therefore, to predict the full-scale turbine performance, it is recommended to perform experiments on the larger turbine in a facility with no blockage effect.

To extend the results presented in this Chapter, the influence of shear velocity profile was included in the CFD model, along with submergence depth and surface waves, and is presented in Chapter 5.

Chapter 4

The Impact of Evaluation Method on the Performance of a Horizontal Axis Marine Current Turbine

A refereed journal paper was published based on this Chapter and a part of Chapter 3 in Journal of Energy. The citation for this journal paper is:

Rahimian M, Walker J, Penesis I. Performance of a horizontal axis marine current turbine–A comprehensive evaluation using experimental, numerical, and theoretical approaches. *Energy*. 2018;148:965-76.

4.1. Introduction

There are several different methods currently available to characterise and analyse the hydrodynamics of a marine current turbine. Selection of an appropriate and accurate method is important at all stages of turbine research, development and implementation. Blade Element Momentum (BEM) theory is a useful tool to attain a quick power prediction of a marine current turbine [18], which can be modified to include environmental influences in the calculations. Numerical simulation is highly useful for the analysis of different hydrodynamic problems, including turbine performance. Computational fluid dynamics (CFD) models provide detail about the flow around the blades; however, they need to be validated by experimental data. Experiments can provide detailed results on scale models and allows the characterisation of turbine performance by controlling different parameters during tests. However, some intrinsic characteristics of a facility may limit the applicability of model experimental results.

Studies that have compared analysis methods include Maalawi and Badawy [85] and Madsen, et al. [86] who both compared the BEM theory with a CFD model. They both showed that a BEM model is less computationally demanding and may be utilised to give accurate performance predictions. However, there is a need for correction under conditions of flow unsteadiness. Javaherchi, et al. [37] conducted both experimental and numerical evaluations of the performance of a horizontal axis hydrokinetic turbine. They used a RANS model for the CFD simulation together with flume testing for validation. Another numerical prediction was performed by Bai, et al. [36] on the power production of a marine current turbine in free surface flow. They validated the CFD model by experimental results from Bahaj, et al. [25]. Kinsey and Dumas [38] investigated the effect of blockage on the performance of an axial and a cross-flow turbine using 3D CFD simulations. They studied some of blockage correction methods and found them more accurate for cross-flow turbine results than axial turbines. Kolekar and Banerjee [39] employed experimental tests as well as CFD modelling to study Reynolds number, boundary proximity, and blockage effects on a marine hydrokinetic turbine performance under various operating conditions.

In this Chapter, an experimentally validated BEM model [21] was modified to model the turbine under a sheared velocity profile. To investigate the effect of sectional Reynolds number on BEM predictions, the 800 mm diameter turbine was also modelled in QBlade, a BEM based software. The accuracy of these models in the performance evaluation of the turbine was assessed compared to the experimental results. Then, the QBlade model as well as the CFD

model from Chapter 2 were employed to study the effect of scaling by simulating the two scales of the turbine and at full-scale. The final part of this Chapter compares results from the numerical model, the experimental tests and the theoretical model, and details the advantages as well as limitations of each analysis method for HAMCT characterisations.

4.2. Theoretical Approach

4.2.1. Blade Element Momentum Theory

Previous studies have showed that BEM (blade element momentum) theory, which is a combination of momentum theory and blade element theory, is able to accurately predict the performance of horizontal-axis turbines, both wind and tidal, when modelling a turbine in a steady and axial condition of flow [21, 22, 86-89]. This theory is based on the assumption that each stream flow passing through the turbine blades can be analysed independently from the rest of the flow. Therefore, the variations in the fluid dynamic quantities occur in the plane along the axial and radial directions from strip to strip, without considering expressly the radial equilibrium among the strips [17]. Some of the recent turbine performance studies using BEM theory include Masters, et al. [90] and Koh and Ng [20]. Masters, et al. [90] extended the BEM model using Monte Carlo and sequential quadratic optimisation in order to predict the performance and loadings of a tidal stream turbine. Koh and Ng [20] studied the effect of Reynolds number and tip loss models on the BEM prediction accuracy compared to experiments.

Basic BEM Model

The theoretical model presented in this Chapter is based on an experimentally validated BEM model developed by Walker, et al. [21]. The basic theory is presented here; for a more detailed approach to the theory please refer to Manwell et al. [19].

To define the differential equation of thrust (equation (4-1)) and torque (equation (4-2)), momentum theory employs conservation of linear and angular momentum equation. It uses a control volume analysis of the forces on the blades based on the axial and angular induction factors, *a* and *a'*.

$$dT = 4F\rho U^2 a(1-a)\pi r dr \quad \textbf{(4-1)}$$

$$dQ = 4F\rho U a'(1-a)\pi r^3 \omega dr \quad \textbf{(4-2)}$$

where F is tip loss correction factor, ω is the turbine rotational speed and U is freestream velocity. Blade element theory is the analysis of the forces over the blade sections, in which the thrust (dT) and torque (dQ) in differential form are expressed based on lift (C_L) and drag (C_D) coefficients as:

$$dT = B\frac{1}{2}\rho U_{rel}^2 (C_L \cos\varphi + C_D \sin\varphi) c dr \quad \textbf{(4-3)}$$

$$dQ = B\frac{1}{2}\rho U_{rel}^2 (C_L \sin\varphi - C_D \cos\varphi) c r dr \quad \textbf{(4-4)}$$

B is the number of blades, U_{rel} is the local relative velocity, c and r are the blade local chord and radius respectively. To find the induction factors a and a', the above thrust and torque equations are equated which result in:

$$a = 1/\left(1 + 4F\sin^2\varphi/(\psi C_L \cos\varphi)\right) \quad \textbf{(4-5)}$$

$$a' = 1/\left(4F\cos\varphi/(\psi C_L) - 1\right) \quad \textbf{(4-6)}$$

where $\psi = Bc/2\pi r$ is the local solidity ratio and $\varphi = \delta + \alpha$; in which α is the local angle of attack and β is the local blade twist. The drag coefficient was assumed to be zero in calculating the induction factors. The inputs of the BEM model include lift and drag coefficients, blade geometry, number of blades and tip speed ratio. The lift coefficients for each section can be calculated using local tip speed ratio (λ_r), local solidity ratio and the relative flow angle (φ) as given in equation (4-7).

$$C_L = 4F\sin\varphi(\cos\varphi - \lambda_r \sin\varphi)/\sigma'(\sin\varphi + \lambda_r \cos\varphi) \quad \textbf{(4-7)}$$

The lift coefficient and angle of attack for each blade section are achieved from the intersection of the C_L curve, obtained from equation (4-7), and the experimental lift curve with respect to the angle of attack. Then, the axial and angular induction factors at each blade section can be calculated. Once a and a' are known power and thrust coefficients can be computed using differential equations (4-8) and (4-9).

$$dC_P/d\lambda_r = \left(8/\lambda^2\right) F \lambda_r^3 a'(1-a)(1-(C_D/C_L)\cot\varphi) \quad \textbf{(4-8)}$$

$$dC_T/d\lambda_r = \left(2/R^2\right)\psi r(1-a)^2 (C_L\cos\varphi + C_D\sin\varphi)/\sin^2\varphi \quad \textbf{(4-9)}$$

where F is tip loss correction factor which is expressed as equation (4-10)[19].

$$F = (2/\pi)\cos^{-1}\left[\exp\left(-(B/2)(1-r/R)/((r/R)\sin\varphi)\right)\right] \quad \textbf{(4-10)}$$

The thrust coefficient of the hub and the root of the blade were added to the blade thrust coefficient to find the total C_T of the rotor using the drag coefficients of semi-sphere, $C_{D,hub}$ = 0.42, and cylinder, $C_{D,root}$ = 1.7 [21].

Accounting for Sheared Inflow

In this work, Walker et al's [21] BEM model was modified using MATLAB to take different, non-uniform flow profiles into consideration. The modified BEM was able to mathematically model the turbine in the CWC and improves our understanding of the effect of ambient characteristics of the flow on the performance of the HAMCTs. In the model, the shear flow profile from Fig. 3.7 in Chapter 3 was inserted as an input and the influence of shear in the code was made by changing the local angle of attack (AoA) as a result of the change in the local relative velocity. The Reynolds number, Re_c, in this paper is calculated based on the blade chord length and Re_{c70} refers to chord length at 70% of the span.

Accounting for Variation in Reynolds Number

In reality, the Reynolds number varies along the blade span due to the varying relative velocity. Conventional BEM theory models do not account for this and assume a single Reynolds number when assigning the lift and drag coefficients at each blade section. In order to account for Reynolds number variation in the BEM calculations, QBlade software [91] was employed to model the 800 mm turbine. Although this software was developed for wind power modelling, it can also be used for hydrokinetic turbines.

The first step in the QBlade model was to estimate the lift and drag curves, using integrated XFoil predictions in the software, in the range of $0.8 \times 10^5 < Re_c < 5 \times 10^5$ for AoAs from -5° to 25°. Fig. 4.1 shows the lift coefficients estimated by the QBlade, which are compared to the fitted experimental curve from [21]. As can be seen there is good agreement among the curves for AoAs before stall, where around and after the stall the 2D wind tunnel has slightly higher values. It may result in different predictions of power coefficients by the QBlade and the BEM model. In addition, an instability can be seen in the C_L values estimated by QBlade for $Re < 2 \times 10^5$. The Montgomerie procedure was then applied to extrapolate the lift and drag curves over

360º of AoA [92]. The 2-bladed rotor was modelled in the software using the turbine geometry from Table 1.1 in Chapter 1. In the model, each blade section was set by previously computed lift and drag data based on the Reynolds number, as shown in Fig. 4.1. As can be seen, there are unstable C_L predictions for low Reynolds numbers. These curves only were used by the QBlade in some low TSRs for sections closer to the root of the blade where the Re is smaller. Thus, the QBlade predictions are more reliable for the optimal operational condition and mostly for TSRs higher than 5. Then, in the QBlade software, an iterative BEM analysis was performed using a convergence criterion of 0.001 and a relax factor of 0.3. Different graphs can be plotted from the analysis, such as C_P and C_T curves. Prandtl's correction factors were utilised to account for the root and tip losses of the blades [93, 94].

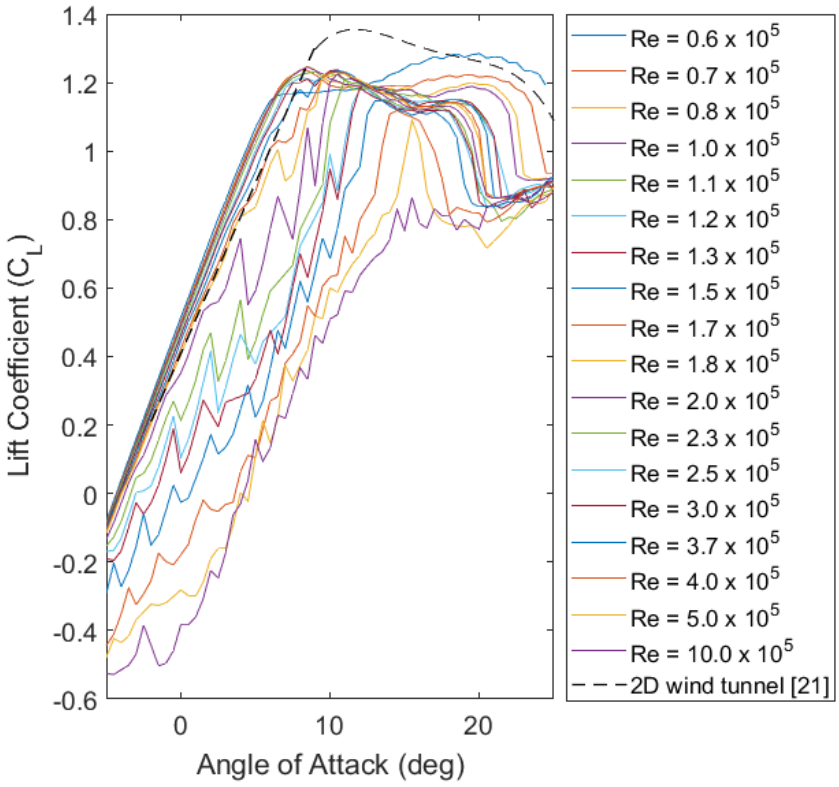

Fig. 4.1. Comparing Lift coefficient of NACA63-618 estimated by the QBlade with the 2D wind tunnel [21]

An approach for 3D correction was used in the QBlade model using the Viscous Inviscid Interaction Method developed by Snel, et al. [95] to correct the model for using 2D lift coefficient data in the calculation of a 3D model. The performance prediction of the 800 mm turbine was performed for flow velocities of 1, 1.3 and 2 m/s to investigate the effect of Reynolds number on the results. The results were validated using the CWC results. The full-

scale turbine was also modelled to provide an estimate of ultimate power production at 2 and 3 m/s of flow velocity.

4.3. Results and Discussion

4.3.1. Modified BEM Model for shear

The original MATLAB BEM model [21] was modified to account for the effect of shear flow on the performance evaluation of the larger turbine in the CWC as described in Section 4.2.1. The results are plotted in Fig. 4.2. Aside from the slightly higher C_P values of the BEM model with shear at TSR > 7, no major changes are seen compared to the basic BEM curve. The main reason is that BEM theory calculates parameters in annular sections, over which the average flow velocity does not vary significantly for the shear flow at the CWC. Thus, the effect of shear on the angle of attack and consequently lift coefficient will be minimised in the calculations. The discrepancy of the two BEM models with the CWC results is not significant, e.g. ~ 6% at TSR = 6.5.

4.3.2. Effect of Scaling and Reynolds Number

QBlade Results

The C_P curves from the QBlade calculations of the 800 mm turbine model as well as the full-scale turbine with a diameter of 16 m are also depicted in Fig. 4.2. This figure provides a better understanding of the effect of Reynolds number on the results. Different Reynolds numbers over the blade sections due to the variation in relative flow velocity and chord length were considered in the QBlade estimations. The QBlade predictions for an inflow velocity of 1.3 m/s were in good agreement with the CWC results, especially for TSRs < 6.5. The QBlade results for the scale model and the full-scale turbine at 2 m/s are slightly higher than the CWC results at 1.3 m/s for TSRs < 7. At an inflow velocity of 1 m/s, QBlade predicted lower C_P values due to lower lift coefficients at Reynolds numbers lower than 2×10^5. No further increase was observed in the QBlade predictions of C_P by increasing the flow velocity more than 2 m/s. Compared to the BEM models, QBlade at an inflow velocity of 1.3 m/s predicted slightly higher C_P values for TSRs lower than 7 and then smaller power coefficients for higher TSRs. However, they are generally in good agreement with each other. It shows that using local sectional Reynolds numbers in the BEM prediction may be not worth the effort to achieve more accurate results compared to the model with a single reference Reynolds number. This is consistent with the outcomes from Koh and Ng [20]. It can be said that the BEM model with a

reference Reynolds number is accurate enough to predict the performance when the turbine is assessed in a condition with *Re* independency.

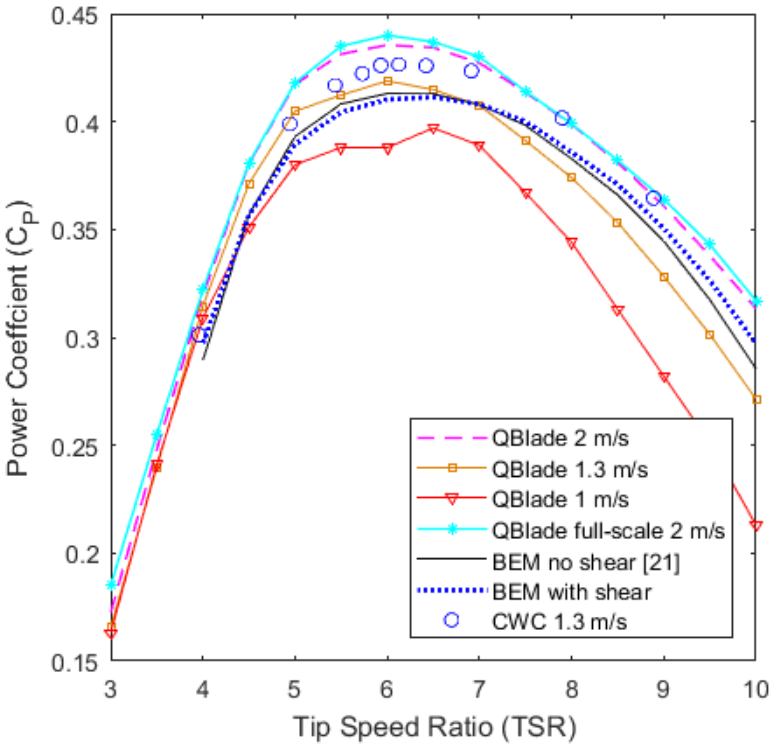

Fig. 4.2. Accounting for Reynolds number and shear inflow in of the turbine performance evaluation using BEM predictions and QBlade

CFD Results

The CFD approach explained in Chapter 2 was also employed to investigate the effect of scaling and Reynolds number on the evaluation of turbine performance. The simulations were implemented on the smaller turbine at inflow velocities of 1.25 m/s and 2 m/s as well as for the larger turbine at 2 m/s. Fig. 4.3 shows the C_P and C_T curves from these simulations together with similar towing tank results. For the smaller turbine, the simulation results at 1.25 m/s match with the towing tank test results at the same speed. By increasing the inflow velocity to 2 m/s the CFD C_P values increase as well, similar to what happens in the towing tank results. For the larger turbine although the CFD values are less than the experimental results, it is still higher than the smaller turbine CFD curve. The CFD prediction for the full-scale turbine is a better fit for the larger scale model towing tank results at 2 m/s for the entire range of TSRs. As can be seen, the maximum C_P of full-scale turbine is 0.44 occurring at TSR ~ 7. The CFD approach gives similar conclusions to both the experimental and theoretical methods about the effect of scaling and Reynolds number on the performance evaluation.

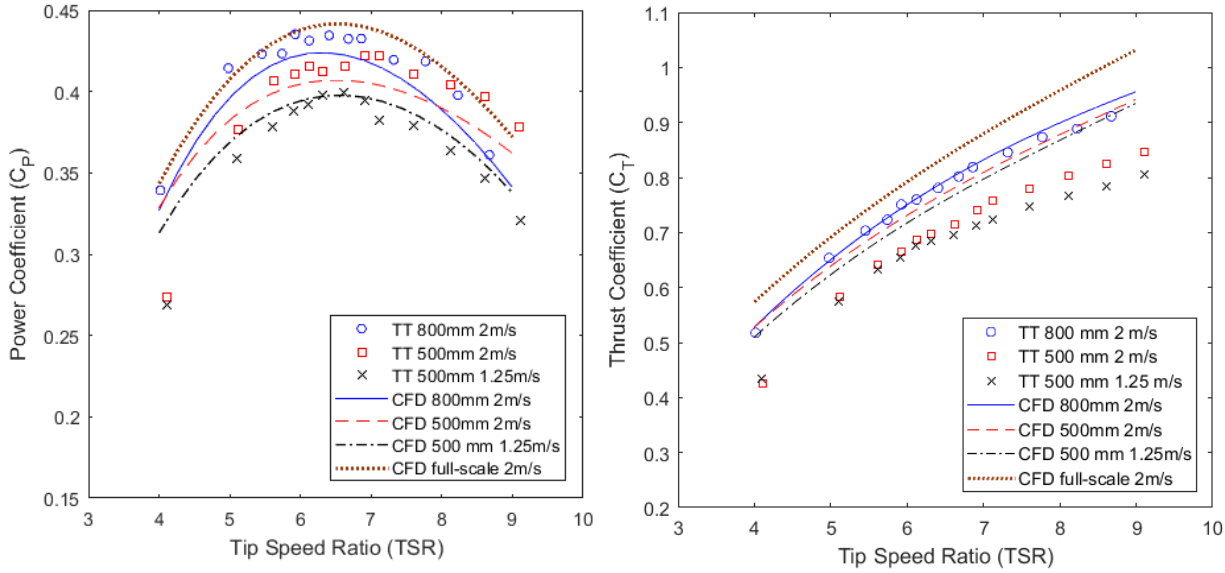

Fig. 4.3. Accounting for scale effect in the turbine performance assessment using CFD simulations

4.4. Comparison of Turbine Performance Evaluation Methodologies

The different turbine performance assessment methods are compared in Fig. 4.4 for the 800 mm diameter turbine model. In this figure, the CFD simulations (Chapter 2) and the towing tank experiments (Chapter 3) are presented at an inflow velocity of 2 m/s and the CWC experiments (Chapter 3) are presented at the maximum inflow velocity in that facility of 1.3 m/s. All the presented results are blockage corrected. The experimental results from Walker, et al. [21] at the United States Naval Academy are also shown for comparison. The curve from the theoretical BEM model (Chapter 4) is based on the MATLAB calculations using lift and drag coefficients from the 2D wind tunnel tests from [21] and the flow velocity profile of the CWC.

Both the CFD and the BEM model underestimated the maximum C_P by ~ 7%, compared to the towing tank and the CWC results, respectively. The maximum power coefficient of the 800 mm diameter scale model was 0.44 at TSR ~ 6.5 in the towing tank and 0.42 at TSR ~ 7 in the CWC. The experimental results were affected by facility bias due to different flow conditions and blockage ratios. Flow conditions in the towing tank were uniform and steady, whilst in the CWC the turbine was tested under a shear flow profile and with turbulence. The unsteadiness in the CWC was due to presence of the tank pumps and arguably provided conditions more similar to the flow conditions at a real deployment site than the towing tank. However, since the towing tank provides an ideal condition for testing, it is possible to study

the effect of a single parameter, such as submergence depth, wave, blockage and boundary proximity, without the interference of shear and turbulence.

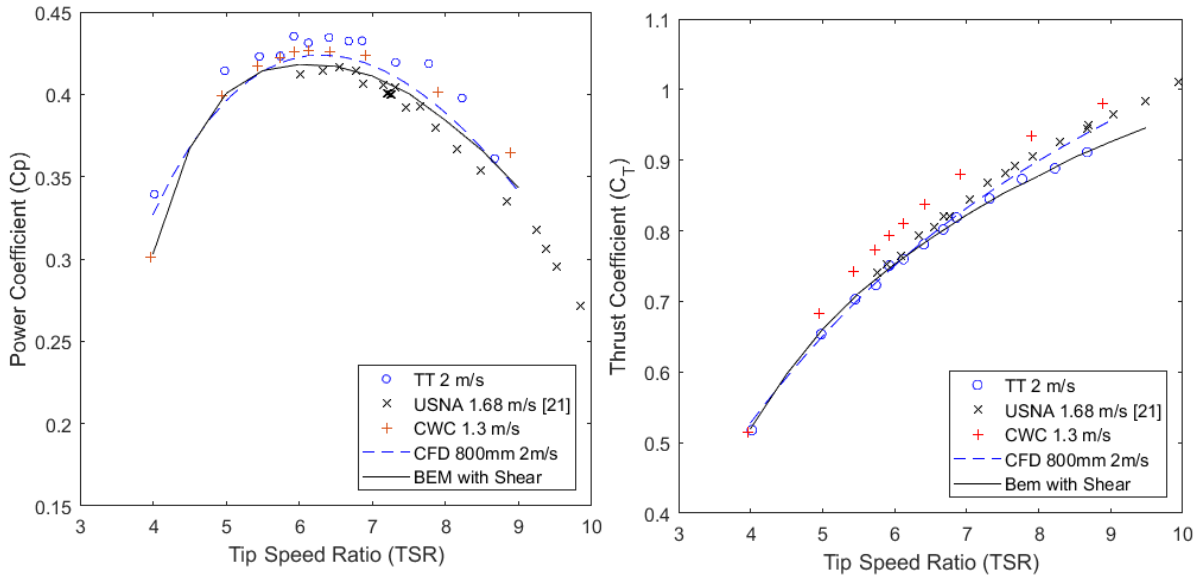

Fig. 4.4. Comparing the methods employed for performance evaluation of 800 mm turbine

In addition, the size of facility can limit the selection of scale model size, where the blockage ratio is high, e.g. 10% for the 800 mm scale model in the towing tank. Comparing the two scale models results in the towing tank, after blockage correction and where Reynolds number independency was achieved showed that even though the performance curves were generally similar, the larger turbine had larger C_P values, approximately 5% higher at TSR ~ 6, than the smaller model. Interestingly, the C_P results of the 500 mm turbine in the AMC towing tank match with the USNA results of 800 mm model, where blockage effect were negligible in the two facilities. It can be inferred that the 500 mm model was a better option for test in the AMC towing tank. On the other hand, since the maximum inflow velocity in the CWC was 1.3 m/s, the Reynolds number independency was not achievable for the smaller scale model. Thus, for test in the CWC the 800 mm turbine was the better choice. Overall, although the experimental method provides reliable performance results, the influence of various parameters associated with this approach should be carefully accounted for in analysing the results.

The CFD results revealed that, in the absence of blockage, the scale effect is primarily related to Reynolds number. The difference between the CFD and the experiments concerning the scale effect was the influence of blockage in the experimental results, even after blockage correction, which also extended the discrepancy between the two scale models performance

curves. The external domain in the CFD model was set large enough to have no blockage effect on the turbine performance. It shows the advantage of CFD in characterising the turbine hydrodynamics by varying a single parameter, while others are controlled. Compared to the BEM theory, CFD has shown to be an appropriate tool for studying the effect of various parameters, such as flow unsteadiness, on the turbine hydrodynamic characteristics [32, 35, 58, 96]. Therefore, the validated numerical model was developed to study the effect of shear flow profile, submergence depth and wave on the turbine performance, presented in the next Chapter.

Overall, considering the uncertainty of the experimental results, the CFD and BEM were quite successful in predicting the maximum power prediction of the turbine. Thus, the validated numerical and theoretical models were employed to predict the ultimate power production of the full-scale turbine with 16 m diameter. Based on QBlade results, in ideal conditions the turbine at TSR ~ 6 can generate 0.37 MW and 1.25 MW for inflow speeds of 2 m/s and 3 m/s, respectively. This shows the importance of the deployment site flow velocity in terms of power production. The results from CFD simulation showed maximum power output of 0.37 MW at inflow speed of 2 m/s.

In addition to the above discussions, the different methodologies can be compared in terms of the relative ease of use as well as the associated cost and time for the performance assessment of a HAMCT. QBlade was the easiest tool to provide quick and fairly accurate performance predictions. BEM theory was the next easiest method to use; however, the accuracy of the result depends on the lift and drag coefficients employed in the code, which in the case of using experiments to determine these coefficients, the cost and time of the method will increase.

Conversely, achieving a reliable CFD model that can assess the performance of a turbine can be challenging. There are many parameters involved in the CFD modelling, from generating grids to solver setup, which must be considered in order to have a trustworthy CFD model. However, once the model is validated it provides detailed information about the hydrodynamics of the turbine that cannot be achieved by the other methods. CFD also provides the ideal platform to account for various environmental parameters, which affect the turbine performance, such as shear velocity, turbulence and surface waves. The cost and time needed to employ this method depend on the commercial package cost and the availability of High Performance Computing (HPC) systems.

The experimental method is the most appropriate way for establishing if a parameter has an impact on an outcome. Experiments play an essential role in the performance evaluation of HAMCTs by providing performance data in realistic conditions and validating the results of the theoretical and numerical methods, BEM and CFD. However, there is no doubt that the experimental method is the most expensive method of those assessed. It is susceptible to possible failures during testing, which would add on to the cost and time as well as human error. In addition, the experimental results are affected by the test conditions limiting the applicability of the results. Other factors, such as availability of testing facility, required equipment and technical support, influence the time and cost of an experiment.

4.5. Conclusion

A Blade Element Momentum theory (BEM) model was modified to account for the effect of shear flow in the performance evaluation of the larger turbine (800 mm diameter) in the CWC. Although the BEM C_P curve is in good agreement with the experimental curves for TSRs < 6, it is a better fit for the USNA results for the entire range of TSRs. The main impact of shear on the performance of the turbine was a change in input power, kinetic energy flux, as well as a cyclic effect on the loadings with no significant influence on the mean power output. BEM theory employs annular sections over the rotor swept area to calculate different parameters, which reduces the effect of shear in the model.

The study of Reynolds number effect on the performance using the QBlade software showed an increase in C_P curves with augmentation of the flow velocity and associated Reynolds number. Comparing the BEM model and the QBlade results revealed that using lift and drag coefficients from a single reference Reynolds number is accurate enough and the use of a local sectional Reynolds numbers for performance prediction is unnecessary. Compared to the experimental method, BEM theory is a quicker and cheaper tool for performance prediction of HAMCTs under steady conditions. The accuracy of BEM results was reasonable in condition with Reynolds number independency. It can also investigate the effect of Reynolds number on the turbine performance, provided lift and drag coefficients are available over a range of Reynolds numbers, whether using experimental data or XFoil predictions.

A steady state CFD model was employed to simulate the larger turbine model. A reasonable correlation was seen between the CFD and experimental results, which validates the CFD model to be used for predicting the full-scale turbine performance. The CFD model was

developed to study the effect of scaling on the performance results. The effect of scaling was found to be due to Reynolds number, where the larger turbine with higher Re had higher C_P values. However, this discrepancy between the two scale model C_P curves was higher in the experimental results due to the presence of blockage.

The experiments in the towing tank provided the turbine performance in the steady flow condition. The larger turbine was under high blockage effect in the towing tank where even after correction the results were higher than the smaller turbine. The intrinsic shear flow profile with turbulence in the CWC provided a condition more similar to the real environment. However, Reynolds number independency for the 500 mm turbine was not achieved, given the limitation in the maximum facility flow speed.

This Chapter compared experimental results from three different facilities, a theoretical model and CFD. Each method was able to predict the performance of the turbine and has its place in the performance analysis of HAMCTs. BEM and CFD can be done at the desktop and can provide detailed information about the flow through the turbine and the associated torque and loads on the turbine assembly. However, these theoretical and numerical models must be compared with experimental results to be valid.

Despite the ability of QBlade and BEM in providing quick and fairly accurate performance predictions, the underlying XFoil predictions of lift and drag coefficients are only acceptable in the expected operating range and provide poor results elsewhere. If available, it is recommended that experimental lift and drag data are used to validate the XFoil predictions, hence providing a more reliable tool for performance prediction of HAMCTs.

Achieving a reliable CFD model for the performance assessment of a turbine can be challenging due to the parameters involved in the numerical modelling, from generating grids, to solver setup. However, once the model is validated it provides detailed information about the hydrodynamics of the turbine that cannot be achieved by the other methods.

The experimental results are affected by the test conditions limiting the applicability of the results. However, experiments play an essential role in the performance evaluation of HAMCTs by providing performance data in realistic conditions and validating the results of the theoretical and numerical methods, BEM and CFD

Chapter 5

The Influence of Shear Flow and Waves on the Performance Characteristics of a Horizontal Axis Marine Current Turbine

This chapter has been submitted for publication in the Journal of Applied Energy, and at the time of writing is under review. The citation for the research article is:

Rahimian M, Walker J, Penesis I. The influence of shear flow and waves on the performance characteristics of a horizontal axis marine current turbine. *Journal of Applied Energy*. 2018.

5.1. Introduction

Turbine performance is influenced by various parameters, such as the flow condition of deployment site, which may be different from that the turbine was designed. Thus, it is crucial to ensure that the performance of a turbine is optimal for a particular site during the primary design stages. Various flow conditions that a turbine may experience are shear velocity profile due to seabed friction, change in flow direction, turbulence and fluctuations in the flow, depth variation and surface waves. Although there are some studies striving to assess the effect of these conditions on the turbine performance, more investigation is required to address the influence of each flow condition as well as interaction of them on the hydrodynamic characteristics of HAMCTs.

Xu [57] utilised the viscous/potential flow method to numerically simulate a marine turbine in non-uniform flow. He reported an overall reduction of efficiency when the turbine is subject to a shear velocity profile, due to a drop in the mean velocity of the effective wake. A method was developed by Forbush, et al. [49] to account for sheared flow in the performance assessment of a cross-flow hydrokinetic turbine. They proposed temporally- and spatially-averaged inflow velocities in the performance analysis to achieve consistent results. Lewis, et al. [97] characterised the vertical profile of the flow at two tidal sites using Acoustic Doppler Current Profiler (ADCP). They utilised a 3D tidal model to extrapolate the simulated profile to all potential tidal sites in the Irish Sea. They described the high temporal variability of the flow by generalised extreme value theory. They found that it is important to include a roughness coefficient to describe the spatial variation of the flow.

Adamski [98] specifically performed a numerical investigation on the operating characteristics of a horizontal axis marine current turbine in presence of the free surface using computational fluid dynamics (CFD). They employed the virtual blade model and volume of fluid methods to model the turbine performance near the free surface. They concluded that the effect of the free surface is related to an increase in the blockage ratio and constraint of the wake expansion. Moreover, little variation was observed in power coefficient at low blockage ratio because of the change in vertical position of the turbine. Kolekar and Banerjee [39] studied the effects of Reynolds number, blockage, and surface proximity on the performance of a hydrokinetic turbine. They observed an enhancement in performance when decreasing the immersion depth of the turbine. However, performance decreased when the tip clearance to the

free surface was less than half the rotor radius, where the free surface restricted the wake expansion and propagation process.

Lust, et al. [51] and Luznik, et al. [99] performed experimental studies on the impact of surface waves on the performance characteristics of scale model tidal turbines. Experiments yielded similar average power coefficients for conditions with and without waves. However, the instantaneous power generation and blade loadings were significantly affected by the waves. They identified a correlation between the wave vertical velocity and the measured torque. In an investigation by Galloway, et al. [52] on the effect of waves and rotor misalignment on tidal stream turbines, it was found that the wave frequency had more of an effect on the blade loading than the wave height. Although yaw loadings are not comparable to wave loadings, they still reduce power and thrust captured by rotor. Bai, et al. [36] employed an immersed boundary method to simulate the performance of a marine current turbine. They used two free surface models to investigate the impact of surface waves on the turbine. They validated the models with published experimental results. Noruzi, et al. [35] carried out a numerical study on the effect of wave and depth on a marine turbine performance. They found that when the turbine installation depth is less than 20% of the total water depth, gravity waves play an important role in the turbine performance. Tatum, et al. [42] studied the effect of waves on a tidal turbine's characteristics. They found that the magnitude and period of changes in power and thrust depend on the wave parameters. They recommended the inclusion of waves in marine turbine models in conditions where turbine is positioned in a depth less than half of the wavelength.

In this Chapter, a CFD model was developed using two numerical methods to account for shear, surface waves and free surface proximity. These two CFD models were compared to find the best numerical approach for turbine performance studies under the above-mentioned conditions. Results from the CWC experiments in Chapter 3, were utilised to validate the CFD models for shear. The towing tank results at the Australian Maritime College (AMC) [54] were employed for depth and wave model validation. Finally, the hydrodynamic characteristics of the HAMCT were assessed under different waves, shear flow profiles and submergence depths using the experimentally validated CFD model.

5.2. Numerical Models

In this work, the influence of four operating conditions (case studies) on the turbine performance were investigated using CFD modelling. The CFD boundary conditions were set according to the study case. The first case investigated the effect of shear flow velocity profile (shear case). The second case was designed to study the effect of free surface proximity (depth case). The third case was to find the influence of surface waves (wave case). The final case was defined to investigate the interaction of shear and waves on the performance of the turbine (shear-wave case). Two CFD approaches, single-phase and volume of fluid models were employed in this Chapter to model the above case studies.

5.2.1. The Single-Phase Model

The CFD approach recommended in Chapter 2 was employed to setup the single-phase (SPh) model. Water was the only fluid considered in the model. Two domains were generated around the rotor. The cylindrical inner domain was to provide the turbine rotation, located 2 m from inlet, and the other domain to resemble the testing tank. The aim was to validate the CFD model using experimental data from the two testing facilities of the Australian Maritime College (CWC and towing tank). Thus, the outer domain of the numerical model was set at 10 m long; however, the width and the depth changed according to the cross-sectional size of the actual testing tanks. A region with 0.5 m height was considered on the top of the outer region to account for the upper area of the free surface in all simulations. The domains together with the boundary conditions are shown in Fig. 5.1. A hybrid mesh method was used to generate grids over the model. A structured mesh was used over the turbine blades surfaces with higher resolution over the leading and trailing edges; together with prismatic elements for inflation layers, providing $Y^+ \sim 30$. This range of Y^+ enables the *k-ω* SST turbulence model to use the wall function model for flow calculations over the wall. Other regions were discretised using tetrahedral grids. The total number of approximately 4.5×10^6 grids was found to be optimal based on the mesh independency study.

The Reynolds-averaged Navier-Stokes (RANS) method was selected to solve the equations of continuity and momentum conservation. ANSYS CFX R15.0 was employed to setup the solver. The second order backward implicit scheme and a high-resolution scheme were utilised to discretise the time derivative and advection terms, respectively. Since the angular position of the blades is important due to the non-uniformity of the flow in both the shear and wave

cases, the sliding mesh method was utilised to simulate the rotation of the turbine. However, prior to that a moving reference frame (MRF) technique was used to generate initial data for the sliding mesh simulations. This reduces the required computational time to achieve convergence in the transient solution [100]. Transient solutions were performed with a total time of 20 s and time step of 0.01 s. The use of smaller time steps showed no significant effect on the results. The sidewalls and the bottom were set as free slip walls. The outlet and the top boundary were modelled as an entrainment opening, able to endure possible reverse flow in the boundary, with zero relative pressure. The inlet flow velocity and turbulence intensity were set according to each case study condition.

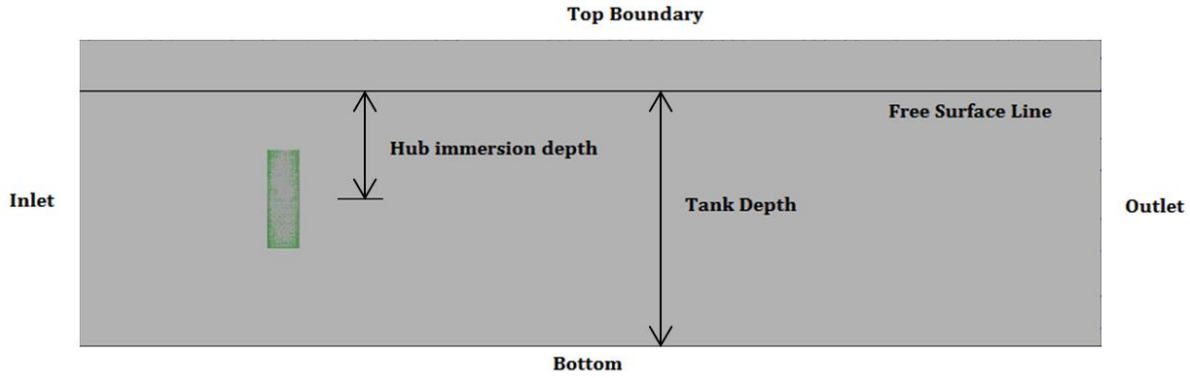

Fig. 5.1. The domains of the CFD model and the boundary conditions

5.2.2. The Volume of Fluid Model

It is known for HAMCTs that the turbine rotor should be positioned closer to the free surface where the flow has usually higher velocity [101]. Therefore, it is important to investigate the effect of the free surface on the performance of the turbine. The volume of fluid (VOF) method was selected to model the free surface in the CFD turbine model. The VOF model is based on an Eulerian approach for volume-tracking the fluid passing through a single grid [102]. The model considers the effect of buoyancy using a density difference method. The model setup was based on the SPh model with some differences due to the volume fractions of air and water in the outer domain boundaries. The top boundary had a water volume fraction of zero. The inlet was divided into a water inlet with water height of the actual testing tank and an air inlet with a height of 0.5 m. The downstream pressure profile, due to the effect of gravity on the fluid, and volume fraction at the outlet were defined using user defined functions.

5.2.3. Wave and Shear Modelling

The wave study was performed using both the VOF model and the SPh. The stretched linear wave theory was employed to model the waves in simulations to represent the non-linearity of the waves because of their high amplitude, see [103] for the theory details. User defined functions were utilised to specify the wave velocity at the inlet using equations (4-1) and (4-2):

$$u_{wx} = \omega_w A_w \frac{\cosh(kz)}{\sinh(kH)} \cos(\omega_w t) \quad \textbf{(5-1)}$$

$$u_{wz} = \omega_w A_w \frac{\sinh(kz)}{\sinh(kH)} \sin(\omega_w t) \quad \textbf{(5-2)}$$

where k, ω_w and A_w are the wavenumber, the angular frequency and the amplitude of wave. H is the depth and z is vertical distance from the bottom. Velocity in y-direction was set to zero. The Dissipation Relation was used to determine the wave number k as in equation (5-3):

$$\omega_w^2 = gk \tanh(kH) \quad \textbf{(5-3)}$$

To study the effect of shear velocity profile on the turbine performance using the CFD models, the velocity U_z at height z from the bottom was set using equation (5-4) [104]. Various power laws (γ) and roughness coefficients (β) present different velocity profile. H is the total water depth and $\bar{U}$ the depth averaged velocity. The velocity across the inlet width was presumably constant.

$$U_z = \left(\frac{H - z}{\beta H} \right)^{1/\gamma} \bar{U} \quad \textbf{(5-4)}$$

To add the shear case to the wave model, the velocity profile was specified using a simple power law defined in equation (5-4) in a way that the flow speed at the hub was equal to the condition without shear.

5.2.4. Validation

To validate the model for the shear case, the velocity profile data from the ADV measurements in the CWC, shown in Chapter 3 Fig. 3.7, were inserted at the inlet with a turbulence intensity of 10%. Simulations were run at TSR ~ 6 and 7 for three different hub immersion depths of 0.5 m, 1.1 m and 1.6 m.

The results from the towing tank experiments conducted by Sos, et al. [54] were used for validating the waves and depth case models. Their experiments were conducted in the AMC towing tank on the 500 mm diameter turbine model. Two hub immersion depths of 0.31 m and 0.76 m were selected for simulation at an inflow velocity of 1.25 m/s and TSR = 6.5. The parameters of the wave applied for validating the CFD simulations of the 500 mm scale model are outlined in Table 5.1.

Table 5.1. Characteristics of case studies applied to the turbine in CFD simulations

Case	U (m/s)	Depth (m)	Period (s)	Height (m)	Comment
w1 (validation)	1.25	0.31, (0.76)	1.7	0.07	Same wave parameters as [54], TSR = 6.5
w2	1.25	0.31	4	0.07	-
w3	1.25	0.31	1.7	0.15	-
s (validation)	1.3	0.5, 1.1, 1.6	-	-	Velocity profile data from ADV (Chapter 3)
s1	1.25	0.31, 0.76	-	-	$\beta = 1$, $\gamma = 7$
s2	1.25	0.31, 0.76	-	-	$\beta = 1$, $\gamma = 9$
w1 + s1	1.25	0.31, 0.76	1.7	0.07	$\beta = 1$, $\gamma = 7$
w1 + s2	1.25	0.31, 0.76	1.7	0.07	$\beta = 1$, $\gamma = 9$

5.3. Case Studies

To study the impact of changing depth as a wave passes a turbine, the validated CFD model was utilised to simulate the turbine in a submergence depth of 0.31 m. Moreover, to study the effect of changing the wave period and wave height, two other wave cases were simulated as outlined in Table 5.1. The wavelength was calculated for each waveform using equation (5-3). For the shear effect study, two velocity profiles were added to the inlet using a power law with $\gamma = 7$ and 9. The roughness coefficient (β) was considered to be 1. The flow velocity at the hub was 1.25 m/s. The interaction of shear and waves was also studied by introducing the above shear velocity profiles to the case w1. Since the simulations were performed in a confined domain with the same cross-sectional dimension as the AMC towing tank, the presented computational results for C_P and C_T were corrected for blockage using the method proposed by [25]. As an example, the blockage correction resulted in 2.5% and 1.5% reduction in C_P and C_T at TSR = 6 for the towing tank simulations, respectively.

5.4. Results and Discussion

5.4.1. CFD Model Validation

Validation for Shear Flow Profile

Fig. 5.2 shows the Single Phase model results at TSR ~ 6 and the VOF results at TSR ~ 7 from the turbine simulation when the CWC velocity profile was set at the inlet. The fitted curve from the CWC experiments at the depth 1.1 m was plotted for comparison. Fig. 5.2a shows the C_P and C_T values calculated using the flow velocity at the hub and Fig. 5.2b shows values obtained using equivalent flow velocity. Using the equivalent flow velocity led to a better correlation of the CFD results with the experiments. The SPh model under-predicted the turbine performance compared to the experimental curve; whilst the VOF model overestimated the C_P values for immersion depths of 1.1 m and 0.5 m. The maximum discrepancy of the CFD models and the experimental results was approximately 6%; thus, both the CFD models were in good agreement with the experiments. The VOF model was employed in this work to study the effect of shear cases, using a power law with γ of 7 and 9, on the performance of the turbine. The reason for this selection is related to the ability of the two CFD models in wave and free surface modelling, explained later in this Chapter.

Validation for Submergence Depth

Since the SPh model is not able to capture the effects of the free surface, only the VOF model was utilised to study the impact of free surface proximity on turbine performance. The turbine power coefficients predicted by the VOF model in the two hub immersion depths are plotted in Fig. 5.3. The fitted experimental curve was plotted based on the results obtained at a depth of 0.31 m by [54]. The VOF result at a depth of 0.31 m collapses on the experimental curve, while a slight increase in C_P can be seen for the depth of 0.76 m. Power coefficient's of approximately 0.421 and 0.414 were predicted by the VOF model at a depth of 0.76 m and 0.31 m, respectively, a discrepancy of ~1.6%. Fig. 5.4a shows the pressure coefficient over the blade at an angular position of zero. As can be seen, the pressure difference between the two sides of the blade, accounting for the blade loadings, reduces by decreasing the proximity to the free surface. The results from the VOF model are consistent with a reduction in the power coefficient reported by Sos, et al. [54], Kolekar and Banerjee [39] when the tip immersion depth is less than half of the turbine radius.

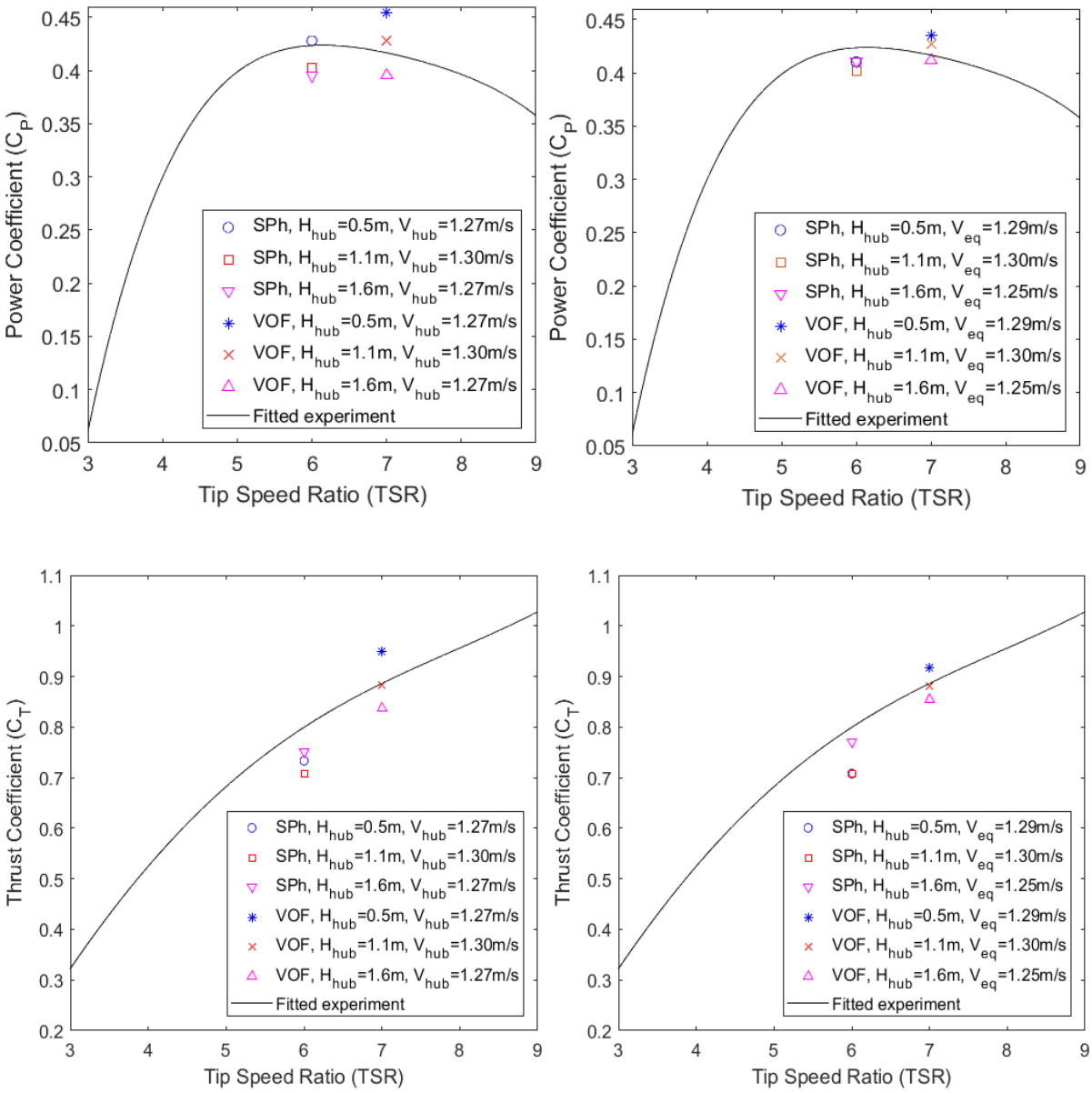

(a) Hub flow velocity **(b) Equivalent flow velocity**

Fig. 5.2. Validation of the single-phase and the VOF model for shear using fitted experimental curve at 1.1 m depth (case s from Table 5.1)

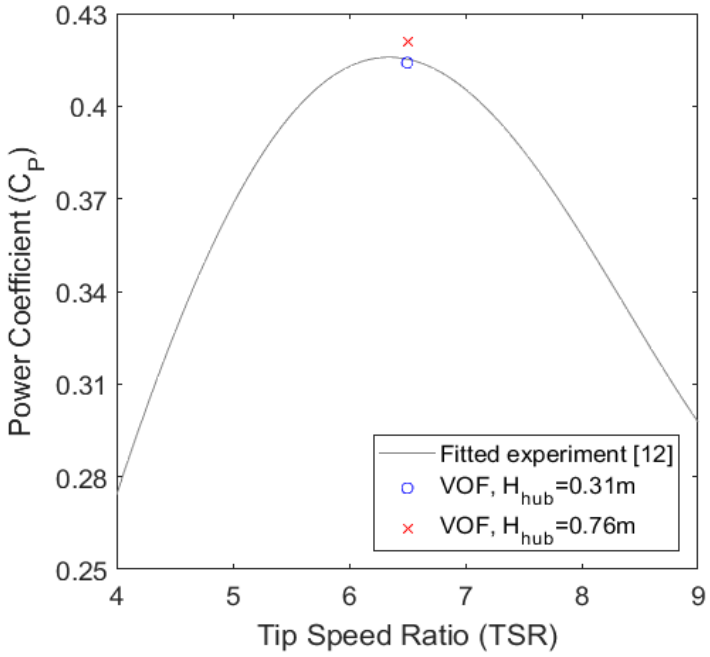

Fig. 5.3. The VOF model validation for depth case using AMC towing tank results

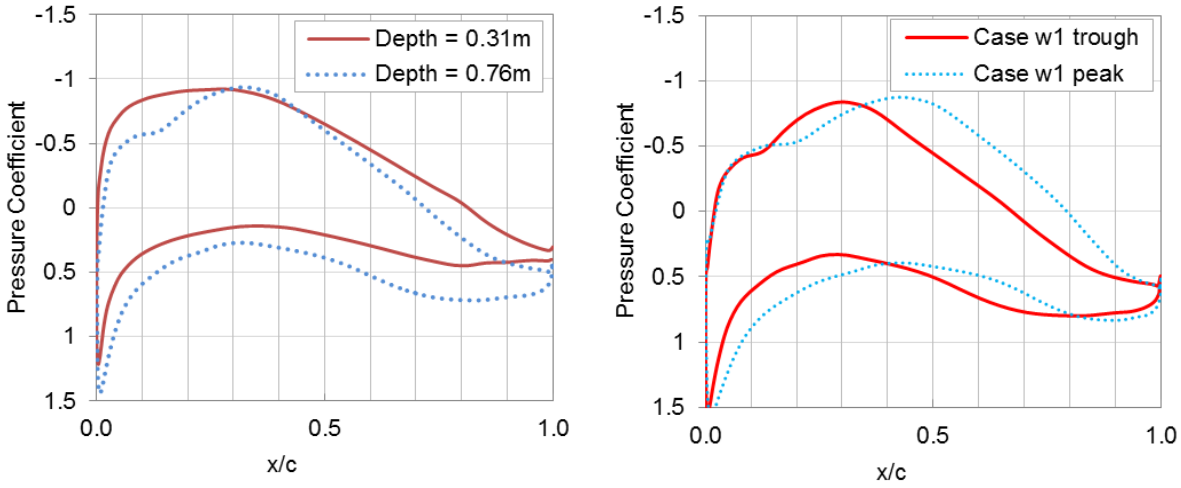

(a) Depth effect **(b) Wave Effect**

Fig. 5.4. Pressure coefficient over the turbine blade (a) at two immersion depths and (b) under case w1 at depth of 0.76 m

Fig. 5.6 shows the VOF results for torque over each blade and the resultant torque during a simulation for the two submergence depths. As can be seen torque over a blade is periodic due to the vertical gradient of the hydrostatic pressure and the free surface effect accounted in the VOF model over one rotation. The cyclic fluctuation on a blade is 2.3% and 24.1% of the mean torque for 0.76m and 0.31m of submergence depth, respectively, as presented in Table 5.2. The blades experience a larger variation in torque for a smaller proximity to the free surface where the rotor deforms the free surface, shown in Fig. 5.5 for the depth of 0.31 m. The difference between the crest and trough of the surface deformation behind the rotor with the surface level

was 0.057 m and 0.041 m, respectively. The deviation of the turbine resultant torque for 0.31 m of depth is ~2.6%. Similar behaviour was observed for thrust. The minimum torque and thrust on a blade occur when the blade is close to the free surface before the angular position of 90^{o} from the horizontal axis.

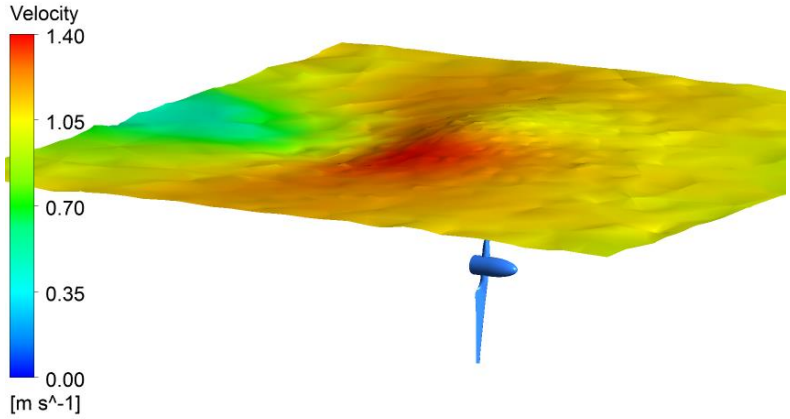

Fig. 5.5. Free surface deformation due to the turbine rotation

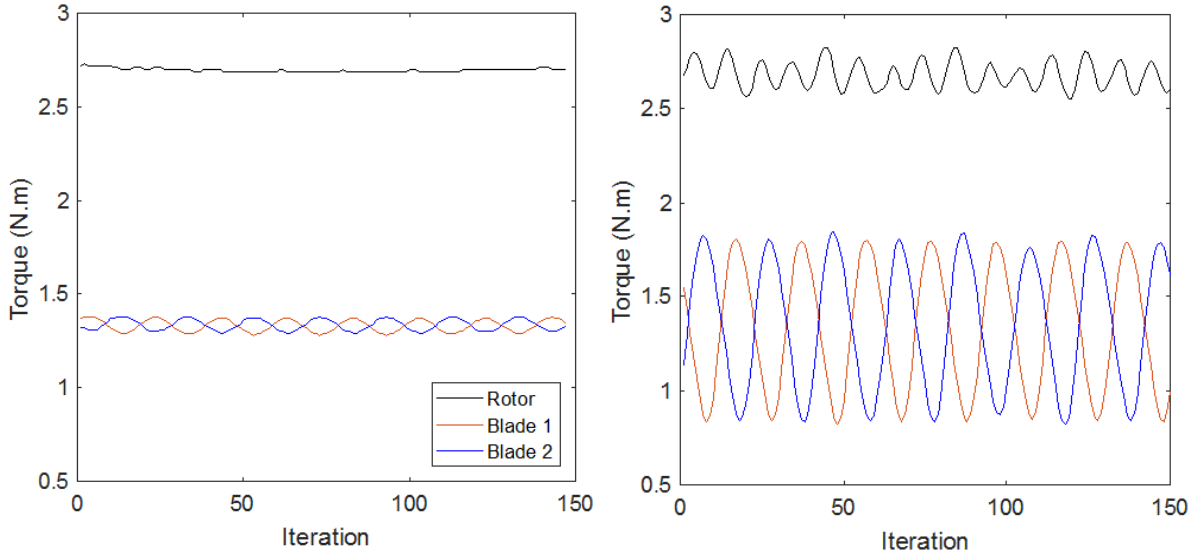

(a) Depth = 0.76 m

(b) Depth = 0.31 m

Fig. 5.6. The VOF simulations results of torque over each blade and the total torque of turbine in two submergence depths

Table 5.2. Cyclic fluctuations of torque over a single blade and rotor for simulation cases

Study Case	Depth = 0.76 m		Depth = 0.31 m	
	Single Blade	**Rotor**	**Single Blade**	**Rotor**
Uniform Flow	2.3%	0%	24.1%	2.7%
s1	6.9%	0.54%	23.9%	2.9%
w1	2.27%	0%	23.5%	1.5%
w1 + s1	6.2%	0.75%	22.5%	2.4%

Validation for Waves

The wave experiments in the AMC towing tank on the 500 mm diameter model [54] were simulated for a TSR of 6.5 using the VOF and the SPh models. The time-averaged values of C_P and C_T from the simulations are shown with a dashed line in Fig. 5.7. The turbine rotor was not close enough to the surface to constrain wake expansion and affect the performance. Thus, it was expected from the literature [52, 99] that waves should have little effect on the mean values of the power and thrust coefficients of the turbine. The time-averaged value of C_P from the VOF simulations have good agreement with the AMC experimental results; whilst, the single-phase underestimated it, as shown in Table 5.3. The time-averaged C_T was slightly over predicted by the two CFD methods. The maximum torque and thrust expel on a blade in the opposite angular position, after 270º.

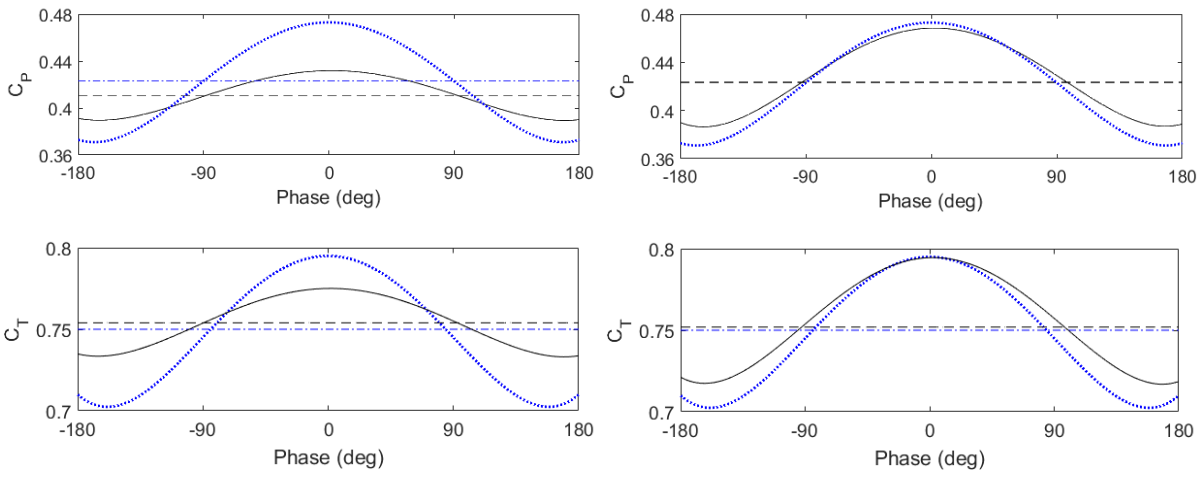

(a) Single-phase **(b) VOF**

Fig. 5.7. Phase averaged results from the simulation of the validation wave case at U = 1.25 m/s and TSR = 6.5. Solid line relates to the phase-average parameter; dashed line represents the time-averaged values. Blue dotted line is phase-averaged and blue dash-dotted line is time-averaged from the experiments [54]

It is also important to validate the CFD models for the variation of C_P and C_T over a wave phase. The phase-averaged values are depicted in Fig. 5.7 with a solid line. Table 5.3 lists the variation range together with the time averaged values of power and thrust coefficient from CFD models as well as the towing tank experiments at TSR = 6.5. Compared to the SPh, the VOF model was a better fit for the AMC results, which can be due to effect of free surface and buoyancy modelling in the VOF, providing conditions more akin to the reality. Therefore, the VOF model was selected to study the effect of waves, using the cases outlined in Table 5.1, on the performance of the turbine.

Fig. 5.8 and Fig. 5.9 shows the velocity distribution over the horizontal and vertical planes crossing the turbine for the SPh and the VOF simulation, respectively. It can be seen that the velocity along the domain in the VOF simulation is not as harmonic as the SPh, which can be attributed to the effect of free surface constraining the wake expansion.

Table 5.3. The turbine performance results from simulations and the AMC experiments under the wave condition

Method	Variable	Time averaged	Variation Range
CFD (SPh) – Case w1	**C_P**	0.41	0.390 - 0.432 (10.2%)
	C_T	0.77	0.753 - 0.788 (4.5%)
CFD (VOF) – Case w1	**C_P**	0.42	0.379 - 0.467 (20.9%)
	C_T	0.76	0.718 – 0.793 (9.8%)
Experiments [54]	**C_P**	0.42	0.373 - 0.473 (23.5%)
	C_T	0.75	0.710 – 0.801 (12.1%)

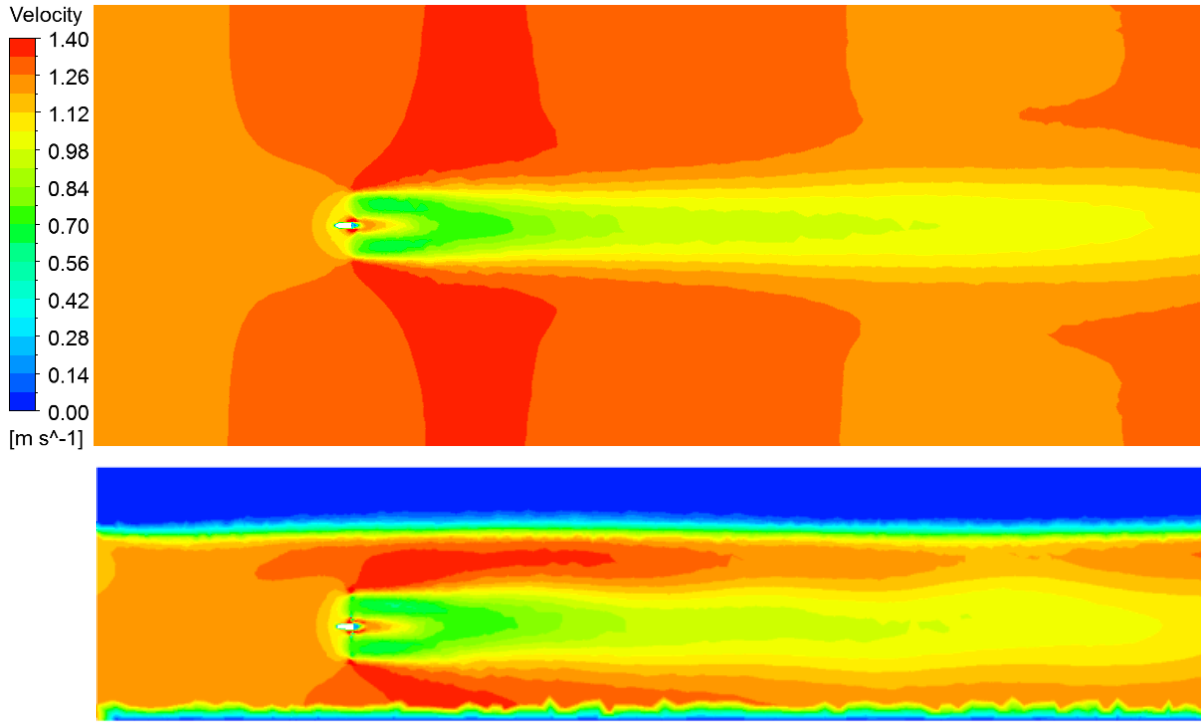

Fig. 5.8. Velocity distribution over the turbine planes in VOF simulation

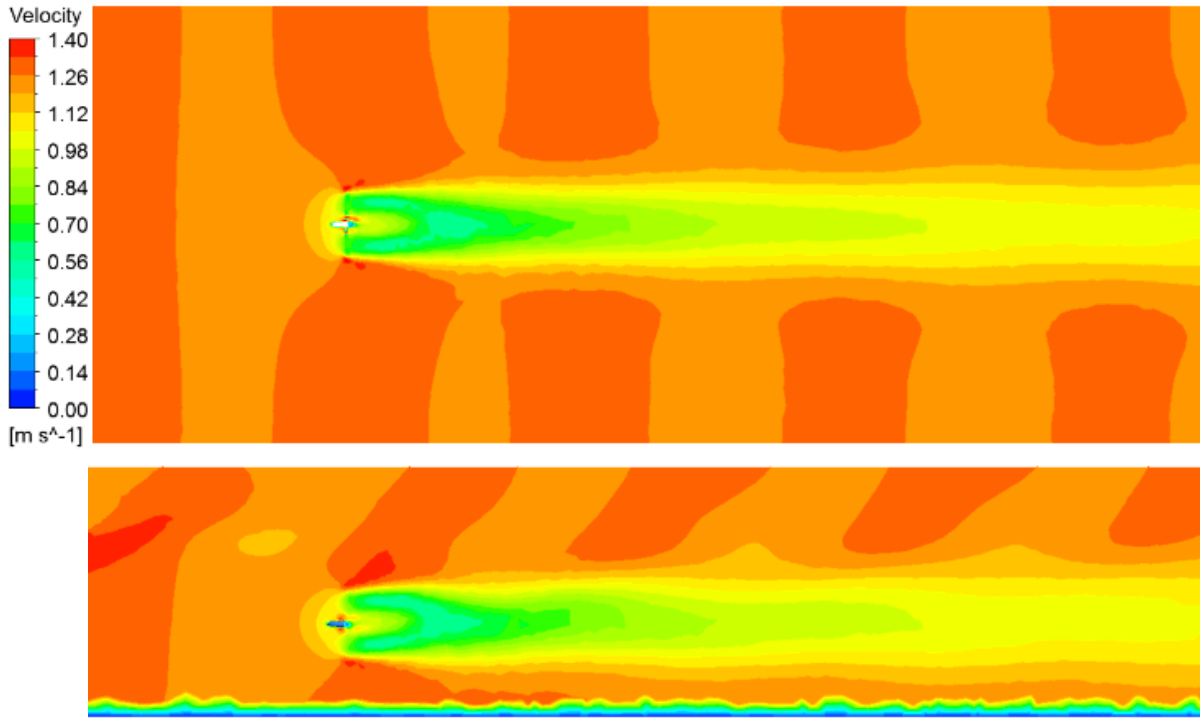

Fig. 5.9. Velocity distribution over the turbine planes in single-phase simulation

5.4.2. Effect of Shear Flow Velocity Profile

Fig. 5.10 shows the instantaneous torque over the blades and the rotor in uniform and shear velocity profiles for the VOF simulations at a hub immersion depth of 0.76 m and TSR ~ 6.5. Cyclic torque fluctuation on an individual blade was higher for the turbine under shear velocity

profile (γ = 7). The resultant torque deviated within 0.54% of the mean value. The same shear velocity profile at the depth of 0.31 m generated a higher range of deviation in the total torque value, ~2.9%. According to the torque fluctuations outlined in Table 5.2, for different depths and the conditions with and without shear velocity profile, it can be inferred that in the depth of 0.31 m, the free surface is dominant compared to the shear in terms of generating fluctuations in the turbine torque output. The torque fluctuation of an individual blade increased slightly once the shear velocity profile was introduced to the flow.

For shear cases, maximum blade loadings still occur at an angular position of 270^o at the depth of 0.31 m, while they happen at 90^o for the depth of 0.76 m where the flow had the highest velocity values in the profile. Therefore, in the depth of 0.76 m, the free surface is less influential and the shear velocity profile is dominant.

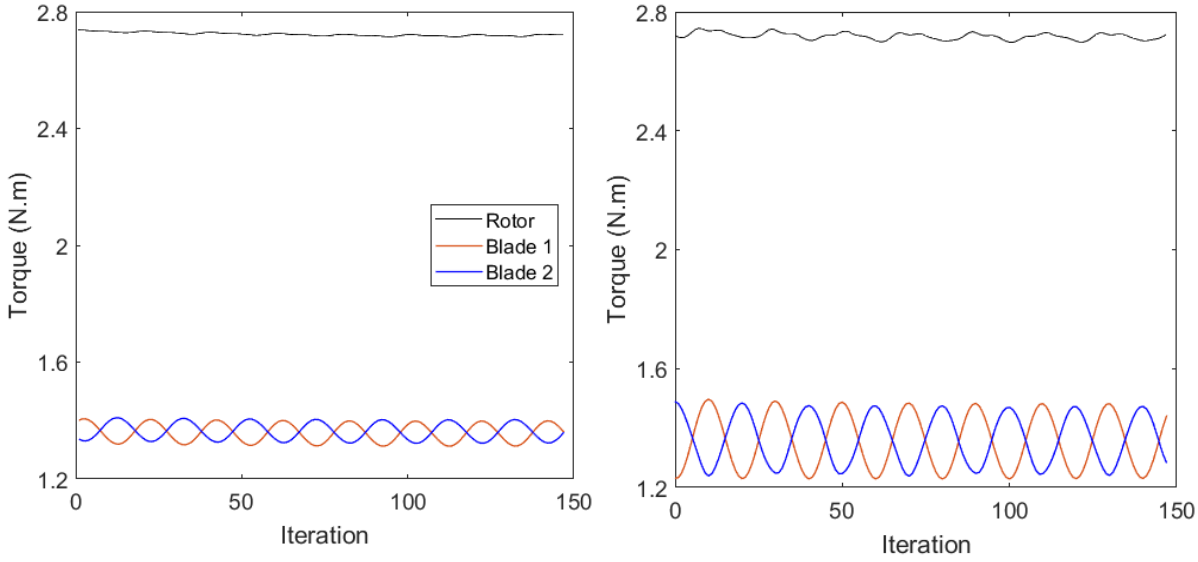

(a) Uniform velocity **(b) Shear velocity profile**

Fig. 5.10. The VOF simulation results of torque over each blade and the resultant torque of the turbine in condition with and without shear velocity profile at TSR ~ 6.5 and hub immersion depth of 0.76 m

Compared to the condition with uniform flow, mean values of C_P and C_T showed little change to the applied velocity profiles, provided the equivalent flow velocity was employed in the calculations. Fig. 5.11 depicts the velocity distribution over the vertical plane in the VOF simulations of the turbine with and without shear velocity profile. It can be seen that the bypass flow around the turbine has higher velocity than the inlet velocity due to the domain confined by walls and free surface and the wake behind the turbine is uneven for the case with a shear velocity profile.

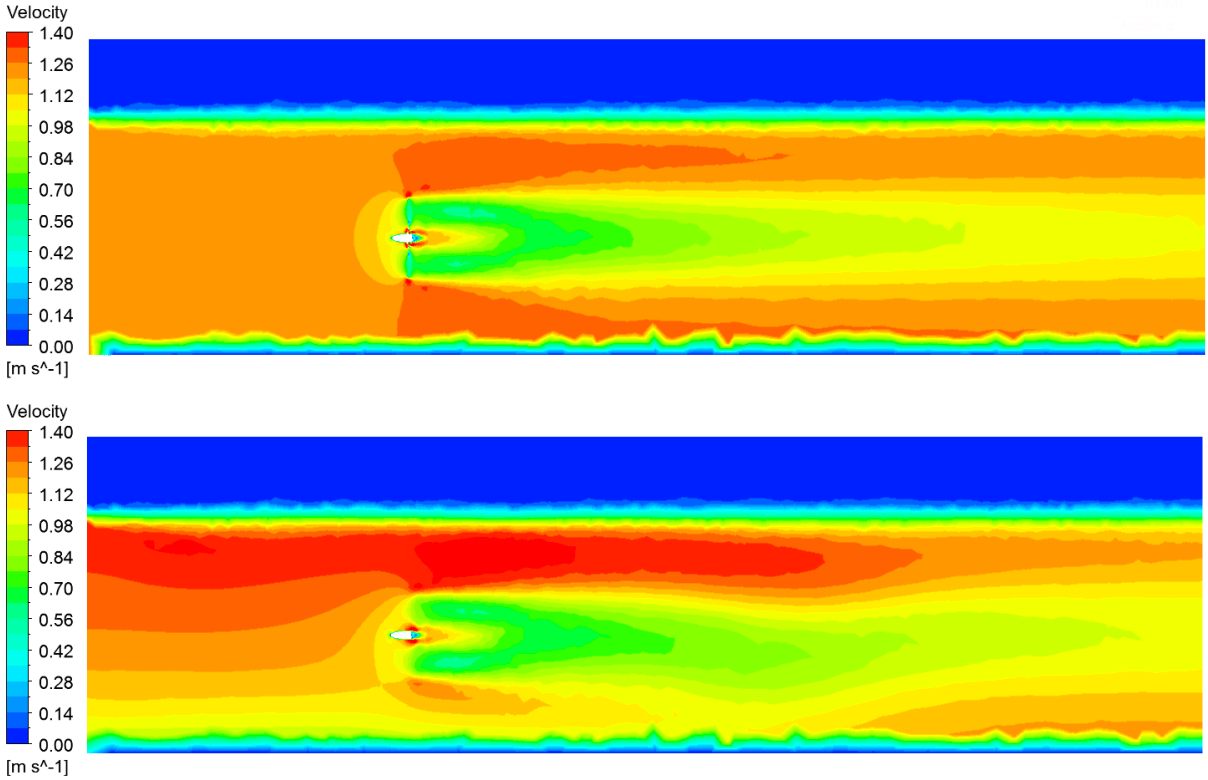

Fig. 5.11. Comparing the velocity distribution over the vertical plane in the VOF simulation with and without velocity profile

5.4.3. Effect of Surface Waves

The wave cases investigated using the VOF model are detailed in Table 5.1. The torque variation over each blade and the rotor under case w1 in the VOF simulation is plotted in Fig. 5.12 for two depths of 0.76 m and 0.31 m. It is seen that in addition to the periodic variation in torque as a result of passing wave in submergence depth of 0.76 m, ~1.5% of fluctuation is added to the turbine torque because of free surface effect in 0.31 m of depth, as in Fig. 5.12b.

The time-averaged values of C_P and C_T of the turbine under case w1 had no significant change when the turbine proximity to the free surface was reduced from 0.76m to 0.31m. It is in contradiction with the finding of the condition without waves. It can be associated with a net velocity imposed by Stokes drift, as reported in [51] (see [105] for details of Stoke drift velocity). Hence, the wave simulation data were corrected for Stokes drift, which led to slightly smaller time-averaged values of C_P and C_T at the depth of 0.31m than the 0.76m.

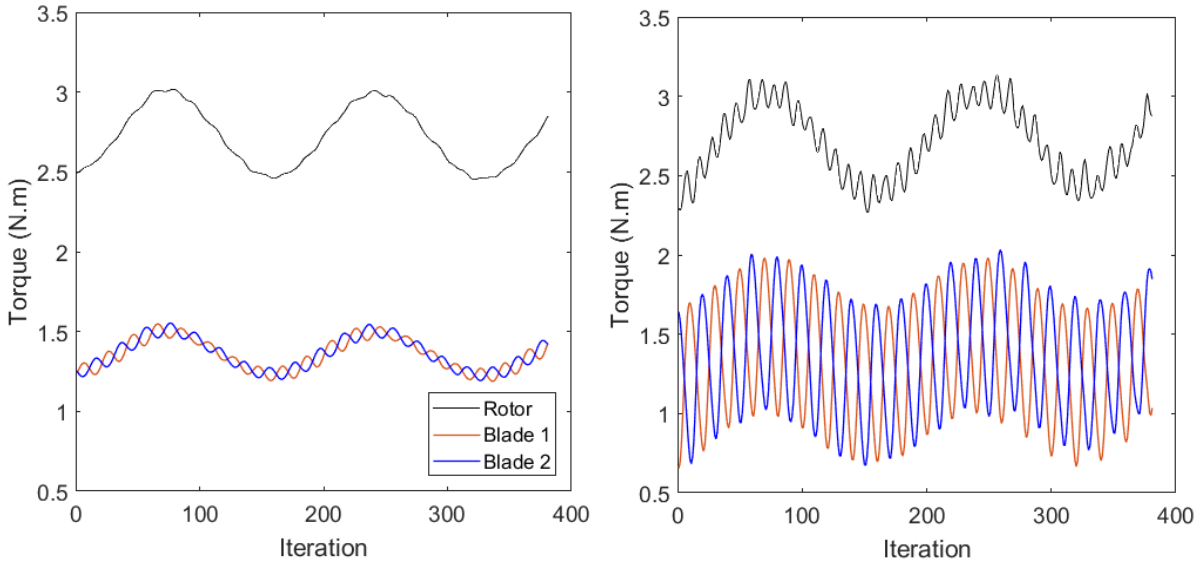

(a) Depth = 0.76m **(b) Depth = 0.31m**

Fig. 5.12. The VOF results of torque over each blade and the resultant torque of the turbine model under wave case 1 condition at TSR ~ 6.5 and two hub immersion depths

Fig. 5.13 shows the phase average as well as time average C_P values from VOF simulation of the wave cases, as outlined in Table 5.1**,** after correction for Stokes drift. As can be seen, reducing the submergence depth resulted in a slight increase in the variation ranges of phase-averaged values. At the constant submergence depth of 0.31m, there is little change in mean C_P and C_T in different applied wave cases. However, increasing either wave period (case w2) or wave height (case w3) resulted in significant rises in phase-averaged values of C_P, and similarly for C_T. Variation in thrust is important in terms of structural design of blades to endure fatigue due to periodic loadings. Moreover, substantial variation in power reduces the quality of electrical power generation [42]. The maximum and minimum of C_P and C_T occur at the peak and trough of the wave respectively, consistent with the literature [51, 52, 54]. The blade pressure coefficient is shown in Fig. 5.4b for case w1, representing the blade loadings in wave peak and trough at the depth of 0.76m at angular position of zero.

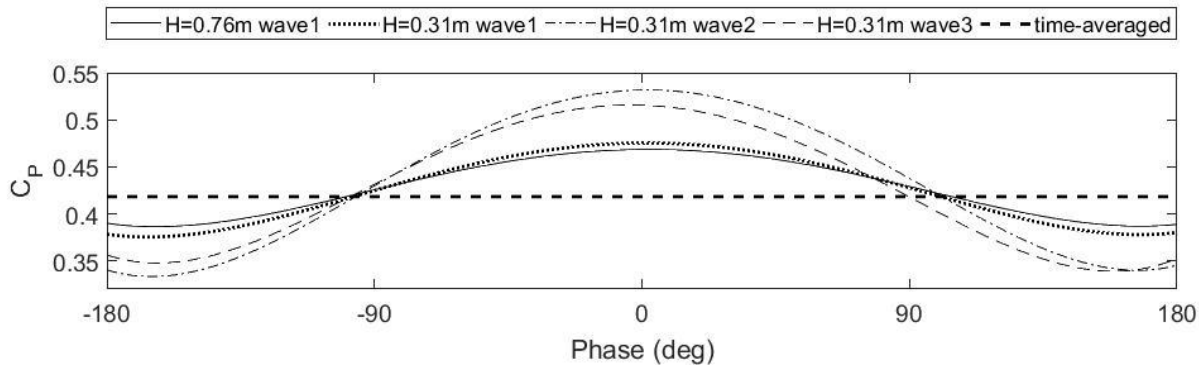

Fig. 5.13. Phase averaged results from the simulation of the wave cases at U = 1.25 m/s and TSR = 6.5. Thick dashed line represents the time-averaged values

5.4.4. Interaction of Wave and Velocity Profile

The performance of the turbine model under the simultaneous influence of shear and waves was studied by simulating case w1 together with a shear velocity profile using a power law of γ = 7 and 9 in two hub immersion depths of 0.31 m and 0.76 m, as outlined in Table 5.1. No significant change was seen in the time-averaged values of C_P and C_T, calculated using the equivalent flow velocity, when the submergence depth reduced from 0.76 m to 0.31 m, similar to what was seen in the wave condition without shear. Correcting the simulation data for Stokes drift resulted in lower values for the depth of 0.31 m. Comparing the wave simulation results for each depth before and after adding shear velocity profile, either using power law of 7 or 9, showed little change in the time-averaged and phase-averaged values of C_P and C_T, provided the equivalent flow velocity be utilised in analysis. As can be seen in Table 5.2, the fluctuation of resultant torque on the rotor is higher than the case w1 with uniform inlet velocity for the two depths.

5.5. Conclusion

The effect of free surface proximity, shear flow velocity profile and surface waves on the hydrodynamic characteristics of a two-bladed horizontal axis marine current turbine was investigated using numerical approach. A CFD model was developed to account for shear and waves in the performance evaluation of the turbine. The volume of fluid and the single-phase model were the two numerical approaches utilised to simulate the turbine performance. The CFD models were validated against the experimental results from the CWC and the towing tank. Comparison between the two CFD models showed that both the single-phase model and the VOF model were accurate enough in predicting the turbine performance under the sheared flow condition, but the VOF comes with higher computational costs. However, the VOF model

in wave conditions had closer agreement with the experiments than the single-phase model. Moreover, the single-phase model was not able to account for the effect of free surface proximity on the turbine performance. Therefore, the VOF was selected to study the turbine performance under the effect of wave and shear in various submergence depths.

The effect of reducing the free surface proximity to less than half of the radius was a reduction in the C_P and C_T values only for the condition without waves. In the presence of waves, changing the turbine submergence depth made no significant change to the mean C_P and C_T values, however resulted in a slight increase in the phase-averaged values. Different outcomes obtained from the simulations with and without waves when the free surface proximity was reduced can be attributed to the effect of Stokes drift in wave conditions. Correcting the wave case data for Stokes drift resulted in smaller mean values of C_P and C_T for smaller proximity to the free surface. For all the study cases, the cyclic fluctuations of torque and thrust experienced by the blades and rotor were increased when the proximity to the free surface was reduced.

Introducing the shear velocity profiles, with two different power law (γ), had little impact on the mean values of power and thrust coefficients when the equivalent flow velocity was utilised for the performance analysis. However, ranges of torque and thrust on the blades are higher over a rotation compared to the condition with uniform flow.

For 0.76 m of depth where the influence of the free surface was less, the maximum torque and thrust on an individual blade occurred at an angular position of 90^o where the velocity values are higher in the profile. The maximum torque and thrust on a blade over a complete rotation occurred in an angular position before 270^o in uniform inflow velocity.

The different applied wave cases had negligible impact on the time-averaged values of C_P and C_T. Increasing wave period and wave height, performed in separate simulation cases, significantly raised the phase-average values of C_P and C_T. The maximum and minimum of C_P and C_T coincide with the wave peak and wave trough respectively.

Provided the equivalent flow velocity is employed in the calculations and the data is corrected for Stokes drift, the time averaged and phase-averaged values of C_P and C_T from the turbine simulations under waves and shear velocity profile matched with the wave case without shear.

Overall, there was no change on the mean power and thrust coefficients of the turbine as a result of shear velocity profile or small proximity to the free surface or when surface waves are applied. However, these conditions increase the fluctuations of torque and thrust on the individual blades and the rotor, which is important in terms of higher risk of structural failure in the blades due to fatigue and reduction of the power output quality.

Chapter 6

Summary, Conclusions and Future Work

6.1. Summary

The focus of this work was to investigate the hydrodynamic characteristics of a horizontal axis marine current turbine under the influence of various environmental conditions and to comprehensively evaluate the available methodologies for characterising turbine performance. The two overarching research questions for this project were:

"How do flow conditions, such as shear inflow velocity, waves and submergence depth, and evaluation parameters, such as blockage and model scale, influence the performance of HAMCTs?"

"What are the best approaches to characterise the hydrodynamic performance of HAMCTs in steady and unsteady flow conditions?"

This chapter presents an overall conclusion of the outcomes and provides the key research findings in relation to these research questions and their contributions to the field of marine renewable energy. Recommendations for future research along with discussions on the limitations of the study are given.

To initiate this research, a three-dimensional computational fluid dynamics (CFD) model of the turbine was developed in Chapter 2. The purpose of the CFD model was to evaluate the different numerical approaches available in order to find the best practice for turbine performance modelling. Extensive verification and validation was conducted on the proposed CFD models to ensure their accuracy in the performance evaluation of the turbine against experimental data obtained in this work and provided in literature. The focus was to evaluate the impact of modelling techniques, including the selection of turbulence model, boundary layer model, single blade or full turbine model, transient or steady solution, and rotation method of the rotor. Comparisons were made among the above techniques by assessing their accuracy in predicting the turbine power coefficient against experimental data.

To extend the study on turbine performance, an experimental investigation was performed on two turbine scale models at two hydrodynamic facilities, a towing tank and a circulating water channel (CWC), presented in Chapter 3. The aim of these experiments was to study the performance of the turbine under different operating conditions including steady/unsteady flow, blockage ratio, Reynolds number, and model scale. An uncertainty analysis was performed to determine the validity range of the turbine performance data.

In Chapter 4, a blade element momentum (BEM) theory model was developed to assess the performance of the turbine in uniform and shear flow profiles. QBlade software and the CFD model from Chapter 2 were utilised to study the effect of Reynolds number on the results. A discussion of the employed performance evaluation methods in Chapters 2, 3 and 4 was presented, including the benefits and limitations of each method.

In the last Chapter, the CFD model from Chapter 2 along with a volume of fluid (VOF) model was developed to account for shear flow velocity, submergence depth and waves in the assessment of turbine performance. The two CFD models were compared in terms of their simulation accuracy against experimental results from Chapter 3 as well as the literature.

6.2. Findings and Limitations

6.2.1. CFD Modelling in Steady Conditions

- Turbulence models: Although the results from BSL EARSM[2] can reasonably predict the turbine performance for a range of TSRs, k-ω SST results in closer agreement with the experiments.

- MRF/Sliding Mesh: The results from both the moving reference frame (MRF) and the sliding mesh method had a close agreement with the experimental data. The convergence criteria were achieved faster in MRF. Although the sliding mesh simulations are more realistic to the actual turbine operation, it comes with higher computational costs.

- Boundary layer models: The wall-function model had the best agreement with the experimental data with less computational time compared to the other models. The transitional gamma-theta model and the near wall model were computationally demanding due to the required finer mesh for these methods and they had higher truncation errors.

- Single blade/Whole rotor: Convergence achievement for simulations on a single blade instead of the whole turbine were significantly faster. However, the whole rotor model

[2] Baseline Explicit Algebraic Reynolds Stress Model

had higher C_P values and closer agreement to the experiments than the single blade model.

- Overall, the steady MRF simulation on the whole turbine using the wall-function with k-ω SST model provided the best balance between accurately predicting the turbine performance and modelling the flow physics with computational time.

- Limitations: The number of parameters studied in the CFD model was limited because performing the simulations were time excessive, especially in transient solutions. The number of available licences and CPUs also limited using high performance computing (HPC) systems. A general concern about the CFD method is the accuracy of results, i.e. they must be validated by experimental data. Another limitation of CFD is the quality of mesh that highly depends on the practitioner's skills, which will affect the accuracy of results as well as the required time for modelling.

6.2.2. Model Scale Testing

- The turbine performance was evaluated using dimensional analysis performed on the measured data. The maximum power coefficient of the 800 mm diameter turbine was 0.44 at TSR ~ 6.5 in the towing tank and is 0.42 at TSR ~ 7 in the CWC.

- Facility bias: The type of testing facility affected the turbine performance, and was found to be a result of different flow conditions and blockage effects. The blockage correction on the towing tank results led to a 12% reduction in C_P for the larger turbine. The difference between the corrected C_P values of the two scale models, even for Re independent conditions, was due to high blockage effects on the 800 mm rotor in the towing tank. It was found that the AMC towing tank results of 500 mm turbine, compared to 800 mm turbine model, were a better match with the USNA towing tank results of 800 mm turbine with negligible blockage. Therefore, it is suggested that experiments are conducted in facilities with little blockage effect.

- Shear flow profile: Using the equivalent flow velocity calculated using the kinetic energy flux through the swept area of the turbine instead of the inflow speed at the hub in the dimensional analysis of the CWC data resulted in a better correlation with the towing tank results. It shows the importance of selecting the correct flow velocity for performance analysis. The effect of a shear velocity profile on the power production of

the turbine is mostly related to the change in kinetic energy, which should be considered for turbine performance assessment. Therefore, it is recommended to use the equivalent flow velocity, a better representative of the kinetic energy, for turbine performance evaluation in shear flow conditions.

- Scaling effect: Although the performance curves for the two scale models were similar, the 800 mm model had higher C_P values than the 500 mm model, ~ 4% at TSR 6 for inflow velocity of 2 m/s. The combined impact of Reynolds number and blockage effect were the main causes of the difference in the results of the two scale models. The smaller turbine operates at lower Reynolds numbers than the larger turbine, in a similar test condition, which causes lower lift coefficients and hence lower power coefficients. A Reynolds number based on the chord at 70% of the blade span of 2×10^5 was found to be the criterion for Reynolds number independency.

- Limitations: The experiments in the CWC were only implemented for one flow velocity, the maximum velocity possible for the facility, in which Reynolds number independency was not achieved for the 500 mm turbine model. The experiment in the towing tank was limited to carriage speed up to 2 m/s due to the vibration of the testing setup in the higher speeds. For the two facilities, the maximum TSR for experiments was 9 since higher rotational speeds damaged the test rig once. In addition, the results for the larger turbine in the towing tank were affected by considerable blockage, which even after correcting for blockage did not match with the USNA results with little blockage, especially for higher TSRs. Thus, the size of testing tank is another limit that should be kept in mind when the scale of a turbine model for testing is decided.

6.2.3. Theoretical Modelling

- BEM model with shear: No significant changes were found in the performance results by adding a shear velocity profile in the BEM model. BEM theory employs annular sections over the rotor swept area to calculate different parameters, which reduces the effect of shear in the model. The C_P curve obtained from the BEM model with shear was in good agreement with the experimental data.

- Reynolds number effect: The study of Reynolds number effect on the performance using QBlade software showed that C_P values rise when the flow velocity increases up to 2 m/s. The use of the local sectional Reynolds number to allocate the lift and

drag coefficients in the BEM model only provided marginal improvements; using a single reference Reynolds number is sufficient.

6.2.4. CFD Modelling in Unsteady Conditions

- CFD approach: Both the single-phase model and the VOF model were accurate in predicting the turbine performance in the sheared flow condition. Under wave conditions, the VOF model had closer agreement with the experiments than the single-phase model. In addition, the single-phase model was not able to account for the effect of free surface proximity on turbine performance. Therefore, the VOF was found to be the better CFD model to study turbine performance in conditions with waves and shear in different submergence depths.

- Free surface proximity: Reducing the free surface proximity to less than half of the rotor radius caused a reduction in the C_P and C_T values, for conditions without surface waves. In the presence of waves, the proximity reduction resulted in no significant change to the mean values and a slight increase in the phase-averaged values. However, correcting the wave case data for Stokes drift resulted in smaller mean values of C_P and C_T for closer proximity to the free surface. For all the study cases, the torque and thrust fluctuations on the blades and rotor were increased when the proximity to the free surface was reduced, which is important in terms of blade fatigue and power output quality.

- Shear velocity profile: No significant changes in the mean values of the power and thrust coefficients were found for shear cases when the equivalent flow velocity was utilised for the performance analysis. However, fluctuations of torque and thrust on the blades increased compared to the condition with no shear, important in terms of fatigue and power quality.

- The maximum torque and thrust on a blade over a complete rotation occurred at an angular position before 270^o for any depths in uniform flow velocity. It is the same for the smaller proximity to the free surface, in condition with shear. However, in the deeper location where the free surface was not influential, for the condition with shear, the maximums occurred at an angular position of 90^o where the velocity values are higher in the profile.

- Surface waves: The effect of surface waves was negligible on the time-averaged values of C_P and C_T. However, the phase-average values of C_P and C_T significantly increased when either wave period or wave height was augmented. The maximum of C_P and C_T coincide with the wave peak and the minimum with the wave trough for all the studied wave cases.

- Wave and shear interaction: The time-averaged and phase-averaged values of C_P and C_T from the turbine simulations with wave and shear velocity profile were consistent with the wave results without shear if the equivalent velocity was employed in the calculations and the data was corrected for Stokes drift.

- Overall, the above-mentioned conditions increase the fluctuations, either cyclic or periodic, of torque and thrust experienced by the individual blades and the rotor, which is important to account for due to higher risk of structural failure in the blades, induced by fatigue, as well as the quality reduction of the turbine power output.

- Limitations: Due to the number of grids and complexity of the problem, the computational time required for solving the CFD models was excessive. Performing the simulations even using a HPC were computationally demanding for the VOF model, e.g. the simulation time required to get a single point on the C_P curve for the turbine under wave and shear using VOF model on 32 cores of HPC was approximately 4 days.

6.2.5. Comparing Assessment Methods

- The experimental results were affected by facility bias due to different flow conditions and blockage ratios. The flow was uniform and steady in the towing tank, whilst it was turbulent and had a shear velocity profile in the CWC. The unsteadiness in the CWC arguably provided conditions more like the flow conditions at a real deployment site than the towing tank. However, due to the steady condition of the towing tank, the effect of a single parameter could be studied without the interference of shear and turbulence.

- The discrepancy between the towing tank results of the two scale models, after blockage correction and where Reynolds number independency was achieved showed that the 500 mm model was a better option for testing in the AMC towing

tank, where the blockage ratio was less than 10%. Compared to the 800 mm turbine, the 500 mm turbine results from the AMC towing tank was a better fit to the 800 mm turbine results from the USNA towing tank with a large tank. Thus, the size of testing tank can limit the applicability of the results.

- The blockage effect was minimised by employing a large domain in the CFD models, which showed that, in zero blockage, the scale effect is primarily related to Reynolds number. It is an advantage of CFD in characterising the turbine hydrodynamics that a single parameter can be studied while others are controlled. Compared to the BEM theory, CFD has shown to be an appropriate tool for studying the effect of various parameters, such as flow unsteadiness, on the turbine hydrodynamic characteristics.

- Theory: QBlade was the easiest tool to provide quick and fairly accurate performance predictions. BEM theory was the next easiest method to use; however, the accuracy of the result depends on the lift and drag coefficients employed in the code.

- CFD: Achieving a reliable CFD model for the turbine performance assessment can be challenging. There are many parameters, from generating grids to solver setup, which can affect the simulation results. However, once the CFD model is validated, detailed information can be obtained about the turbine hydrodynamics, not achievable by the other methods. CFD provides the ideal platform to account for various environmental parameters affecting the turbine performance.

- Experiment: Experiments are the most appropriate methodology for establishing if a parameter has an impact on an outcome. They play an essential role in the performance evaluation of HAMCTs by providing performance data in realistic conditions and validating the results of the theoretical and numerical methods. Physical scale model tests are also considered the most advanced techniques for the prediction of the hydrodynamic performance of marine current turbines. However, it is an expensive method, prone to unforeseen failures and human error, and as such should be undertaken using internationally adopted guidelines and procedures to reduce any uncertainty in the findings.

- Each method was able to predict the performance of the turbine and has its place in the performance analysis of HAMCTs. BEM and CFD can be done at the desktop and can provide detailed information about the flow through the turbine and the associated torque and loads on the turbine assembly. However, these theoretical and numerical models must be compared with experimental results to be valid.

6.3. Implications of the Research

The broad motivation behind this research was to progress the development of tidal power, a source of marine renewable energy, and hence contribute to the lessening of our reliance on fossil fuels for global energy requirements. The core aim of this work was to evaluate the performance of a horizontal axis marine current turbine in both steady and unsteady flow conditions. To find the best practice for performance evaluation, an in-depth investigation on the various methods and their limitations and benefits was completed. This allows quantification of the parameters of importance relative to the environmental conditions at a deployment site.

Experiments, CFD and theoretical models were implemented to investigate the hydrodynamic characteristics of a horizontal axis marine current turbine in both steady and unsteady flow conditions. Fig. 6.1 and Fig. 6.2 show the turbine performance obtained in different cases using the employed methods for the two scale models at TSR~6.5. Such a comprehensive study, which brings all these methods together to investigate the performance of HAMCTs in different operational conditions, is rare. The research characterises the difference between the performance predicted in a steady flow condition and the actual turbine performance in the unsteady flow conditions of the real environment. The presented results are a guide for designers to develop a profound understanding of a turbines hydrodynamics in order to enhance the performance according to the environmental condition of an intended deployment site.

In addition, developmental investigations were performed on the methodologies and the capabilities of each to study the turbine hydrodynamics. The CFD work studied the impact of mesh resolution, Y^+ in the near wall, turbulence model, boundary layer model, and solution method on the CFD results to accurately predict the performance of the turbine. The performance of two numerical approaches, i.e. single-phase and volume of fluid, was also evaluated to account for shear and surface waves in the turbine modelling. This signified many

considerations in performance evaluation of HAMCTs, which have been neglected in most previous studies.

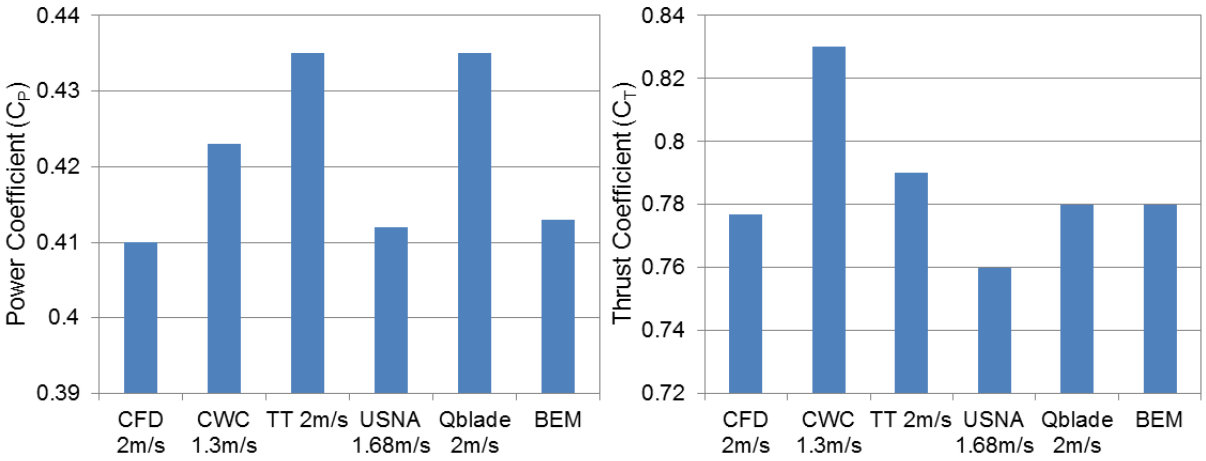

Fig. 6.1. Performance of the 800 mm turbine at TSR~6.5 obtained from different assessment methods

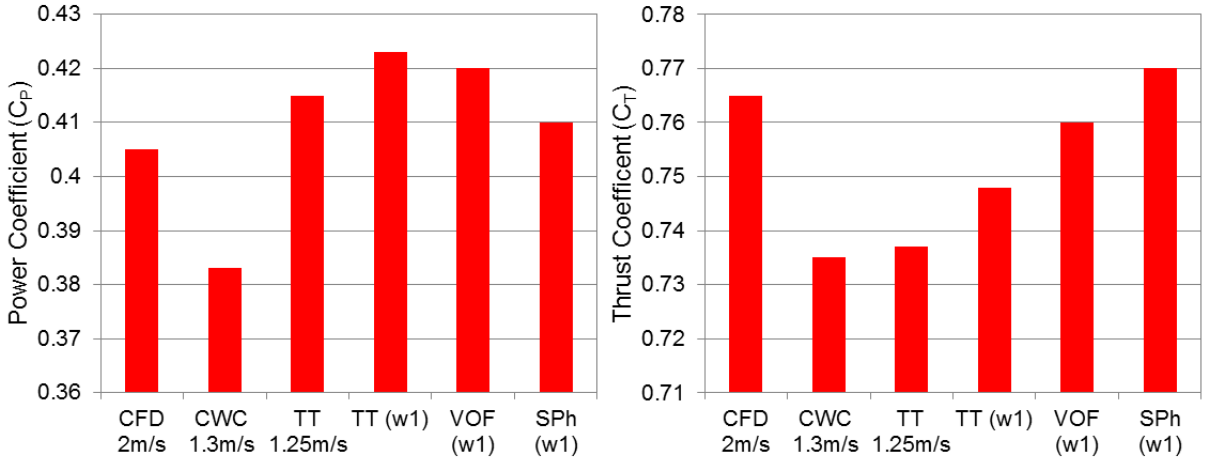

Fig. 6.2. Performance of the 500 mm turbine at TSR~6.5 obtained from different assessment methods

The experimental work in this thesis is of significant value by providing results on scaling effect, facility bias and shear velocity profile as there are few or no studies in the public domain that experimentally characterise the performance of HAMCTs under the effect of these parameters.

The theoretical work showed the limitation of BEM theory in modelling the turbine in unsteady conditions as well as its ability to provide reasonably accurate performance curves in the steady flow condition.

The research presented in this thesis provides a broad insight into the hydrodynamics of HAMCTs that will frame the basis and support for future research on horizontal axis marine current turbines. Having the ability to model the turbine in unsteady conditions provides turbine designers with a more accurate prediction of the turbine hydrodynamics in the real environment, allowing the optimisation of turbine design for a particular deployment site during the primary design stages. Finally, the research provides a very valuable data set that can be used to remove current barriers to the deployment of this important source of renewable energy, and begin to lessen our reliance on fossil fuels.

6.4. Future Work

The work performed in this thesis could be extended to the following:

- Conduct experiments to investigate the effect of blockage in more detail, using tests in facilities with different cross-sectional areas. There is a need to measure the flow velocity in different locations around the turbine to record the wake and bypass velocities. In addition, the CFD model from this thesis could be developed to study the blockage effect, which provides more detailed data.

- The bottom proximity is another parameter important to be studied for sites with shallow water. Enough free surface clearance should be considered for deploying a turbine, allowing for the traffic of surface vessels. However, closer proximity to the bottom means lower velocities in the flow profile, because of seabed friction, which reduces the performance. An optimum depth can be defined using CFD simulations for an intended deployment site.

- Turbulence intensity is also of considerable importance due to possible reduction in power output as well as increased risk of fatigue. To conduct the experiment, different turbulence intensities could be generated in the flow using a grid. This could be investigated on a single turbine or arrays of turbines working in the wake of each other. CFD is also capable of modelling turbulence; however, simulations using LES or DNS are required instead of RANS, to accurately model the turbulence, which requires higher computational power.

- Most of investigations and discussion presented in this thesis were related to the performance and ability of the turbine on power production. Using the experimental

and the numerical models in this work, a deeper study on the structural loadings of the turbine could be implemented, which is important for the material selection and fabrication of the full-scale turbine. Experiments could be conducted by installing strain gauges on the blades. The numerical method could be developed to account for fluid-structure interaction (FSI).

- Using the CFD models developed in this work, a deep analysis of blade design could be performed. This would aim for a reduction in structural loading and increase of power production of the turbine. The optimised design could be fabricated and tested experimentally to validate any design enhancements.

References

[1] Clark RH. Elements of tidal-electric engineering: Wiley-IEE; 2007.

[2] Boyle G. Renewable energy power for a sustainable future. Oxford University Press; 2004.

[3] Behrens S, Griffin D, Hayward J, Hemer M, Knight C, McGarry S, Osman P, Wright J. Ocean renewable energy: 2015-2050, an analysis of ocean energy in Australia. 2012.

[4] IEA. International Energy Agency Key World Energy Statistics. 2016.

[5] Seng Y, Koh LL, Koh SL. Marine Tidal Current Electric Power Generation: State of Art and Current Status, Renewable Energy. In: Hammons TJ, editor.: InTech; 2009.

[6] Khaligh A, Onar OC. Energy Harvesting ' Solar, Wind, and Ocean Energy Conversion Systems'. Illinois Institute of Technology2008.

[7] Atlantis Resources corporation Ltd; https://www.atlantisresourcesltd.com, 2015.

[8] Andritz Hydro Hammerfest `AHH Technologies'; http://www.hammerfeststrom.com, 2013.

[9] Marine Current Turbines Ltd, SeaGen Technology; www.marineturbines.com, 2013.

[10] Magagna D, MacGillivray A, Jeffrey H, Hanmer C, Raventos A, Badcock-Broe A, Tzimas E. Wave and tidal energy strategic technology agenda. SI ocean. 2014;44.

[11] Ocean S. Ocean energy: cost of energy and cost reduction opportunities. Strategic Initiative for Ocean Energy (SI OCEAN) May. 2013.

[12] Magagna D, Uihlein A. Ocean energy development in Europe: Current status and future perspectives. International Journal of Marine Energy. 2015;11:84-104.

[13] Uihlein A, Magagna D. Wave and tidal current energy – A review of the current state of research beyond technology. Renewable and Sustainable Energy Reviews. 2016;58:1070-81.

[14] Belloni C. Hydrodynamics of Ducted and Open-Centre Tidal Turbines: University of Oxford; 2013.

[15] Grimwade J, Hails D, Robles E, Salcedo F, Bard J, Kracht P. Review of Relevant PTO Systems. MARINET, 2012 Cork.

[16] Batten WMJ, Bahaj AS, Molland AF, Chaplin JR. The prediction of the hydrodynamic performance of marine current turbines. Renewable Energy. 2008;33:1085-96.

[17] Benini E. Significance of blade element theory in performance prediction of marine propellers. Ocean Engineering. 2004;31:957-74.

[18] Masters I, Williams A, Croft T, Togneri M, Edmunds M, Zangiabadi E, Fairley I, Karunarathna H. A Comparison of Numerical Modelling Techniques for Tidal Stream Turbine Analysis. Energies. 2015;8:7833-53.

[19] Manwell JF, McGowan JG, Rogers AL. Wind Energy Explained: Theory, Design and Application. 2nd ed: John Wiley and Sons Ltd.; 2009.

[20] Koh WXM, Ng EYK. Effects of Reynolds number and different tip loss models on the accuracy of BEM applied to tidal turbines as compared to experiments. Ocean Engineering. 2016;111:104-15.

[21] Walker JM, Flack KA, Lust EE, Schultz MP, Luznik L. Experimental and numerical studies of blade roughness and fouling on marine current turbine performance. Renewable Energy. 2014;66:257-67.

[22] Bahaj AS, Batten WMJ, McCann G. Experimental verifications of numerical predictions for the hydrodynamic performance of horizontal axis marine current turbines. Renewable Energy. 2007;32:2479-90.

[23] Myers L, Bahaj AS. Power output performance characteristics of a horizontal axis marine current turbine. Renewable Energy. 2006;31:197-208.

[24] Goundar JN, Ahmed MR, Lee Y-H. Numerical and experimental studies on hydrofoils for marine current turbines. Renewable Energy. 2012;42:173-9.

[25] Bahaj AS, Molland A, Chaplin J, WMJ.Batten. Power and thrust measurements of marine current turbines under various hydrodynamic flow conditions in a cavitation tunnel and a towing tank. Renewable Energy. 2007:407-26.

[26] Myers L, Bahaj AS. Wake studies of a 1/30th scale horizontal axis marine current turbine. Ocean Engineering. 2007:758-62.

[27] Gaurier B, Davies P, Deuff A, Germain G. Flume tank characterization of marine current turbine blade behaviour under current and wave loading. Renewable Energy. 2013;59:1-12.

[28] Tutar M, Veci I. Performance analysis of a horizontal axis 3-bladed Savonius type wave turbine in an experimental wave flume (EWF). Renewable Energy. 2016;86:8-25.

[29] Ross H, Polagye B. Blockage Effects on Current Turbine Performance and Wake Characteristics. EWTEC 2017 Cork, Ireland.

[30] Gaurier B, Germain G, Facq JV, Johnstone CM, Grant AD, Day AH, Nixon E, Felice FD, Costanzo M. Tidal Energy "Round Robin" Tests: Comparisons between towing tank and circulating tank results. International Journal of Marine Energy. 2015;12:87-109.

[31] Maganga F, Germain G, King J, Pinon G, Rivoalen E. Experimental characterisation of flow effects on marine current turbine behaviour and on its wake properties. IET Renewable Power Generation. 2010;4:498.

[32] Tedds SC, Owen I, Poole RJ. Near-wake characteristics of a model horizontal axis tidal stream turbine. Renewable Energy. 2014;63:222-35.

[33] Hall TJ. Numerical simulation of a cross flow marine hydrokinetic turbine [master of Engineering]: University of Washington; 2012.

[34] Lawson MJ, Li Y, Sale DC. Development and verification of a computational fluid dynamics model of a horizontal-axis tidal current turbine. ASME 2011 30th International Conference on Ocean, Offshore and Arctic Engineering, 2011. American Society of Mechanical Engineers, 711-20.

[35] Noruzi R, Vahidzadeh M, Riasi A. Design, analysis and predicting hydrokinetic performance of a horizontal marine current axial turbine by consideration of turbine installation depth. Ocean Engineering. 2015;108:789-98.

[36] Bai X, Avital EJ, Munjiza A, Williams JJR. Numerical simulation of a marine current turbine in free surface flow. Renewable Energy. 2014;63:715-23.

[37] Javaherchi T, Seydel J, Stelzenmuller N, Aliseda A. Experimental and Numerical Analysis of a Scale-Model Horizontal Axis Hydrokinetic Turbine. Proceedings of the 2nd Marine Energy Technology Symposium (METS2014), 2014.

[38] Kinsey T, Dumas G. Impact of channel blockage on the performance of axial and cross-flow hydrokinetic turbines. Renewable Energy. 2017;103:239-54.

[39] Kolekar N, Banerjee A. Performance characterization and placement of a marine hydrokinetic turbine in a tidal channel under boundary proximity and blockage effects. Applied Energy. 2015;148:121-33.

[40] Mcnaughton J, Rolfo S, Apsley D, Afgan I, Stallard T, Stansby P. CFD Prediction of Turbulent Flow on an Experimental Tidal Stream Turbine using RANS modelling. 1st Asian Wave and Tidal Energy Conference in host publication, 2012 Jeju Island, South Korea.

[41] Tatum S, Allmark M, Frost C, O'Doherty D, Mason-Jones A, O'Doherty T. CFD modelling of a tidal stream turbine subjected to profiled flow and surface gravity waves. International Journal of Marine Energy. 2016;15:156-74.

[42] Tatum S, Frost CH, Allmark M, O'Doherty DM, Mason-Jones A, Prickett PW, Grosvenor RI, Byrne CB, O'Doherty T. Wave–current interaction effects on tidal stream turbine performance and loading characteristics. International Journal of Marine Energy. 2016:161-79.

[43] Miley SJ. A catalog of low Reynolds number airfoil data for wind turbine applications. Department of Aerospace Engineering: Texas A&M University; 1982.

[44] XFoil 6.96; http://web.mit.edu/drela/Public/web/xfoil/;, 2006.

[45] Make M, Vaz G. Analyzing scaling effects on offshore wind turbines using CFD. Renewable Energy. 2015;83:1326-40.

[46] Giahi MH, Dehkordi AJ. Investigating the influence of dimensional scaling on aerodynamic characteristics of wind turbine using CFD simulation. Renewable Energy. 2016;97:162-8.

[47] Bardal LM, Sætran LR, Wangsness E. Performance Test of a 3MW Wind Turbine – Effects of Shear and Turbulence. Energy Procedia. 2015;80:83-91.

[48] Wagner R, Courtney M, Gottschall J, Lindelöw-Marsden P. Accounting for the speed shear in wind turbine power performance measurement. Wind Energy. 2011;14:993-1004.

[49] Forbush D, Polagye B, Thomson J, Kilcher L, Donegan J, McEntee J. Performance characterization of a cross-flow hydrokinetic turbine in sheared inflow. International Journal of Marine Energy. 2016;16:150-61.

[50] Masters I, Orme J, Chapman J. Towards realistic marine flow conditions for tidal stream turbines. Proc 7th European Wave and Tidal Energy Conference, 2007 Porto

[51] Lust EE, Luznik L, Flack KA, Walker JM, Van Benthem MC. The influence of surface gravity waves on marine current turbine performance. International Journal of Marine Energy. 2013;3-4:27-40.

[52] Galloway PW, Myers LE, Bahaj AS. Quantifying wave and yaw effects on a scale tidal stream turbine. Renewable Energy. 2014;63:297-307.

[53] Buckland H. Combined Current, Wave and Turbulent Flows and their Effects on Tidal

Energy Devices [Ph.D thesis]: Swansea University.; 2013.

[54] Sos M, Johnston L, Walker J, Rahimian M. The impact of waves and immersion depth on horizontal axis tidal turbine performance. 12th European Wave and Tidal Energy Conference (EWTEC2017), 27 August-1 September 2017 Cork, Ireland. 1-8.

[55] Wu H-n, Chen L-j, Yu M-h, Li W-y, Chen B-f. On design and performance prediction of the horizontal-axis water turbine. Ocean Engineering. 2012;50:23-30.

[56] Baltazar J, De Campos JF. Hydrodynamic analysis of a horizontal axis marine current turbine with a boundary element method. Journal of Offshore Mechanics and Arctic Engineering. 2011;133:041304.

[57] Xu W. Numerical Techniques for the Design and Prediction of Performance of Marine Turbines and Propellers [Master of Enginnering]: The University of Texas at Austin; 2010.

[58] Shi W, Wang D, Atlar M, Seo K. Flow separation impacts on the hydrodynamic performance analysis of a marine current turbine using CFD. Proceedings of the Institution of Mechanical Engineers, Part A: Journal of Power and Energy. 2013;227:833-46.

[59] Gunawan B, Michelen C, Neary VS, Coe RG, Johnson E, Fontaine A, Meyer RS, Straka W, Jonson M. Model validation using experimental measurements from the garfield thomas water tunnel at the applied research laboratory (arl) at penn state university. 2014.

[60] Menter FR. Turbulence modeling for engineering flows. Ansys, Inc. 2011.

[61] Menter FR. Two-equation eddy-viscosity turbulence models for engineering applications. AIAA journal. 1994;32:1598-605.

[62] Menter F, Garbaruk A, Egorov Y. Explicit algebraic Reynolds stress models for anisotropic wall-bounded flows. Progress in Flight Physics, 2012. EDP Sciences, 89-104.

[63] Wallin S, Johansson AV. An explicit algebraic Reynolds stress model for incompressible and compressible turbulent flows. Journal of Fluid Mechanics. 2000;403:89-132.

[64] Blanco JM. Investigation of turbine interactions in a tidal device. 2009.

[65] Ansys C. Release 15.0, CFX-"Solver theory guide". Technical report, Ansys; 2013.

[66] ANSYS. ANSYS CFX-Solver Modeling Guide. 15th ed. 275 Technology Drive, Canonsburg PA 153172013.

[67] Rhie C-M. Numerical study of the flow past an isolated airfoil with separation. Dissertation Abstracts International Part B: Science and Engineering[DISS ABST INT PT B- SCI & ENG]. 1982;42:1982.

[68] Slater JW. Examining spatial (grid) convergence. Public tutorial on CFD verification and validation, NASA Glenn Research Centre, MS. 2006;86.

[69] Sutrisno, Prajitno, Purnomo, W SB. The performance & flow visualization studies of three-dimensional (3-D) wind turbine blade models. 2016;1737:060016.

[70] John D. Anderson J. Fundamentals of Aerodynamics. Fifth ed: McGraw-Hill; 2011.

[71] Otto W, Rijpkema D, Vaz G. Viscous-flow calculations on an axial marine current turbine. ASME 2012 31st International Conference on Ocean, Offshore and Arctic Engineering, 2012. American Society of Mechanical Engineers, 369-82.

[72] Micallef D, Akay B, Ferreira CS, Sant T, Bussel Gv. The origins of a wind turbine tip vortex. Journal of Physics: Conference Series. 2014;555:012074.

[73] Liu J, Lin H, Purimitla SR. Wake field studies of tidal current turbines with different numerical methods. Ocean Engineering. 2016;117:383-97.

[74] SonTek. SonTek/YSI ADVField/Hydra Operation Manual Acoustic Doppler Velocimeter (Field) Technical Documentation. USA2001.

[75] Cea L, Puertas J, Pena L. Velocity measurements on highly turbulent free surface flow using ADV. Experiments in Fluids. 2007;42:333-48.

[76] Mycek P, Gaurier B, Germain G, Pinon G, Rivoalen E. Experimental study of the turbulence intensity effects on marine current turbines behaviour. Part I: One single turbine. Renewable Energy. 2014;66:729-46.

[77] Mycek P, Gaurier B, Germain G, Pinon G, Rivoalen E. Experimental study of the turbulence intensity effects on marine current turbines behaviour. Part II: Two interacting turbines. Renewable Energy. 2014;68:876-92.

[78] ITTC. Uncertainty Analysis Instrument Calibration. 25th ITTC2008. p. 1-14.

[79] Boer Jd. Marin Propulsion Dynamometer- User Manual- Final Report. Marin Technology Transfer2014.

[80] Marinet. Review of Tow Tank Limitations. Marine Energy System Testing - Standardisation and Best Practice: Marine Renewable Infrastraucture Network; 2014.

[81] Figliola RS, Beasley DE. Theory and Design for Mechanical Measurements. Fifth ed: Jon Wiley & Sons Inc.; 2011.

[82] Ross SM. Introduction to probability and statistics for engineers and scientists: Academic Press; 2014.

[83] Coleman H, Steele W. Engineering application of experimental uncertainty analysis. AIAAJ. 1995;33.

[84] Wagner R, Courtney SM, Larsen JT, Paulsen SU. Simulation of shear and turbulence impact on wind turbine performance. Technical University of Denmark; 2010.

[85] Maalawi KY, Badawy MT. A direct method for evaluating performance of horizontal axis wind turbines. Renewable and Sustainable Energy Reviews. 2001;5:175-90.

[86] Madsen HA, Mikkelsen R, Øye S, Bak C, Johansen J. A Detailed investigation of the Blade Element Momentum (BEM) model based on analytical and numerical results and proposal for modifications of the BEM model. Journal of Physics: Conference Series, 2007. IOP Publishing, 012016.

[87] Sant T. Improving BEM-based Aerodynamic Models in Wind Turbine Design Codes: University of Malta, Delft University Wind Energy Institute; 2007.

[88] Lanzafame R, Messina M. Fluid dynamics wind turbine design: Critical analysis, optimization and application of BEM theory. Renewable energy. 2007;32:2291-305.

[89] Batten WMJ, Bahaj AS, Molland AF, Chaplin JR. Experimentally validated numerical method for the hydrodynamic design of horizontal axis tidal turbines. Ocean Engineering. 2007;34:1013-20.

[90] Masters I, Chapman J, Willis M, Orme J. A robust blade element momentum theory model for tidal stream turbines including tip and hub loss corrections. Journal of Marine Engineering & Technology. 2011;10:25-35.

[91] Marten D. QBlade Short Manual V.08. Hermann Föttinger Institute of TU Berlin2015.

[92] MONTGOMERIE B. Methods for Root Effects, Tip Effects and Extending the Angle of Attack Range to +-100deg, with Application to Aerodynamics for Blades on Wind Turbines and Propellers. FOI Swedish Defence Research Agency, Scientific Report FOI-R-1035-SE; 2004.

[93] Glauert H. Airplane Propellers. Aerodynamic Theory: A General Review of Progress Under a Grant of the Guggenheim Fund for the Promotion of Aeronautics. Berlin, Heidelberg: Springer Berlin Heidelberg; 1935. p. 169-360.

[94] Shen WZ, Mikkelsen R, Sørensen JN, Bak C. Tip loss corrections for wind turbine computations. Wind Energy. 2005;8:457-75.

[95] Snel H, HOUWKING R, VAN BUSSEL GJW, BRUINING A. Sectional Prediction of 3D Effects for Stalled Flow on Rotating Blades and Comparison with Measurements. European Community Wind Energy Conference, 1993.

[96] Mason-Jones A, O'Doherty DM, Morris CE, O'Doherty T. Influence of a velocity profile & support structure on tidal stream turbine performance. Renewable Energy. 2013;52:23-30.

[97] Lewis M, Neill SP, Robins P, Hashemi MR, Ward S. Characteristics of the velocity profile at tidal-stream energy sites. Renewable Energy. 2017;114:258-72.

[98] Adamski SJ. Numerical Modeling of the Effects of a Free Surface on the Operating Characteristics of Marine Hydrokinetic Turbines [Master of Science]: University of Washington; 2013.

[99] Luznik L, Flack KA, Lust EE, Taylor K. The effect of surface waves on the performance characteristics of a model tidal turbine. Renewable Energy. 2013;58:108-14.

[100] Rahimian M, Walker J, Penesis I. Numerical assessment of a horizontal axis marine current turbine performance. International Journal of Marine Energy. 2017;20:151-64.

[101] Barltrop N, Varyani KS, Grant A, Clelland D, Pham XP. Investigation into wave—current interactions in marine current turbines. Proceedings of the Institution of Mechanical Engineers, Part A: Journal of Power and Energy. 2007;221:233-42.

[102] Hirt CW, Nichols BD. Volume of fluid (VOF) method for the dynamics of free boundaries. Journal of Computational Physics. 1981;39:201-25.

[103] Wheeler JD. Method for calculating forces produced by irregular waves. Offshore Technology Conference, 1969. I-83-I-94.

[104] Soulsby R. Dynamics of marine sands: a manual for practical applications: Thomas Telford; 1997.

[105] Monismith SG, Fong DA. A note on the potential transport of scalars and organisms by surface waves. Limnology and Oceanography. 2004;49:1214-7.

[106] Whelan J, Graham J, Peiro J. A free-surface and blockage correction for tidal turbines. Journal of Fluid Mechanics. 2009;624:281-91.

[107] Tecnomare SpA, IT Power Ltd. Non-nuclear energy - Joule II, Wave Energy Project Results, The exploitation of tidal marine currents. Luxembourg1996.

[108] Milne IA, Day AH, Sharma RN, Flay RGJ. Blade loads on tidal turbines in planar oscillatory flow. Ocean Engineering. 2013;60:163-74.

[109] Geoscience Australia and BREE, Australian Energy Resource Assessment. 2nd ed: Geoscience Australia, Canberra; 2014.

[110] Massie W, Journée J. Offshore hydromechanics. Delft University of Technology: Delft, The Netherlands. 2001.

[111] Tasmanian Tide Tables; http://www.bom.gov.au/ntc/IDO59001/IDO59001_2016_TAS_TP004.pdf, 2016.

Appendix

The Impact of Waves and Immersion Depth on Horizontal Axis Tidal Turbine Performance

This refereed conference paper was published in the Proceedings of the 12th European Wave and Tidal Energy Conference (EWTEC 2017). The citation for this conference paper is:

Sos M, Johnston L, Walker J, Rahimian M. The impact of waves and immersion depth on horizontal axis tidal turbine performance. *12th European Wave and Tidal Energy Conference (EWTEC2017)*. Cork, Ireland. p. 1-8.